Winter 2008

Offshore vertical datum separations derived from Post-Processed Kinematic (PPK) heights observed along a scheduled ferry route

Nathan C. Wardwell
University of New Hampshire, Durham

OFFSHORE VERTICAL DATUM SEPARATIONS DERIVED FROM POST-PROCESSED KINEMATIC (PPK) HEIGHTS OBSERVED ALONG A SCHEDULED FERRY ROUTE

BY

NATHAN C. WARDWELL
BSc Environmental Science, Alaska Pacific University, 2004

THESIS

Submitted to the University of New Hampshire
in Partial Fulfillment of
the Requirements for the Degree of

Master of Science
in
Earth Science: Ocean Mapping

December, 2008

This thesis has been examined and approved.

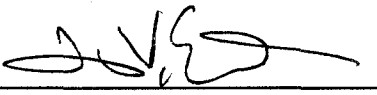

Thesis Director, James V. Gardner
Research Professor of Earth Sciences

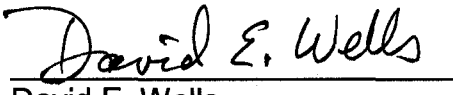

David E. Wells
Adjunct Professor of Ocean Engineering

Lloyd C. Huff
Research Professor of Ocean Engineering

Semme J. Dijkstra
Lecturer of Ocean Engineering

November 17, 2008
Date

DEDICATION

To the memory of my loving parents Kenneth and Lizabeth Wardwell

ACKNOWLEDGEMENTS

Special thanks are due to the National Oceanographic and Atmospheric Administration (NOAA) for funding my research under grant NA05NOS4001153. Thanks are also due to the University of New Brunswick, specifically Dr. Marcelo Santos, for providing the dataset used in this research. I am indebted to the support of the entire community at the Center for Coastal and Ocean Mapping (CCOM) and the University of New Hampshire. Special thanks are necessary for my thesis advisor Dr. David E. Wells for his willingness to discuss least-squares and tidal theory on weekends and holidays. I would also like to extend my gratitude to Dr. Lloyd C. Huff for sharing his knowledge of the field procedures used during the *Princess of Acadia* GPS Project and for his insightful suggestions. Also, I would not have been able to complete this research had it not been the invaluable guidance of my thesis committee chair Dr. James V. Gardner and member Dr. Semme J. Dijkstra. Special thanks go to the director of CCOM Dr. Layer Mayer and the Co-Director of the Joint Hydrographic Center Mr. Andrew Armstrong, without their support I never would have had the opportunity to do this research.

TABLE OF CONTENTS

LIST OF TABLES

LIST OF FIGURES

GLOSSARY

Tidal datum acronyms that are capitalized refer water-levels surfaces that are determined from data collected over a 19-year National Tidal Datum Epoch or have been mathematically corrected to the 19-year equivalent. Tidal datum acronyms that are not capitalized refer to water-level surfaces that are determined from data spanning a month or less.

TERM	DEFINITION
CD	Chart Datum: The low-water tidal datum to which depths on a nautical chart are referenced. Different hydrographic offices use different definitions for Chart Datum. For example Chart Datum in the US is Mean Lower Low Water, whereas Canada is migrating from using Lower Low Water Large Tide to Lowest Astronomical Tide.
CGSJ	GPS base station established at the Canadian Coast Guard Building in Saint John, NB
CGG2000	Canadian Gravimetric Geoid Model of 2000
CHS	Canadian Hydrographic Service
CMM	Comparison of Monthly Means: Method of computing tidal datums from water-level observations spanning less than 19-years.
CO-OPS	Center for Oceanographic Operational Products and Services
DFO	Department of Fisheries and Oceans Canada
DBLS	Dual Baseline Solutions: The weighted average of the single-baseline solutions post-processed with data from GPS base-stations CGSJ and DRHS.
DLW	Mean Diurnal Low Water Inequality: The difference between mean higher high-water and mean lower low-water computed from 19-years of data.

DRHS	GPS base station established at the Digby Regional High School in Digby, NS
dtl	Diurnal Tide Level: The average of mean higher high-water and mean lower low-water computed from a month or less of observations.
DTL	Diurnal Tide Level: The average of mean higher high-water and mean lower low-water computed from 19-years of observations. When 19-years of observations are not available a 19-yr equivalent is computed using either the Comparison of Monthly Means or Tide-by-Tide methods of simultaneous observations.
FIG	International Federation of Surveyors
GEOID99	US Geoid model developed from gravimetric information and GPS ellipsoid heights on leveled bench marks.
GrafNav	A software package developed by Waypoint Consulting Inc. for post-processing raw GPS data.
gt	Great Diurnal Range: The difference between mean higher high-water and mean lower low-water computed from a month or less of observations.
GT	Great Diurnal Range: The difference in height between mean higher high-water and mean lower low-water computed from 19-years of observations. When 19-years of observations are not available a 19-yr equivalent is computed using either the Comparison of Monthly Means or Tide-by-Tide methods of simultaneous observations.
GPS-Hv2.0	Natural Resources Canada software that transforms between orthometric and ellipsoidal heights
HAMELS	Harmonic Analysis Method of Least-Squares: Defined by John D. Boon (2004).
HAMWLS	Harmonic Analysis Method of Weighted Least-Squares
hlw	Higher low-water: The highest of a pair of low-waters.
hhw	Higher high-water: The highest of a pair of high-waters.
ITRF2000	International Terrestrial Reference Frame of 2000

LAT	Lowest Astronomical Tide: The lowest predicted water-level to occur under any combination of astronomical and average meteorological conditions.
LLWLT	Lower Low Water, Large Tide: The average of the lowest low-water from each year of 19 years of predictions.
lhw	Lower high-water: The lowest of a pair of high waters.
llw	Lower low-water: The lowest of a pair of low waters.
mhhw	Mean higher high water: The average of a month or less of higher high-water observations.
MHHW	Mean Higher High Water: The average of 19-years of higher high-water observations. When 19-years of observations are not available a 19-yr equivalent is computed using either the Comparison of Monthly Means of Tide-by-Tide methods of simultaneous observations.
mllw	Mean lower low water: The average of a month or less of lower low-water observations
MLW	Mean Low Water: The average of 19-years of observed low-waters. When 19-years of observations are not available a 19-yr equivalent is computed using either the Comparison of Monthly Means of Tide-by-Tide methods of simultaneous observations.
MLLW	Mean Lower Low Water: The average of 19-years of lower low-water observations. When 19-years of observations are not available a 19-yr equivalent is computed using either the Comparison of Monthly Means or Tide-by-Tide methods of simultaneous observations.
msl	Mean sea level computed from a month or less of hourly water-levels.
MSL	Mean Sea Level: The average of 19-years of hourly water-levels. When 19-yrs of hourly water-levels are not available a 19-yr equivalent is computed using either the Comparison of Monthly Means or the Tide-by-Tide methods of simultaneous observations.
NAD83	North American Datum of 1983

NOAA	National Oceanic and Atmospheric Administration
NOS	National Ocean Service
NTDE	National Tidal Datum Epoch: The 18.6 yr period of the regression of the moon's nodes rounded up to 19 yr. At the time this thesis was written the current NTDE was 1983-2001
PPK	Post-processed kinematic GPS solutions
TByT	Tide-by-Tide: A method for computing monthly mean tidal datums from water-level measurements spanning less than a month.
VTGZ	Virtual Tide Gauge Zone: These are user defined spatial regions. Post-processed kinematic GPS data within these spatial regions are analyzed as if all the data were from one virtual tide gauge.
WebTide	Tidal prediction software developed by the Department of Fisheries and Oceans Canada.
WGS84	World Geodetic System of 1984: Native geodetic reference frame for the Global Positioning System.

PROCESSING FLOW CHART

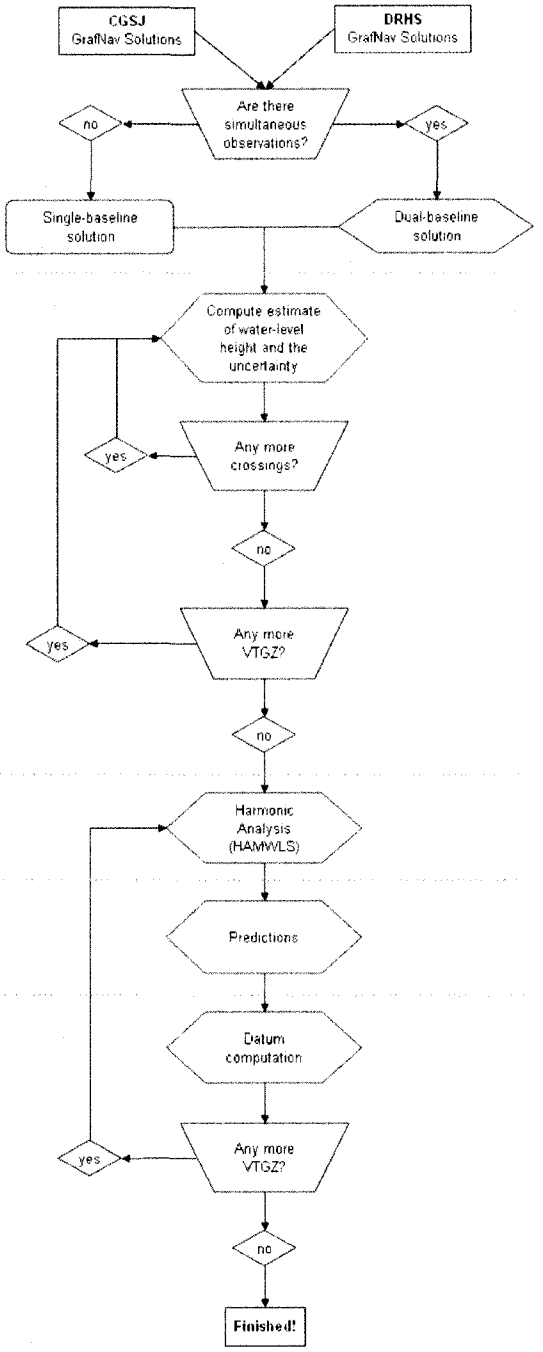

Step 1 - Products

Dataset consisting of single- and dual-baseline solutions

Step 2 - Products

Three datasets for each VTGZ

1. Times
2. Estimated water-level heights
3. Uncertainty estimate for each of the water-level height estimates

Step 3 - Products

Tidal constituents for each VTGZ

Step 4 - Products

Predicted hourly water-levels for each VTGZ

Step 5 - Products

MLLW and MSL for each VTGZ

ABSTRACT

OFFSHORE VERTICAL DATUM SEPARATIONS DERIVED FROM POST-PROCESSED KINEMATIC (PPK) HEIGHTS OBSERVED ALONG A SCHEDULED FERRY ROUTE

by

Nathan C. Wardwell

University of New Hampshire, December, 2008

Eight months of GPS data were used to determine tidal constituents along a ferry route across the Bay of Fundy, Canada. The GPS data were aggregated into 62 spatial zones and analyzed as if all the data within each zone were from a single Virtual Tide Gauge (VTG). Tidal models were developed from the VTG data using a weighted least-squares solution. Chart Datum with respect to the ITRF2000 was computed for each spatial zone using 8 months of predicted water-levels.

The time between ferry crossings results in sampling intervals longer than the tide signal in the Bay of Fundy, thus traditional methods of harmonic analysis are not applicable. Instead, *a priori* knowledge of the tide signal at each end of the ferry route is used to overcome the large and non-uniform sampling intervals. The results were confirmed by a close match between Mean Seal Level and the local Geoid.

INTRODUCTION

The objective of this research was to extract tidal datums from GPS data collected on a moving platform. The results were the separation between a reference ellipsoid and tidal datums along a scheduled ferry route that were computed from water-level predictions. The predictions were based on tidal harmonic constituents resolved from GPS-observed water-level heights. This research focused on the Mean Sea Level (MSL) and Mean Lower Low Water (MLLW) tidal datums because of their importance in geodesy and hydrographic surveying for nautical charts in the US.

These ellipsoid-to-tidal datum separations are the parameters necessary for transforming GPS heights to tidal datums. The transformation parameters reduce a hydrographers reliance on shore-based tide stations. FIG Publication NO 37 (FIG, 2006) shows that if the ellipsoid-to-Chart Datum (MLLW in the US) separation is known hydrographic surveys can be conducted without directly measuring tides (Figure 1).

FIG Special Publication NO 37 shows that traditionally sounding depths on a nautical chart are computed using the equation on the left of Figure 1 where, S is the sounding depth, D is the depth of the water measured by the transducer, Tx is the heave of the vessel, and T is the height of the tide above Chart Datum (CD). FIG Special Publication NO 37 further explains that when soundings are referenced to an ellipsoid the non-tide formula, shown on the right

of Figure 1, is used to compute the sounding depth. The heave and tide parameters in the traditional formula are replaced by the height of the antenna above the transducer (*K*), of the antenna above the reference ellipsoid (*H*), and the ellipsoid-to-CD separation (*N*). It should be noted that in geodesy the variable *N* represents the Geoid undulation, which is the separation between the Geoid and reference ellipsoid. For the purposes of this research *N* represents the separation between chart datum and a reference ellipsoid, which is different from the Geoid undulation.

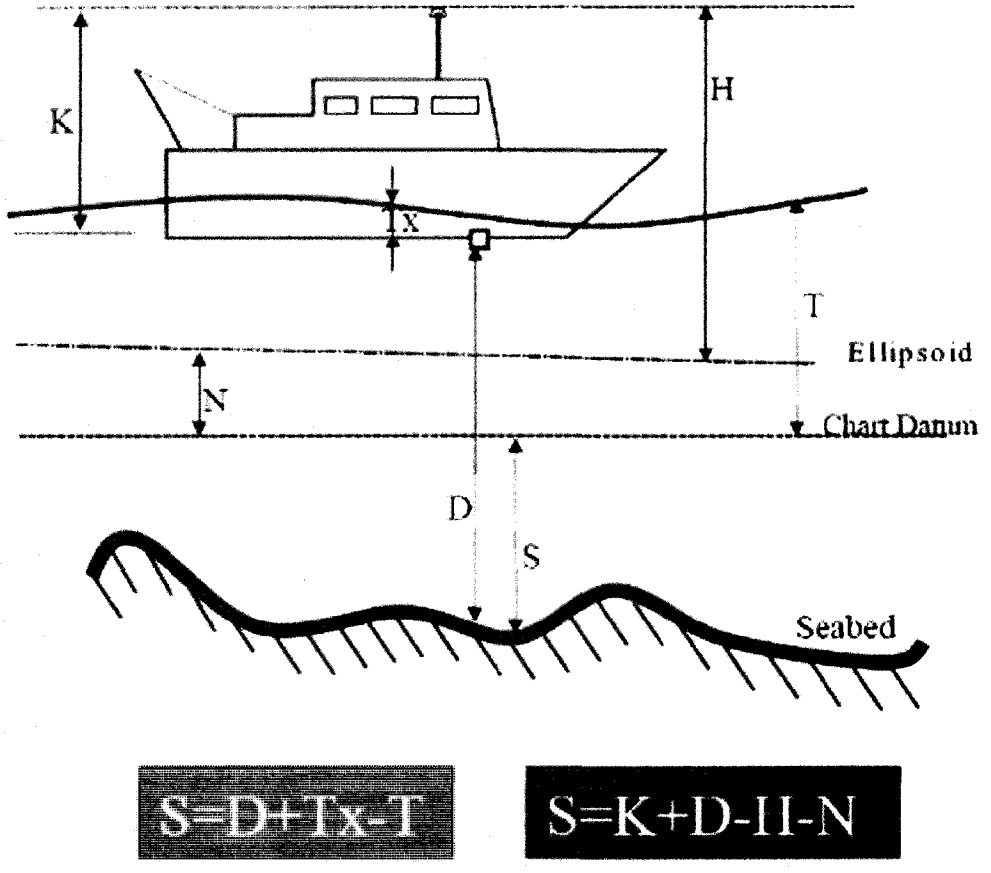

Figure 1 - Traditional (left) and non-tide (right) formulas for computing hydrographic depth soundings (Modified from FIG, 2006).

N varies spatially, an example of this is illustrated in Figure 2, which shows the height MLLW in Saint John, NB and 74 km southeast in Digby, NS. Because *N* varies spatially, it must be either modeled or computed from water-level heights directly referenced to an ellipsoid. For smaller areas *N* is often assumed constant.

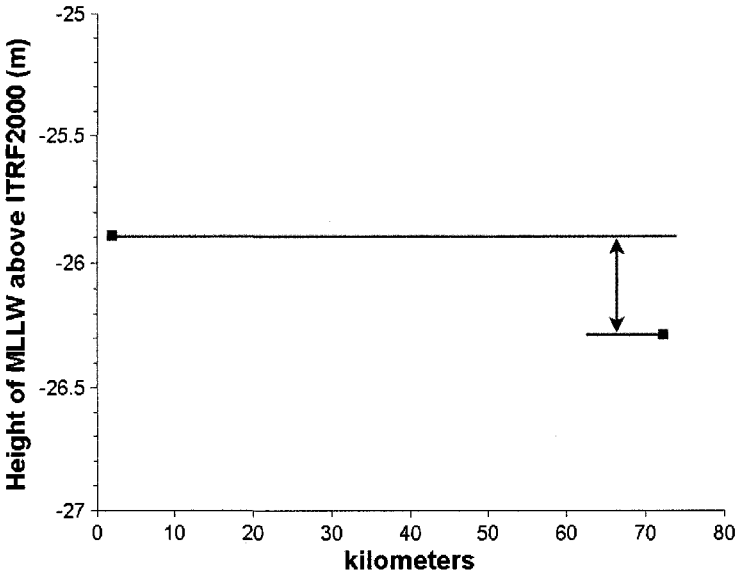

Figure 2 – Difference in height of MLLW at Saint John, NB (blue square) and Digby, NS (red square).

It is relatively easy to derive *N* at a location onshore, especially if a tide station with tidal benchmarks has already been established. A static GPS observation of a tidal benchmark provides the height of the benchmark above the reference ellipsoid. The ellipsoid height and the CD height of the benchmark can then be used to compute *N*.

Locations offshore pose a more difficult problem, because there are no benchmarks and the environment is dynamic. There are two approaches used

for determining *N* at offshore locations. One approach is to compute CD from water-level heights directly referenced to an ellipsoid. The second approach is to model *N* at locations offshore by interpolating between *N* measured at locations onshore.

The data used in this research to answer this question was collected between 7 December 2003 and 25 September 2004 by the University of New Brunswick (UNB) and the University of Southern Mississippi (USM) during the *Princess of Acadia* GPS Project. The *Princess of Acadia* GPS Project was funded by an Office of Naval Research grant in an attempt to better understand the tropospheric effects on high-accuracy GPS positioning in the marine environment, local tidal effects and vertical datum relationships in the Bay of Fundy (Santos et. al., 2004; Wells et. al., 2004). To date, the data collected during this project has contributed to research on improving estimates of tropospheric delay of the GPS signal using a Numerical Weather Prediction model (Cove et. al., 2004; Cove, 2005; Santos et. al., 2005; Nievinski et al., 2005), the UNB3 model (Kim et. al., 2004), nullifying ionospheric delay (Kim and Langley, 2005), and for assessing hydrodynamic models in the Bay of Fundy (Church, 2008).

The *Princess of Acadia* GPS Project used the *Princess of Acadia* ferry to obtain a spatially diverse set of water-level observations. The advantage of using the ferry as a sampling platform instead of a traditionally site specific water-level measurement system is that the ferry transits back and forth between Saint John, NB and Digby, NS 1 to 3 times a day. Thus, it efficiently measures

instantaneous water-levels over a large spatial region. One of the challenges of using the *Princess of Acadia* as a platform for measuring tides is that the sampling interval at any particular location along the ferry's track varies with the frequency of the ferry crossings, which varies from day-to-day and season-to-season. Another challenge is that the ferry takes approximately 3 hrs to transit the 75 km distance between Saint John, NB and Digby, NS. Therefore, even during the busiest month, when the frequency of ferry crossings is at its highest, the period between crossings periodically exceeds the Nyquist sampling interval for resolving the predominant tidal constituent (M2) in the bay from an equally spaced time series.

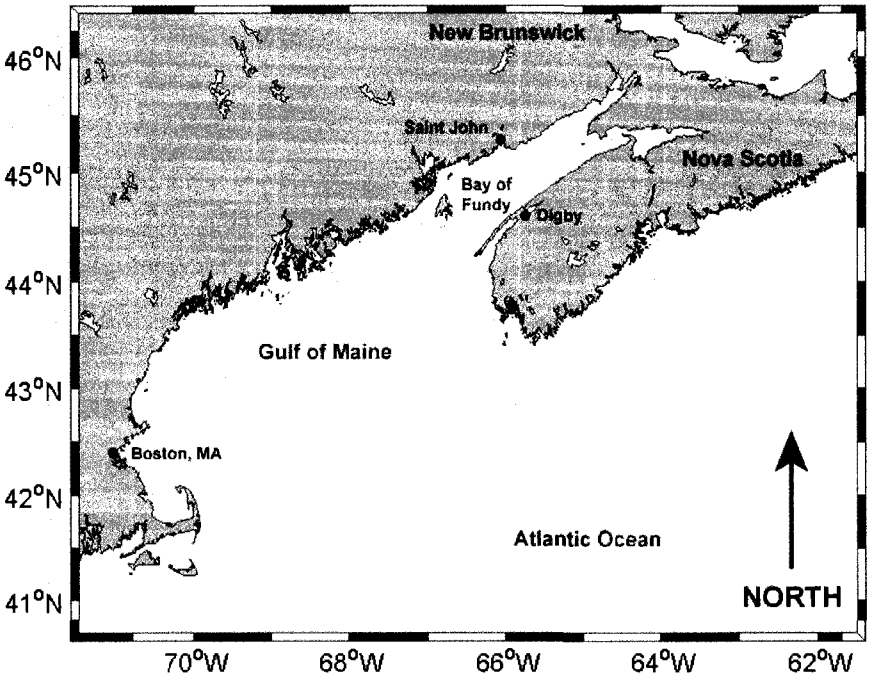

Figure 3 - Map of the Gulf of Maine and the Bay of Fundy.

Document Organization

This thesis is organized in four chapters. Chapter 1 provides background information on tidal theory and vertical positioning with GPS. This chapter concludes with a discussion of how the ellipsoid-to-CD separation values are measured at shore stations and site-specific locations offshore. The end of the chapter also includes a brief introduction to several of the separation models that have been developed by different Hydrographic Offices.

Chapter 2 summarizes the data collected during the *Princess of Acadia* GPS Project. This chapter also describes the methodology used to address the non-uniform sampling interval that resulted from using the *Princess of Acadia* as the measurement platform.

Chapter 3 begins with a discussion of the sampling achieved by the *Princess of Acadia*. This is followed by an analysis of the results from fitting the non-uniform water-level records using two sets of tidal constituents. The amplitude of the constituents and the times of the high and low water-levels predicted using the two sets are compared to data provided by the Canadian Hydrographic Service (CHS) and to predictions derived from the software package WebTide. The chapter concludes with an analysis of the MSL and MLLW heights computed using the methodology described at the end of Chapter 2.

Chapter 4 describes the significant results of this research and gives recommendations for future research.

CHAPTER 1

EQUILIBRIUM TIDE THEORY, MEASUREMENTS, DATUMS AND SEPARATION MODELS

> A model under which it is assumed that the water covering the face of the Earth instantly respond to the tide-producing forces of the Moon and Sun to form a surface of equilibrium under the action of these forces. The model disregards friction, inertia, and the irregular distribution of the land masses of the Earth. The theoretical tide formed under these conditions is known as the equilibrium tide (CO-OPS, 2000)

The equilibrium tide theory provides *a priori* knowledge of the frequencies that contribute tidal energy to a time series of water-level observations (Parker, 2007). The amplitude and phase of these frequencies can be used to predict water-levels, which can then be used to model tidal datums such as MLLW and MSL. MSL is of particular importance, because it allows validation of the Geoid. The Geoid is a model of an equipotential gravity surface that best fits MSL on a global scale (Torge, 2001). There are differences between the Geoid and the observed MSL surface because of water density gradients, ocean currents and varying meteorological conditions (Pugh, 2004). Globally, the maximum differences between the Geoid and MSL are about +/-1m (Torge, 2001)

Tides develop from pulling (gravitational force) and pushing (centrifugal force) of the water on the surface of the earth by the Moon and the Sun (Parker, 2007). Pugh (2004) has shown, using Newton's physical laws, that the

gravitational force a celestial body has on the Earth's oceans is inversely proportional to the cube of the distance the body is from the Earth and directly proportional to the mass of the celestial body (Parker, 2007). Thus, even though the Sun is 27.1 million times larger than the moon the gravitation force imposed on the Earth's surface by the Sun is 0.46 times weaker than that of the Moon because the Sun is 389 times farther from the Earth than the Moon is (Pugh, 2004). Because the gravitational forces developed by the Moon are much larger than the gravitational forces developed by the Sun the remainder of the discussion will focus on the earth-moon system. However, the reader should understand that the discussion is also valid for the earth-sun system.

The earth and moon orbit around the center of mass of the earth-moon system. This common axis of rotation is called the barycenter. The barycenter lies just inside the surface of the Earth (Boon, 2004). The centrifugal force created by this rotation is the force that balances the gravitational forces of the system. The gravitational force and the centrifugal force are equally balanced at the center of the Earth (Parker, 2007). For a point on the Earth's surface that is closer to the Moon than the center of the Earth, the gravitational force will be larger than the centrifugal force. The opposite is true for a point on the Earth's surface that is farther from the Moon than the center of the Earth. The net result of the gravitational and centrifugal forces resulting from the earth-moon system and the earth-sun system are the tide generating forces (Figure 4).

Type of Force	Designation
F_c = centrifugal force due to Earth's revolution around the barycenter	thin arrow
F_g = gravitational force due to the Moon	heavy arrow
F_t = the resultant tide-raising force due to the Moon	double shafted arrow

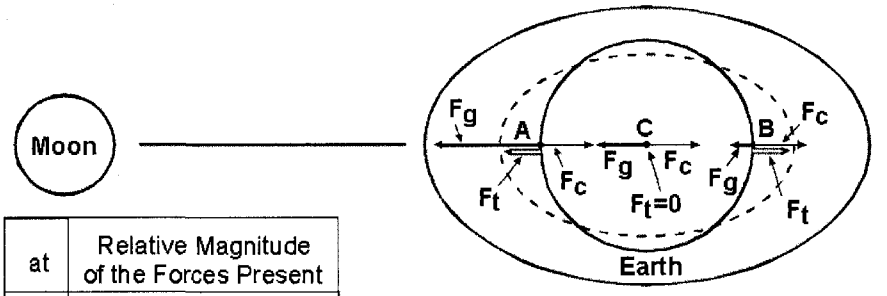

at	Relative Magnitude of the Forces Present
A	$F_g > F_c > F_t$
	v = v
C	$F_g = F_c > 0$
	v = ^
B	$F_g < F_c > F_t$

A north-south cross-section through the Earth's center in the plane of the Moon's hour angle; the dashed ellipse represents a profile through the spheroid composing the tidal force envelope; the solid ellipse shows the resulting effect on the Earth's waters.

Figure 4 - Lunar tide generating forces (from http://co-ops.nos.noaa.gov/restles3.html).

The tide generating force of the moon is 0.0000034 times the gravitational force of the Earth (Boon, 2004). For points on the Earth's surface that are off the Moon's orbital plane there is a horizontal component to the tide generating force (Boon, 2006). This horizontal component is the force vector that moves the oceans on the Earth's surface towards the locations on the Earth's surface that are on the Moon's orbital plane (Parker, 2007). There are two such locations. One is located on the side of the Earth that is closest to the moon, where the gravitational force of the Moon is larger than the centrifugal force of the earth-moon system. The other is located on the side of the earth that is farthest from the Moon where the centrifugal force of the earth-moon system is larger than the

gravitational force of the Moon (Figure 4). The attraction of the water in earth's oceans to these two locations results in two bulges of water. These bulges are referred to as either tidal bulges (Parker, 2007) or the tidal envelope (Hicks, 2006).

Figure 5 shows the vector components of the lunar tide generating forces (thick black lines). Points *A* and *A'* are points on the Earth's surface that are on the Moon's orbital plane. The tide generating forces at these locations are pointing directly away from the Earth's surface. The tide generating forces at the points *B* and *B'* are pointing directly towards the middle of the Earth. For intermediate points *C* and *C'* the tide generating forces are not perpendicular to the Earth's surface. The horizontal component at these and any other intermediate locations is the tractive force that moves water from the intermediate locations to *A* and *A'* (Forrester, 1983).

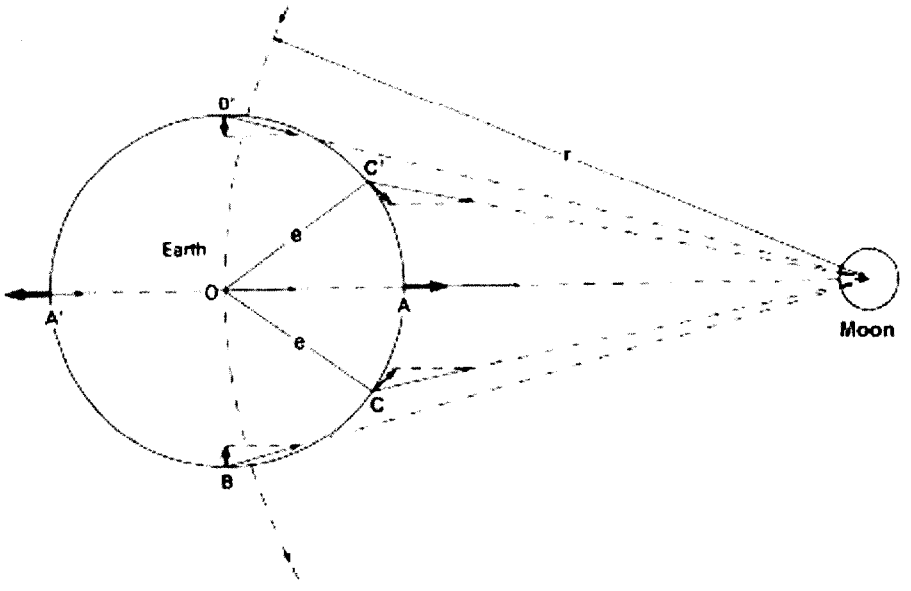

Figure 5 - Horizontal tide force vectors (Modified from Forrester, 1983).

The preceding discussion focused on the tidal envelope developed by the Moon. However, there is also a tidal envelope developed by the Sun (Hicks, 2006). The tidal forces generated by the Sun are smaller than those generated by the Moon thus the solar tide envelop is smaller than the lunar tide envelop. Also, the points on the Earth's surface that are on the Sun's orbital plane are not usually the same points that are on the Moon's orbital plane. The net result of the solar and lunar tide envelopes is the composite tidal envelope (Hicks, 2006). Figure 6 shows a drawing that depicts the lunar, solar, and composite tidal envelopes.

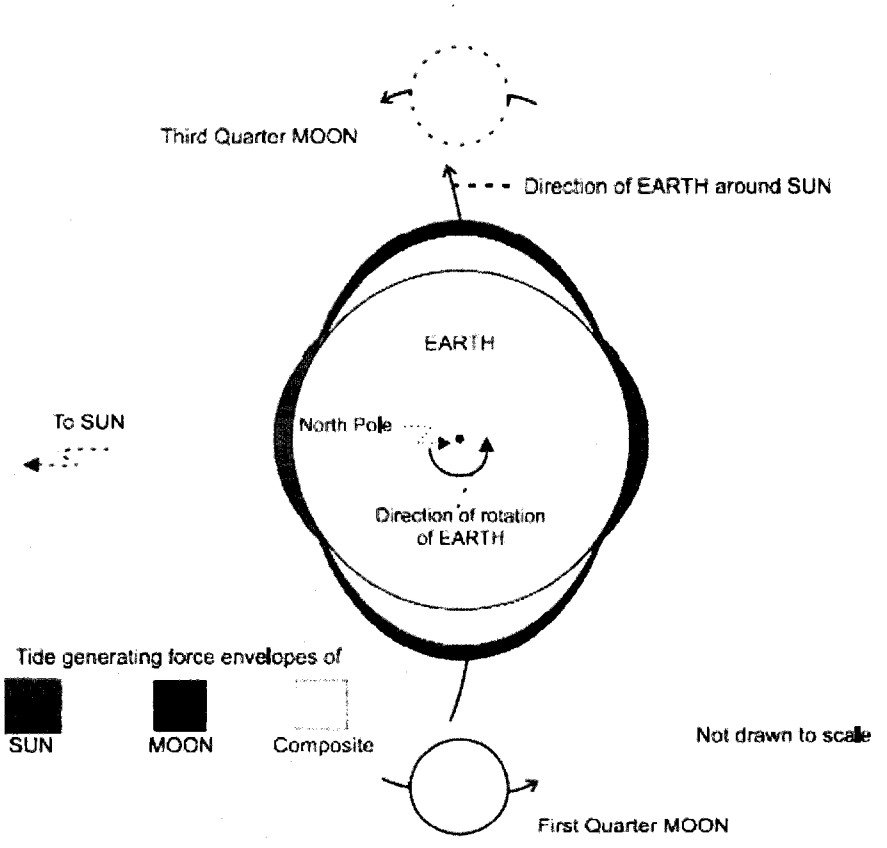

Figure 6 - Drawing of lunar, solar and composite tidal envelopes (Modified from Hicks, 2006).

The size of the composite envelope is not constant, which is one of the factors contributing to the spatial variability in the tides that are observed on earth. The composite envelope is not constant because the tidal forces generated by the Moon and the Sun vary with the distance they are from the Earth and their orientation with respect to the Earth.

Stacy D. Hicks (2006) describes the orbits of the Moon and the Earth as follows. During the Moon's elliptical orbit around the Earth the point at which it is closest to the Earth is called perigee and the point at which it is farthest from the Earth is called apogee. At perigee the Moon is 132,600 km from the Earth. At apogee the moon is 151,800 km from the Earth. The perigee-to-perigee cycle is called the anomalistic month and has a period of 27.55455 days (Figure 7). The elliptical shape of the Moon's orbit around the Earth also varies, which results in a change of the location at which perigee occurs. The period over which it takes the location of perigee to complete a cycle is 8.847 years (Parker, 2007).

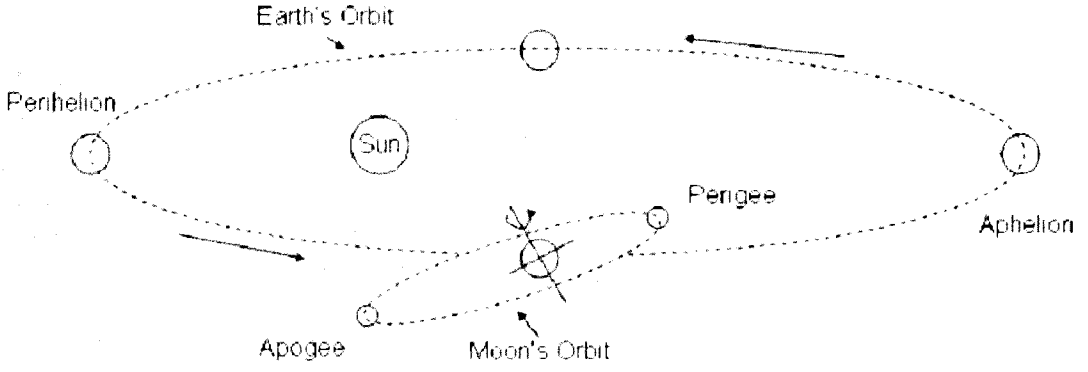

Figure 7 - Drawing of the Moon's elliptical orbit around the Earth and the Earth's elliptical orbit around the Sun (Modified from Parker, 2007).

Hicks (2006) describes the elliptical orbit of the Earth around the Sun to vary by 1,867,351 km over a period of 365.2596 days. When the Earth is closet to the Sun it is considered to be in perihelion. When it is farthest from the Sun it is considered to be in aphelion (Figure 7). The amount of time it takes the Earth to complete a perihelion-to-perihelion cycle is called the anomalistic year.

Changes in declination of the Earth, the Moon, and the Sun are measured with respect to the ecliptic (Figure 8). The ecliptic is the plane defined by the orbit of the Earth around the center of mass of the earth-sun system (Hicks, 2006). The Earth's axis of rotation has a maximum declination of 23.452° with respect to the ecliptic. The summer solstice in the northern hemisphere marks the point at which the northern hemisphere is closest to the Sun. This is also the point that the Sun is at its maximum declination with respect to the Earth's equator. A quarter of its orbit after summer solstice in the northern hemisphere the Sun is directly above the equator. One-quarter of an orbit later the northern hemisphere is now farthest from the Sun marking winter solstice in the northern hemisphere and the point at which the Sun is at its maximum declination south of the Earth's equator (Hicks, 2006).

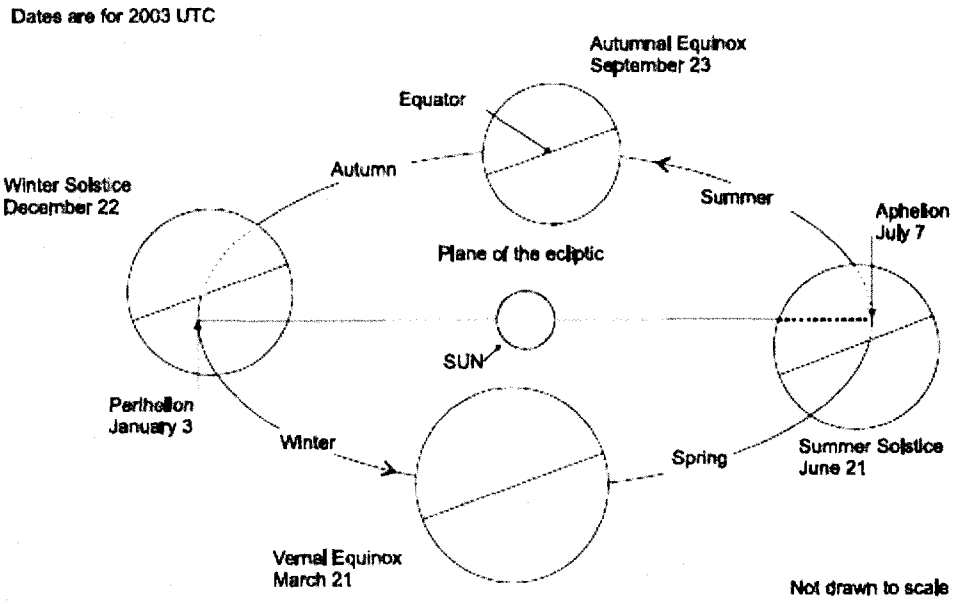

Figure 8 - Drawing of the earth-sun system (Modified from Hicks, 2006).

As described by Parker (2007), the orbital plane of the Moon around the Earth is inclined to the Earth's equator. The maximum angle between the Moon's orbital plane and the Earth's equator is 5° and it takes 18.6 years for this angle to go from 5° north of the earth's equator to 5° south then back to 5° north (Parker, 2007). During this time the position at which the Moon crosses the ecliptic changes. These positions are called lunar nodes. The changes in their position is called the regression of the lunar nodes because their position moves in the opposite direction from which the Earth revolves around its axis, the Moon orbits around the Earth, and the Earth rotates around the Sun (Parker, 2007) (Figure 9).

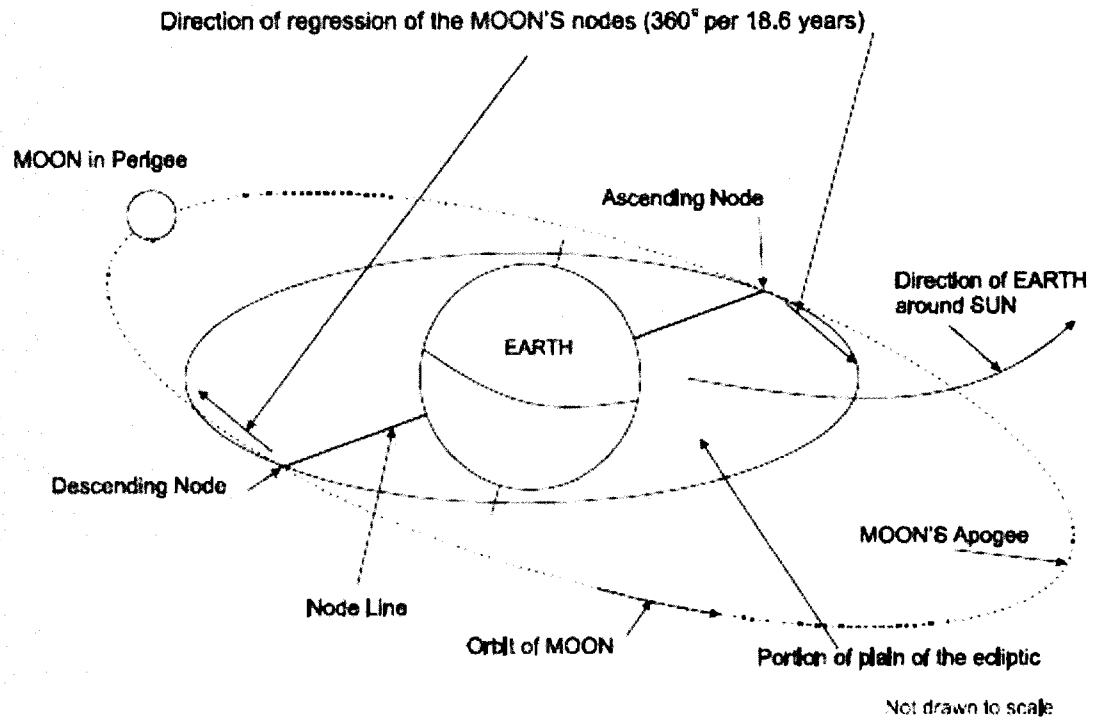

Figure 9 - Drawing of the Moon's orbit around the Earth (From Hicks, 2006).

These variations in distance and declination of the Earth, the Moon, and the Sun control the size of the composite tidal envelope. Cartwright (2000) points out that the periods of the cycles that define these variations have been clearly defined by early astronomers. Linear combinations of the frequencies of these cycles are called tidal harmonic frequencies and are used to describe tidal behavior (Parker, 2007). The period of the six primary cycles that are used to derive the tidal harmonic frequencies are listed in Table 1. The periods listed in Table 1 are the primary benefit of the equilibrium tidal theory because they can be used to derive the tidal frequencies that are used in tidal harmonic analyses.

Table 1 – The six fundamental astronomic periods used to derive tidal harmonic frequencies (modified from Pugh, 2004).

Description	Frequency Symbol	Period (mean solar units)	Degrees per mean solar hour
Mean lunar day (one rotation wrt to the moon)	ω_1	24.8412 hours	14.4921
Tropical month (perod of lunar declination)	ω_2	27.3216 days	0.5490
Tropical year (period of solar declination)	ω_3	365.2422 days	0.0411
Period of lunar perigee	ω_4	8.847 years	0.0046
Period of lunar node regression	ω_5	18.613 years	0.0022
Period of perihelion	ω_6	20,940 years	

Harmonic Analysis Method of Least-Squares (HAMELS)

The equilibrium tide theory discussed in the previous section is a description of how the sea-surface would behave assuming nothing restricts or constrains the water in the oceans from instantaneously responding to the tide generating forces (Pugh, 2004). This assumption is an over simplification because the response of the water in the oceans is restricted by bottom friction and constrained by coastlines (Parker, 2007). These restrictions and constraints dissipate energy from a propagating tidal wave and can transfer energy from one tidal frequency to another (Parker, 2007). The tidal dynamics resulting from these energy changes and shifts result in non-linear effects that are modeled using a hydrodynamic model or by using overtides and compound tides in a harmonic analysis (Parker, 2007). Overtides are higher harmonics of tidal harmonic frequencies. Compound tides are the combination of different tidal harmonic frequencies. Overtides and compound tides are grouped together as shallow-water tidal harmonic frequencies. This research used the Harmonic

Analysis Method of Least-Squares (HAMELS) described by John D. Boon (2004). This method models non-linear effects using shallow-water tidal frequencies.

Although the equilibrium tide is a simplification of this complex ocean's response, it still provides the foundation for developing a prediction model in the form of a linear combination of a set of harmonic functions (Boon, 2004). The general model with *nk* tidal constituents is:

$$\hat{h}_i = h_0 + \sum_{j=1}^{nk} A_j \cos(2\pi f_j t_i) + B_j \sin(2\pi f_j t_i) \quad \textbf{(1)}$$

where:

h_0	= a constant offset
f_j	= frequency of constituent j
t	= time at epoch i
$\hat{h}_i$	= water-level estimate at epoch i
nk	= number of harmonic constituents
A_j	= amplitude of cosine component of constituent j
B_j	= amplitude of sine component of constituent j

The coefficients for equation (1) are obtained using a least-squares procedure that minimizes the squared difference between a height estimate and the observed height, and are appropriate for use only at the location of the observed heights.

Each of the tidal constituents resolved in the least-squares procedure have a unique amplitude (R) and phase (ϕ) of harmonic constituent. R and ϕ are obtained from the coefficients for the prediction model using the equations below:

$$R_j = \sqrt{A_j^2 + B_j^2} \tag{2}$$

$$\phi_j = \tan\left(\frac{B_j}{A_j}\right)^{-1} \tag{3}$$

The uncertainty of the amplitude and phase of a constituent is governed by the sampling interval of the signal, the length of the record, the number of constituents used in the analysis and the amount of noise in the record (Parker, 2007). For evenly-spaced time-series the sampling interval (Δt) defines the highest frequency for which the amplitude and phase can be resolved (Boon, 2004). This frequency is defined as $f_c = 1/(2\Delta t)$ where f_c is the Nyquist or 'cutoff' frequency (Boon, 2004). Analyses of even-spaced time-series at frequencies higher than the Nyquist frequency result in false frequency detections (Boon, 2004). False detections are high-frequency signals that appear in the low-frequency part of the spectrum and are referred to as aliased signals (Scargle, 1982).

Press et. al. (1992) showed, using spectral analysis methods for unevenly spaced data, that when some samples in an unevenly sampled dataset are spaced much closer than the average sample interval, frequencies above the Nyquist frequency can be correctly identified. In fact, Scargle (1982) reports that uneven spacing provides an advantage when aliasing is a problem. Thus, with a *priori* knowledge of the tidal harmonic frequencies that contribute to the signal at a location, the number of frequencies used in a harmonic analysis is reduced.

Also, uneven sample intervals allow for the tidal harmonic frequencies higher than the average sample interval to be resolved (Scargle, 1982).

In order to resolve the individual contribution of two different harmonic constituents, the length of the record being analyzed must be equal to the synodic period (T) of the two constituents (Parker, 2007). This period is the amount of time it takes the two constituents to go from being in-phase to being out-of-phase and back to being in-phase. The synodic period of two constituents is determined using the Rayleigh criterion $T \geq \frac{1}{|f_1 - f_2|}$ where f_1 and f_2 are the frequencies in cycles per day (cpd) of the tidal harmonic constituents to be uniquely identified (Parker, 2007). For example, the frequency of the principal semi-diurnal lunar (M2) and principal semi-diurnal solar (S2) constituents is 1.9323 cpd and 2.000 cpd, respectively. Thus, the synodic period, T, for M2 and S2 is: $T = \frac{1}{|1.9323 - 2.0000|} = 14.765$ days. This period is the spring-neap cycle (Figure 10).

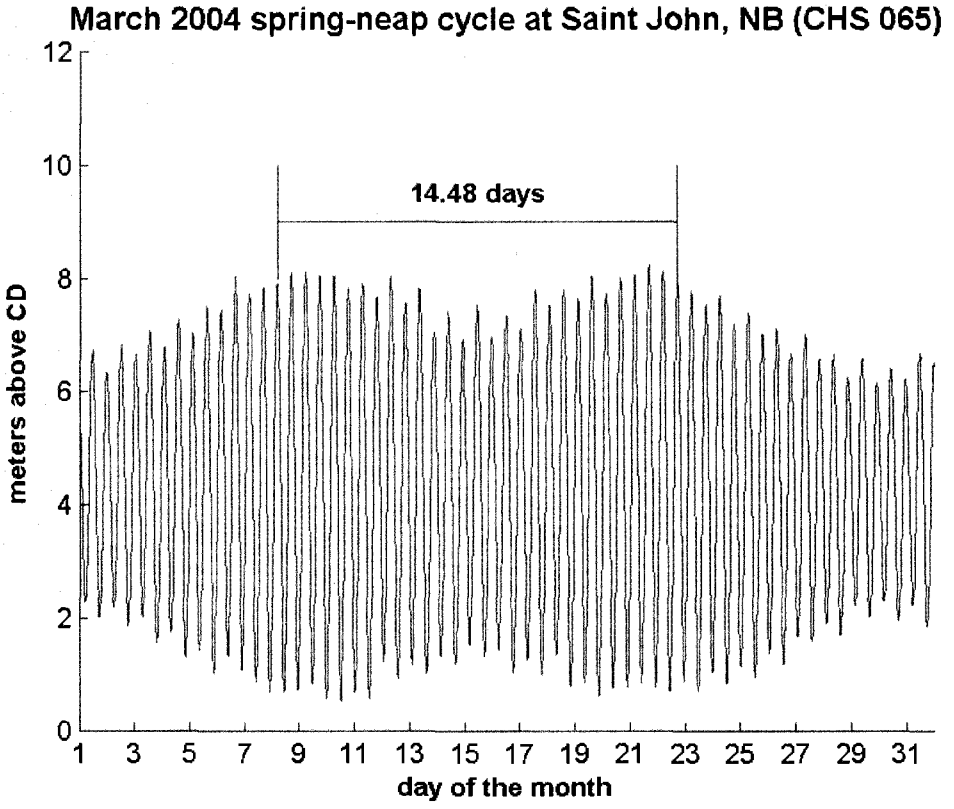

Figure 10 – Spring-neap cycle at CHS 065.

Water-level Measurement Systems

There are many approaches to measuring water-levels. The ones used in this research were float/pulley gauges, a strain gauge and a GPS buoy. Float/pulley gauges have been the standard water-level measurement system for the past 150-years (Pugh, 2004). These systems consist of a wire with a float at one end. The wire goes through a series of pulleys and gears. Attached to the other end of the wire is a counter weight. The float, which rests on the water, goes up and down with the changes of the water-level. The pulleys and gears

are connected to electronic devices that record the changes in the gearing induced by the moving float and counter weight.

A strain gauge is a pressure gauge that has an oscillating crystal for sensing pressure changes. The pressure changes are recorded digitally. Some strain gauges record the combined pressure of the water column and the air above the water column (Pugh, 2004). In order to convert the pressure measurements to depth atmospheric pressure must be accounted for along with water density and gravity (Pugh, 2004). Other strain gauges are vented to the atmosphere, thus water density and gravity are the parameters necessary for converting pressure to depth.

General overview of GPS system

The Global Positioning System (GPS) is one of several Global Navigation Satellite Systems that are used worldwide for accurate 3D positioning. The GPS has been integrated in many fields of science and surveying. There are three different segments to the GPS. The space segment is composed of satellites orbiting in six different planes such that at any location on the Earth's surface, at any time, at least four satellites are visible (El-Rabbany, 2006). As of November 2003 there were 28 Block-II satellites orbiting in the six planes. The control segment consists of manned and unmanned stations located around the world that are used for monitoring and maintaining the satellite orbits and signals (Seeber, 2003). The user segment consists of a GPS receiver connected to an antenna and a person to operate it.

GPS satellites transmit two signals on two different carrier frequencies. These carrier frequencies are L1 and L2. L1 is a 1575 MHz electromagnetic signal that is modulated by 2 binary digital codes (Wells, 1987). The L2 signal is a 1228 MHz electromagnetic signal that is modulated by 1 binary digital code (Wells, 1987). The digital codes are sequences of 0 or 1, where 0 represents no phase reversal of the carrier and 1 represents a phase reversal (Wells, 1987).

The fundamental concept of GPS positioning is based on the one-way travel time of radio waves. GPS receivers use *a priori* knowledge of the exact signal generated in the satellite to duplicate the signal internally. The phase offset between the signal generated in the receiver and the one received from a satellite gives the travel time. Neglecting propagation errors, the product of the travel time and the speed of light give the slant range between the receiver and a satellite. Because this range is affected by satellite and receiver clock errors, orbit errors and atmospheric delay, it is called the pseudorange. Conceptually, the intersection point of three spheres of radius equal to the pseudorange to three different satellites gives the position of the receiver (Seeber, 2003). In practice GPS position fixes are determined by a least-squares fit of predicted pseudoranges to measured pseudoranges for all satellites above the horizon, or above a specific elevation angle (Wells, 2008a).

Tidal Datums

The procedures described in this section and used in this research are those used by NOAA. They are not necessarily the same as procedures used in other countries, including Canada. The Coast and Geodetic Survey Act statutorily authorized the National Ocean Service (NOS) to collect and analyze water-level data in support of their congressional assignments (Gill and Schultz, 2001). This section summarizes the described in NOAA Special Publication NOS CO-OPS 2 (CO-OPS, 2003), which are used in the U.S. for computing tidal datums. These were used because they are well documented. Procedures used elsewhere do not have the same level of documentation.

Tidal datums are of importance because they are legal definitions of private, public, state, federal and international marine boundaries depend on the intersection of the ocean and the land at a specific phase of the tide (Gill and Schultz, 2001) (Figure 11). The intersection of the ocean with the land is defined by tidal datums. An example of a marine boundary defined by a tidal datum is the Exclusive Economic Zone, which is 200 nm from the low-water datum MLLW (Gill and Schultz, 2001). Beyond this 200 nm boundary are international waters. MLLW is also the low-water datum used on nautical charts in the U.S. to reference the depth of the seafloor and submerged hazards (Gill and Schultz, 2001). MSL is another important tidal datum of particular importance because it is the surface to which geodesists attempt to approximate as close as possible with the Geoid (Torge, 2001).

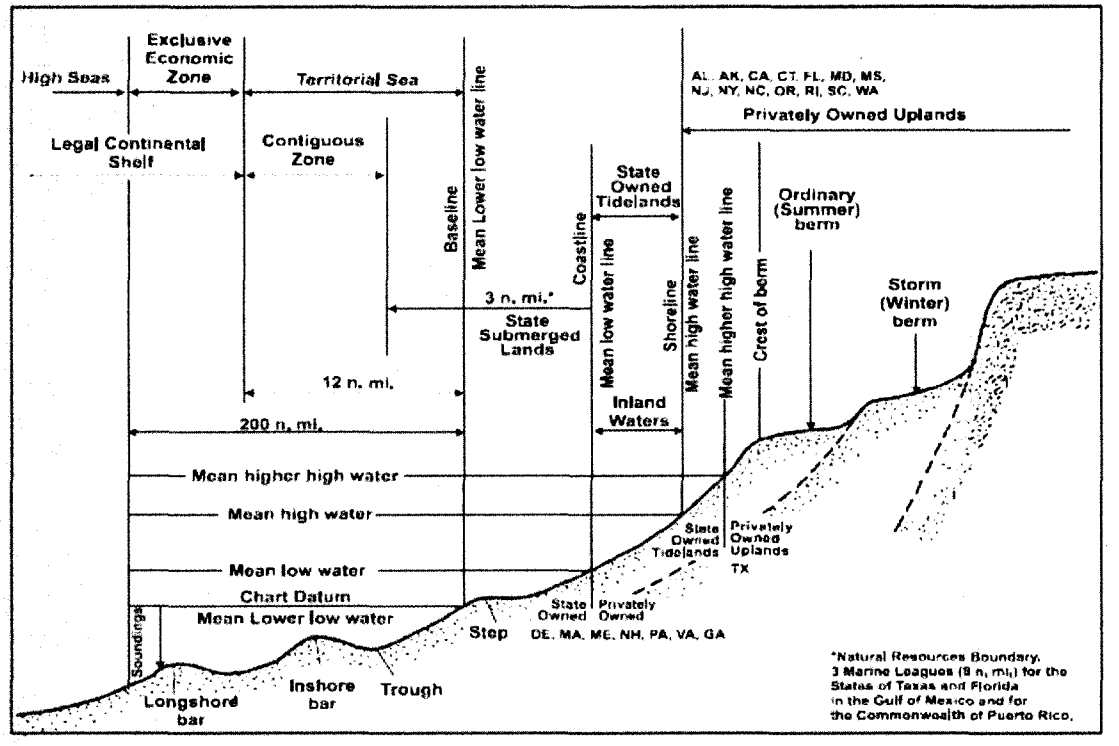

Figure 11 - A drawing of the principal tidal datums that define marine boundaries (From Gill and Schultz, 2001)

Tidal datums are derived from water-level observations. In the U.S., there are three types of tide stations from which water-levels are observed. Primary tide stations are stations that have been installed and operating for at least 19 yrs. The 19-year period of time is used to define a primary station because it encompasses the sufficient amount of time over which the variations introduced from astronomic cycles are averaged out during the computation of tidal datums (Gill and Schultz, 2001). The 19-year period includes the regression of the lunar nodes, which is the longest observable cycle that contributes to variations in water-level heights. Specific 19-year periods of time are adopted by the NOS as National Tidal Datum Epochs (NTDE) (Gill and Schultz, 2001). NTDE defines

the period of time over which water-level observations are used to obtain mean values for computing tidal datums (Gill and Schultz, 2001).

The other two types of tide stations are secondary tide stations, which operate for more than 1-year and less than 19-yrs, and tertiary stations, which operate for less than 1-year (Gill and Schultz, 2001). Data from these stations are not sufficient for independently deriving tidal datums thus they are compared with simultaneous observations from a primary station. Then the data are mathematically reduced to an equivalent NTDE using the procedures described in NOAA Special Publication NOS CO-OPS 2 (CO-OPS, 2003).

The reduction and correction of tidal datums begins with the tabulation of monthly means. Monthly means are tidal datums computed from month-long records of water-level measurements. Monthly means at secondary and tertiary stations are computed using either the Standard or Modified-Range Ratio methods. The Standard method is generally used for stations on the West Coast of the U.S. and in the Pacific Islands. The Modified-Range Ratio method is generally used for stations on the East and Gulf Coasts of the U.S. and in the Caribbean Islands (CO-OPS, 2003).

MLLW computed using the Standard method is derived from the difference between Mean Low Water (MLW) and the Mean Diurnal Low-Water Inequality (DLQ). MLLW computed using the Modified-Range Ratio method is derived from the difference between the Diurnal Tide Level (DTL) and half the Great Diurnal Range (Gt). The Modified-Range Ratio method is used in areas

with semi-diurnal tides because DLQ tends to be very small for those areas (CO-OPS, 2003).

Monthly means are reduced and corrected to a NTDE using the comparison of monthly means (CMM) method. The CMM method compares monthly means at the secondary station to simultaneous monthly means at a primary station. If the tidal record at the secondary station is shorter than a month or spans two partial months then the Tide-By-Tide (TBYT) method is used. The TBYT method compares simultaneous high and low water-levels between a secondary and a primary station instead of simultaneous monthly means (CO-OPS, 2003).

Point-Source Vertical-Datum Separation Values

The separation between a reference ellipsoid, a smooth representation of the equipotential surface of the earth's gravity field that most closely coincides with mean sea level, and the CD, a reference surface derived from locally observed or predicted tidal behavior, varies spatially. The relationship between these two vertical datums (the spatially varying separation) is typically measured at shore-based tide stations using static GPS techniques and offshore using GPS buoys (Figure 12).

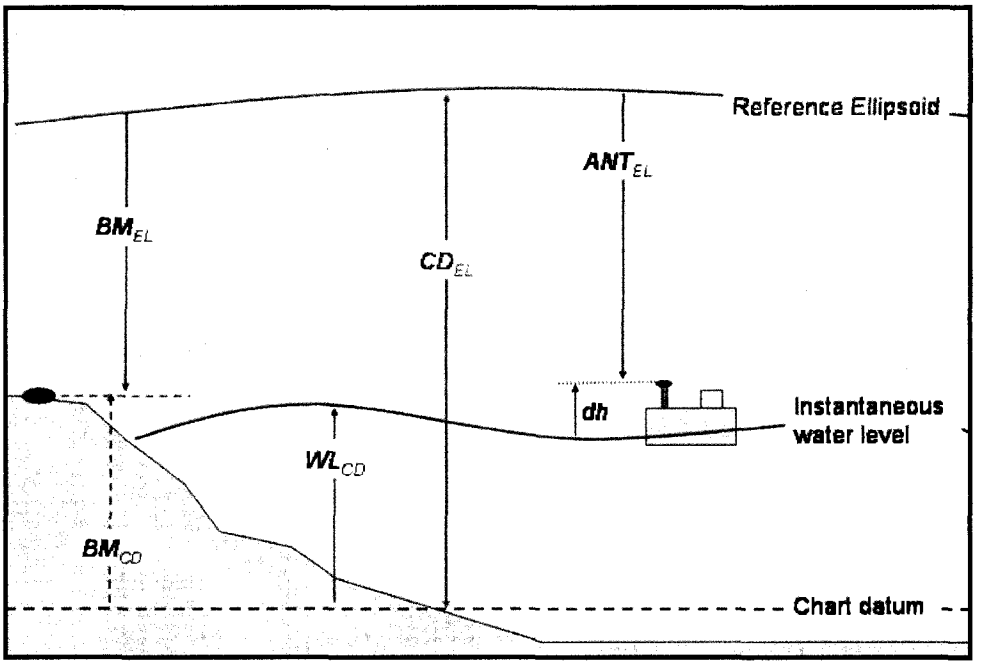

Figure 12 - Vertical relationships of hydrographic surfaces.

Following the convention for computing the separation between a reference ellipsoid and the CD that was used by Arroyo-Suarez et. al. (2005) during their positioning and telemetry buoy research, the separation at a benchmark on shore is:

$$N = BM_{EL} - BM_{CD} \tag{4}$$

where: N = the chart datum to reference ellipsoid separation

BM_{EL} = ellipsoid height of the benchmark

BM_{CD} = chart datum height of benchmark

N is the transformation parameter between the two vertical datums. Assuming CD does not change between a tide gauge and the location at which a GPS buoy is deployed, equation (4) becomes:

$$N = \frac{1}{nwl}\sum_{i=1}^{nwl} WL_{EL}^{i} - WL_{CD}^{i} \quad (5)$$

where: WL_{EL} = water-level height referenced to ellipsoid

WL_{CD} = water-level height referenced to CD

nwl = the number of measurements

i = 1, 2, ..., nwl

Offshore Vertical-Datum Separation Models

There are several offshore vertical-datum separation models that have been developed by different nations. These models relate the geodetic and low-water datums used in the respective countries. Several of the countries and the models they have developed are: the United Kingdom Hydrographic Office's (UKHO) Vertical Offshore Reference Frame (VORF), the Australian Maritime Safety Queensland (MSQ) AUSHYDROID, GPS campaigns by the CHS on the Saint Lawrence River and the Bay of Fundy, and the National Oceanic and Atmospheric Administration's (NOAA) VDATUM project.

The UKHO teamed up with the Danish National Space Centre and the U.K. Proudman Oceanographic Laboratory to develop VORF (Adams, 2004). VORF merges satellite data with long-term and short-term coastal tide station data to model the mean sea-surface. All of the data were referenced to the 3D geodetic datum European Terrestrial Reference Frame of 1989 at an epoch of 1 January-2000 (Iliffe, 2007).

The MSQ developed a separation model for WGS84 and Lowest Astronomical Tide (LAT) called AUSHYDROID (Martin and Broadbent, 2004). The LAT-to-WGS84 separations measured at shore-based tide stations are interpolated offshore based on MSQ tidal-zoning practices (Martin and Broadbent, 2004).

The CHS carried out a GPS campaign in 1995 to determine the separation between CD and NAD83 for the Bay of Fundy (O'Reilly et. al., 1996). Separations measured at 21 tide stations around the bay were used to model the separation offshore (O'Reilly et. al., 1996). Several modeling techniques were used to develop a smooth separation surface of the bay. O'Reilly et. al. (1996) determined that the Kriging and radial basis methods provided the most appropriate representations of the separation surface.

The NOS is in the process of developing vertical datum transformation models for coastal areas around the U.S. as part of the VDATUM project (Hess et. al., 2003; Myers, 2005). A derivative of the VDATUM project is the VDATUM transformation tool. This tool transforms heights between tidal, orthometric and ellipsoidal datums used in the U.S. based on measured and separations between these datums that have been either measured or modeled (Hess et. al., 2003; Myers, 2005). The CD to reference ellipsoidal separation is obtained using a four step process with two datum transformations. The tidal to orthometric datum transformation is based on observed differences in MSL and the National Vertical Datum of 1988 at tidal benchmarks. These differences are spatially interpolated to regularly gridded points using a Kriging algorithm. The orthometric to ellipsoid

transformation is accomplished using the National Geodetic Survey's GEOID99 model (Hess et. al., 2003; Myers, 2005).

Examples of Previous GPS Buoy Projects

Many research projects have been conducted with the purpose of using a variety of different GPS buoys for measuring water-levels. The following paragraphs will describe several of the projects. The list of projects described is not exhaustive, but representative of the work that has been done and are similar to the research in this thesis.

Research conducted by Stephen DeLoach (1996) in the Bay of Fundy near the Saint John harbor investigated the design and implementation of a GPS buoy for deriving tidal datums. The GPS buoy used in his research consisted of a GPS receiver, antenna and a TSS 335B roll, pitch, and heave sensor installed on a Canadian Coast Guard navigation buoy at Saint John, NB. The GPS data were compared to water-level measurements obtained using two different conventional gauges. Daily tide ranges computed from the GPS water-level measurements were within 6 cm of the water-level measurements from the two conventional gauges.

Zilkoski et. al. (1999) conducted a project in the San Francisco Bay to provide centimeter–level positioning of a U.S. Coast Guard vessel using 5 GPS receivers. The goal of the project was to show the potential of using GPS positioning for vessel navigation in harbors and under poor visibility conditions. During this project the Coast Guard vessel was also used to accurately measure

water-levels while the vessel was moving at a constant speed. Their results showed that water-level measurements obtained while the vessel was in motion could be used to measure changes in orthometric heights relative to a reference ellipsoid. They concluded that the GPS has the potential to measure the height of a ship above MLLW.

Yang and Lo (2000) deployed a GPS buoy with Real-Time Kinematic position capabilities near the NOAA tide gauge at Eagle Point, TX. The deployment lasted nearly 11 hrs. The ellipsoid heights for the GPS antenna on the buoy were transferred to the water-level using a static offset. After converting the water-level measurements from the conventional tide gauge and the GPS buoy to MSL there was a mean bias of 1.3 cm between the two, with the measurements from the conventional gauge generally reading higher than the measurements from the GPS buoy. The standard deviation of the differences between the two water-level measurements was 9 mm.

Chen et. al. (2004) investigated the use of improved satellite clock and orbit parameters provided by the International GNSS Service (IGS), formerly the International GPS Service, for kinematic GPS precise point positioning of sea levels. Chen et. al. (2004) were able to achieve decimeter level accuracy for water-level measurements using a GPS buoy.

Wert et. al. (2004) used the satellite based GPS correction system C-Nav, which is developed by C & C Technologies. A C-Nav receiver and antenna were installed on the Canadian Coast Guard Ship Amundsen. This ship was iced in Franklin Bay, North West Territories over winter. The ship was used as a GPS

buoy and GPS heights were used to retrieve tidal heights for the bay. Their results showed that they were able to detect tides in the Arctic to within the specification for IHO Special Order surveys (IHO, 1998).

Arroyo-Suarez et. al. (2005) deployed a GPS positioning and telemetry buoy for 20 days in Sydney, British Columbia's Patricia Bay. The buoy was deployed within 500 m of a permanent CHS tide gauge. The ellipsoid-to-CD separation at two tidal benchmarks was used to transfer the conventional tide gauge data to the reference ellipsoid. Four tidal datums were then computed from the conventional tide gauge data and the data from the GPS buoy: Mean Higher High Water (MHHW), MLLW, Mean Tide Range (Mn) and MSL. The MLLW heights computed from the two different sets of water-level measurements were within 5 cm of each other. The largest difference of 11 cm was for Mn. The smallest difference of 1 cm was for MSL. NOAA Special Publication NOS CO-OPS 1 (CO-OPS, 2000) reports the general accuracy is 4.26 cm for tidal datums computed from a month of data collected on the west coast of the U.S..

CHAPTER 2

PROJECT DESIGN AND COMPUTATION METHODOLOGY

This chapter describes the three types of data collected during the *Princess of Acadia* GPS Project that were used in this research. It also includes a description of the methodology used for computing MSL, MLLW and their uncertainties for each VTGZ.

The data used in this research were collected between 7 December 2003 and 25 September 2004 as part of the *Princess of Acadia* GPS Project (Santos et. al., 2004; Wells et. al., 2004). These data are used to derive tidal coefficients for predicting 8 complete months of water-levels in each VTGZ. Only complete months are predicted so that monthly mean tidal datums can be computed and compared with monthly mean tidal datums from a primary tide station.

The main catalyst of the *Princess of Acadia* GPS Project was the development of methods for improving long baseline kinematic solutions in the marine environment. During the project a high accuracy dual-frequency GPS base station was installed on the north and south sides of the lower Bay of Fundy (Figure 13). A roving receiver was installed on the *Princess of Acadia* ferry. The PPK heights resolved at the GPS antenna on the ferry were the primary data

used in this research. Conventional tide data were collected and a GPS base station was installed in the areas outlined in Figure 13.

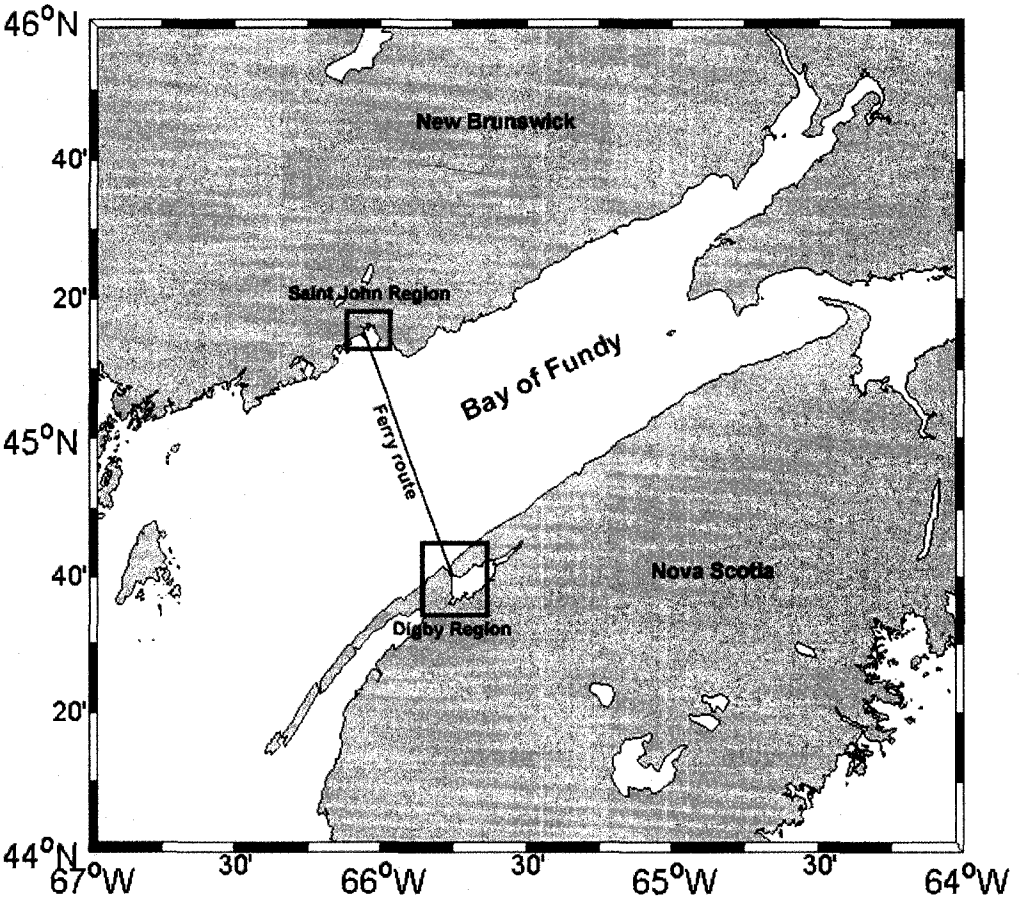

Figure 13 - Area map with the Saint John, NB and Digby, NS vicinities outlined.

Figure 14 and Figure 15 are detailed maps of the areas outlined in Figure 13. These maps show the locations of the CHS tide stations that were installed in both regions. The tide stations are further described in the "Conventional Tide Data" section. The maps also show the relationship between the tide stations and the GPS base stations that were installed for post-processing of the GPS

data logged by the receiver on the ferry. The GPS base stations are further described in the "NovAtel DL-4 GPS Data" section.

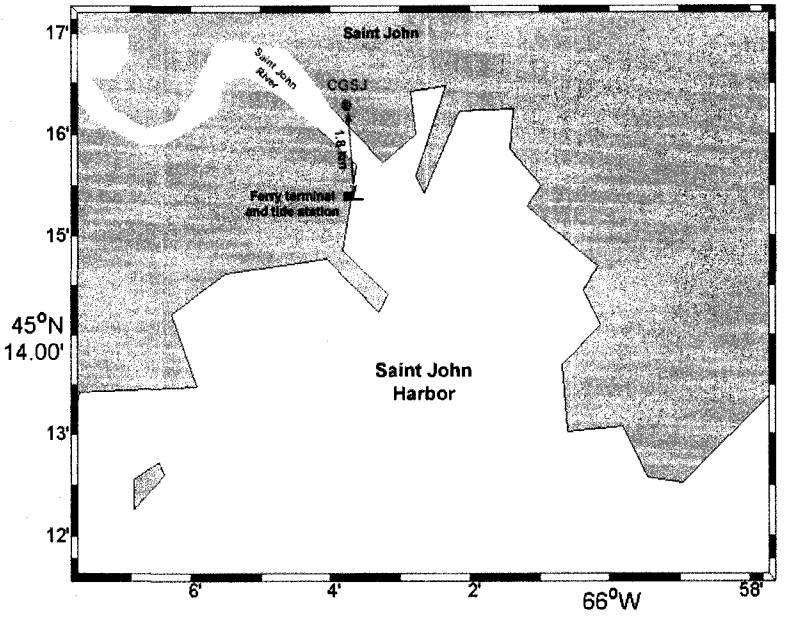

Figure 14 - Area map with the locations of the ferry terminal and GPS base station in Saint John, NB.

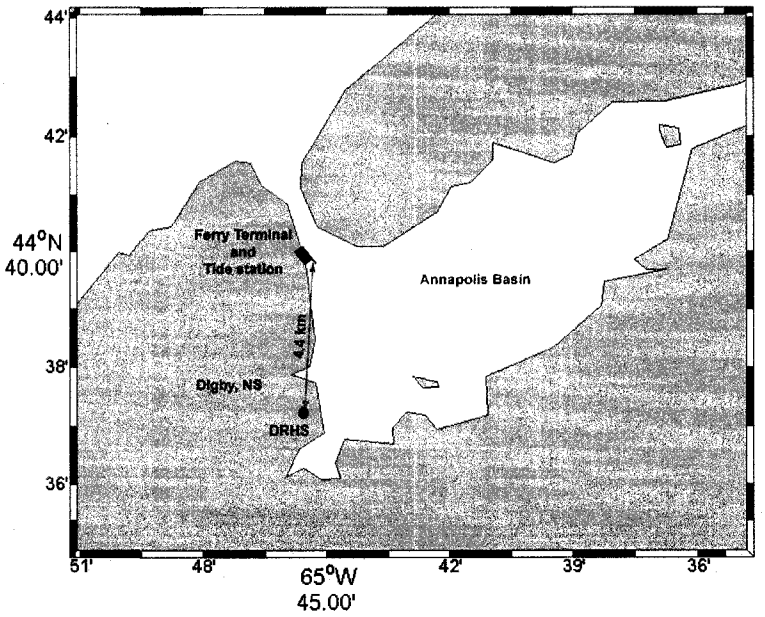

Figure 15 - Area map with the locations of the ferry terminal and GPS base station in Digby, NS.

CROSSBOW Single- and Dual-Accelerometer Data

Vertical acceleration was measured using a CROSSBOW CXL02LF1Z single-axis accelerometer. Roll and pitch were measured using a CROSSBOW CXTA02 dual-axis tilt sensor. Figure 16 shows the accelerometers mounted near the GPS antenna on the *Princess of Acadia*.

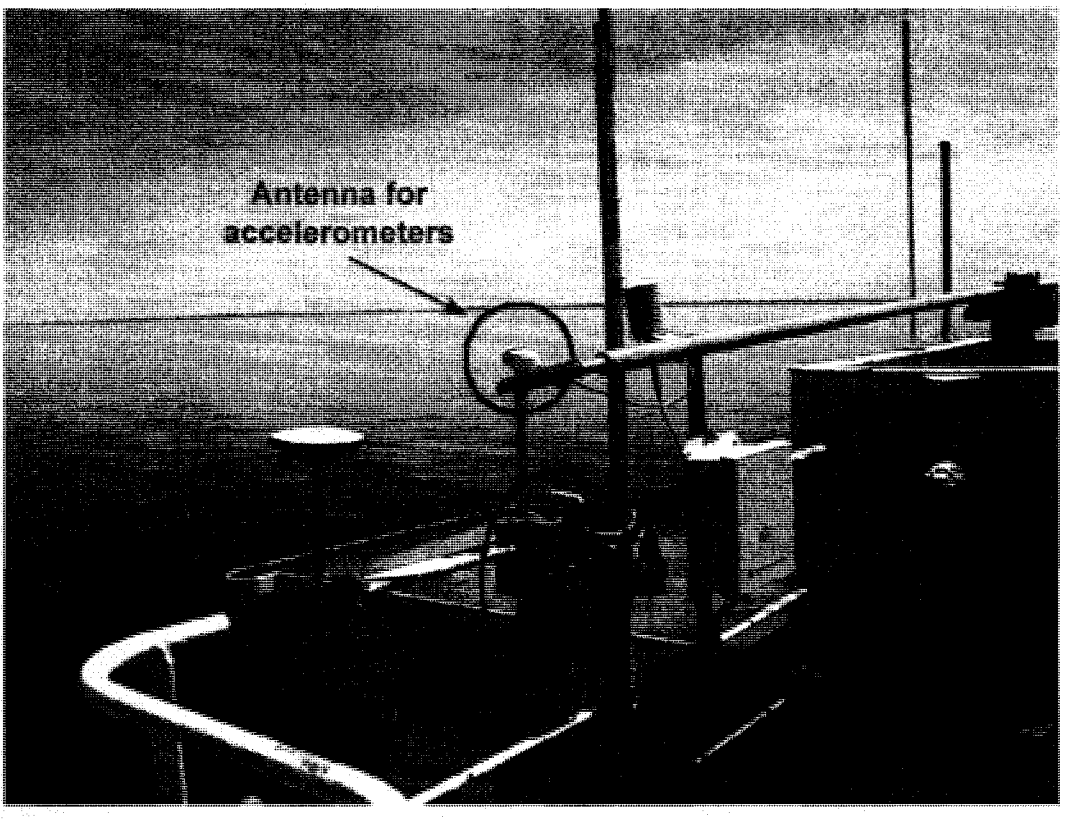

Figure 16 - Location of the accelerometers mounted on the portside of the navigation deck of the *Princess of Acadia*.

Figure 17 shows a 12 hour period of pitch data. The blue line is the pitch values and the green line is the distance the ferry was from the GPS base station CGSJ. This figure shows that while the ferry was docked there is erratic behavior in the pitch values that did not occur during the crossing at the beginning of the day on 8 June 2008.

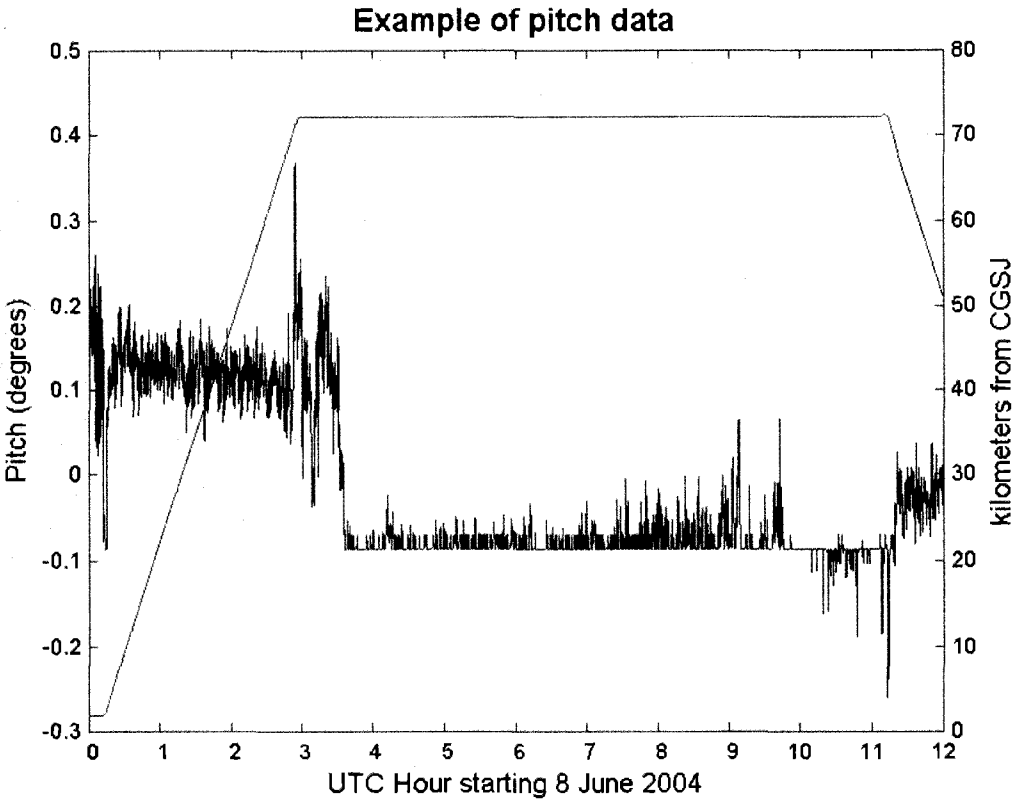

Figure 17 - This is an example of some of the pitch data that was recorded.

A five minute period of time during the crossing at the beginning of 8 June 2008 day is shown in Figure 18. This figure shows pitch periods between 40 and 63 seconds. The pitch values in Figure 17 and Figure 18 are not corrected for X, Y, and Z lever-arm offsets, because the offsets were derived from as-built drawings of the ferry and have large uncertainties. The accelerometer data was time stamped using $GPRMC NMEA strings from a GARMIN 17N. The GARMIN unit turned off intermittently creating a time synchronization problem. Because of the erratic behavior of the accelerometer data (as shown in of the Figure 17), the

uncertainty in the lever-arm offsets and the time synchronization problem the data was not used to correct for roll, pitch and heave of the vessel.

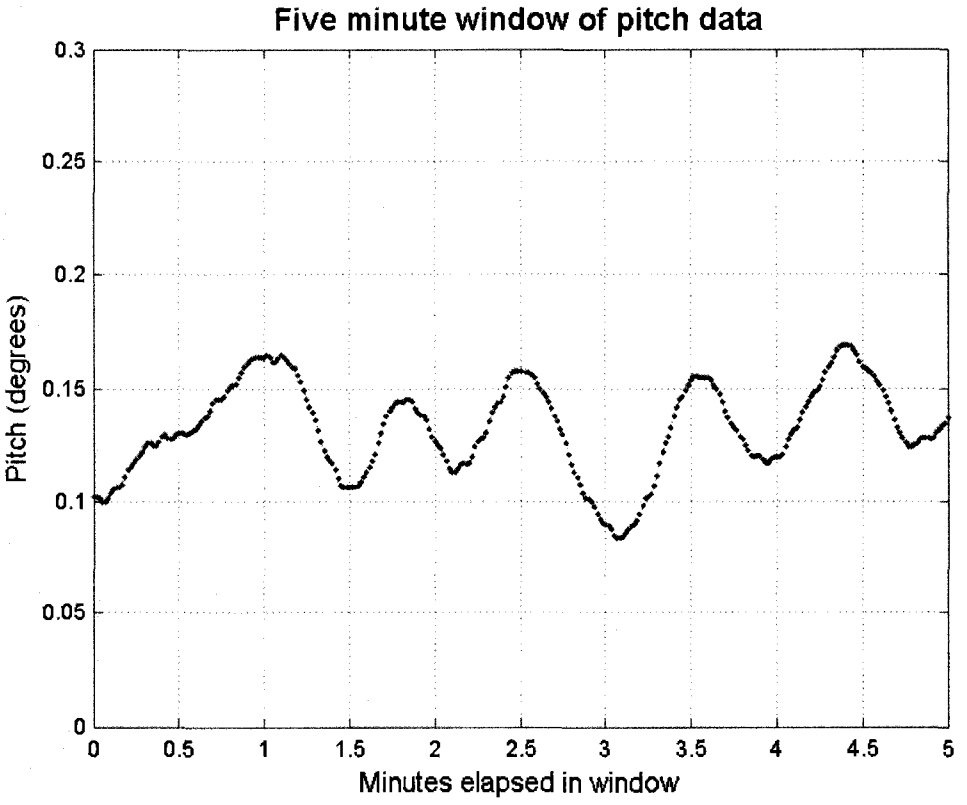

Figure 18 - Five minutes of pitch data recorded while the ferry was crossing from Saint John, NB to Digby, NS.

Conventional Tide Data

The Integrated Science Data Management (ISDM) branch of Canada's Department of Fisheries and Oceans (DFO) manages, archives and distributes data collected by the DFO. Water-level and tidal-benchmark data from any permanent or temporary gauges in the Canadian network can be downloaded from (http://www.meds-sdmm.dfo-mpo.gc.ca/meds/databases/TWL/TWL_e.htm).

Data from CHS tide stations in Saint John, NB (CHS 065) and Digby, NS (CHS 324) were used during this research. Station CHS 065 was originally established on the eastside of the Saint John River at the Pugsley Terminal in 1896. The station was moved in 1999 by the CHS to the Bay Ferry Terminal in Saint John, NB (Figure 14 and Figure 19) and is now part of the CHS Atlantic's Permanent Water-level Network (MacAulay et. al., 2008). The primary sensor at this station during the *Princess of Acadia* GPS project was a float/pulley system (Table 2). The location of the tide station and three of the tidal benchmarks are shown in Figure 19.

Table 2 - Information about the type of gauge installed at Saint John, NB and Digby, NS. The geographic coordinates were obtained using a handheld GPS.

Town	Province	Station No.	Longitude (Deg. W)	Latitude (Deg. N)	DCP	Primary	Back-up	Stilling well
Saint John	New Brunswick	065	66.060	45.255	Sutron 8210	float/pulley	strain gauge	yes
Digby	Nova Scotia	324	65.757	45.660	Sutron 8210	float/pulley	na	yes

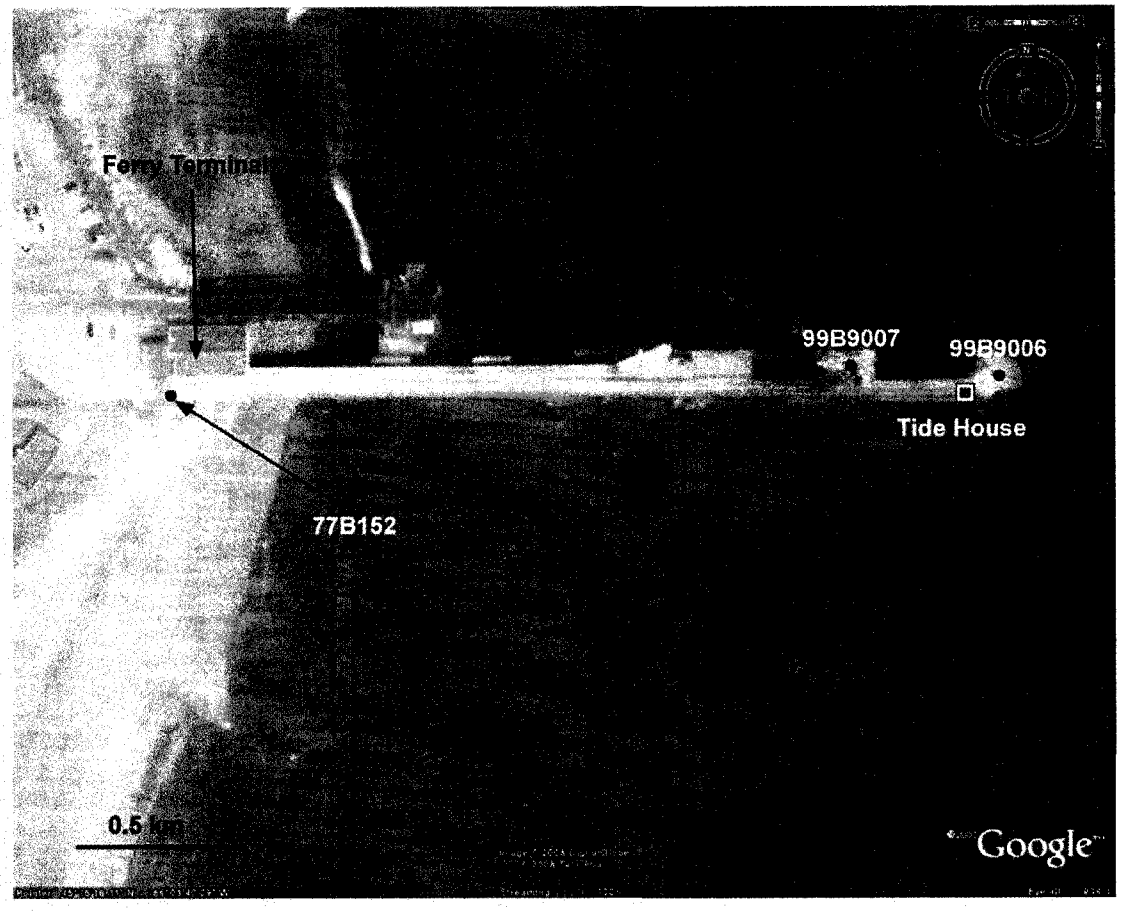

Figure 19 - Sketch of Canadian Hydrographic tide station CHS 065 and three tidal benchmarks. The tidal benchmark IDs are in white.

Tide station CHS 324 was a temporary station installed on 02 October 2003 and removed 10 December 2004 (Figure 20). The tide station consisted of one float/pulley system (Table 2) and was located at the southern end of the ferry terminal. Three tidal benchmarks were installed at station CHS 324 to verify the stability of the tide gauge and to maintain CD at the ferry terminal (Figure 21).

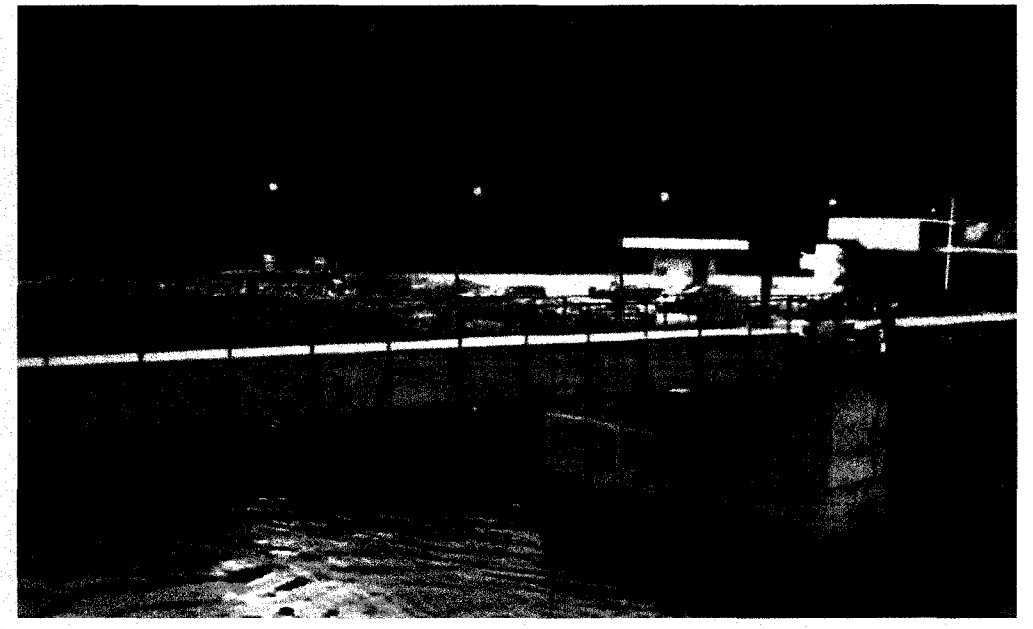

Figure 20 - Picture of the stilling well (green vertical pipe) and tide house (green box at the top of the stilling well) for the tide gauge at Digby, NS (From Santos et. al., 2004).

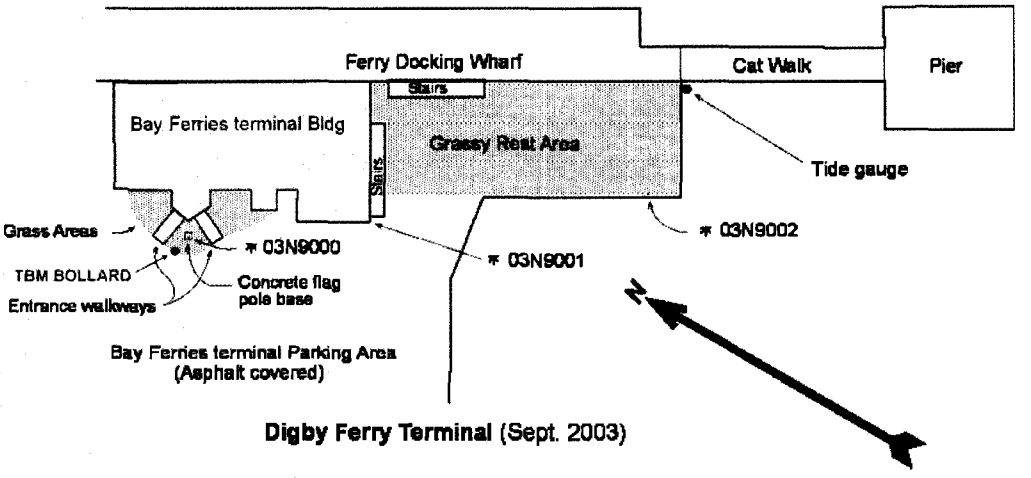

Figure 21 - Benchmark sketch for CHS tide station 324. This sketch was downloaded from the CHS tide and water-level website.

The tidal benchmarks at the CHS 065 and CHS 324 tide stations were checked for stability on 11 August 2008 and 13 August 2008, respectively. Table 3 and Table 4 show the results from the spirit levels conducted during the stability checks. For the determination of CD heights from the 2008 spirit levels at CHS 065 tidal benchmark 99B9006 is used as the control. Tidal benchmark 03N9000 is used as the control for the determination of CD heights from the spirit levels at CHS 324. The benchmark designated BOLLARD in Table 4 is a temporary benchmark (TBM) established during the 2008 leveling. This TBM was established to provide a mark that could be observed with a GPS.

Table 3 - Comparison of CD height of tidal benchmarks at tide station CHS 065 that are published by the CHS to the CD height of the same benchmarks determined from spirit levels on 11 August 2008.

Abstract of leveling for Saint John, NB (CHS 065)

Benchmarks: 99B9006, 99B9007, 77B152
Number of benchmarks: 3
PBM: 99B9006
Date: 11 Aug 2008

all values in meters

From	To	Fwd	Rev	Delta	Mean	CD Elevation CHS	CD Elevation 2008	Difference	BM Name
						10.553	10.553		99B9006
99B9006	99B9007	0.010	-0.010	0.000	0.0100	10.563	10.565	-0.002	99B9007
99B9007	77B152	0.179	-0.177	0.002	0.1780	10.741	10.741	0.000	77B152

Table 4 - Comparison of CD height of tidal benchmarks at tide station CHS 324 that are published by the CHS to the CD height of the same benchmarks determined from spirit levels on 13 August 2008.

Abstract of leveling for Digby, NS (CHS 324)

Benchmarks:	03N9000, 03N9001, 03N9002
Temporary benchmark:	BOLLARD
Number of benchmarks:	4
PBM:	03N9000
Date:	13 Aug 2008

all values in meters

From	To	Fwd	Rev	Delta	Mean	CD Elevation CHS	CD Elevation 2008	Difference	BM Name
						10.963	10.963		03N9000
03N9000	03N9001	-0.311	0.309	-0.002	-0.3100	10.653	10.653	0.000	03N9001
03N9001	03N9002	-0.315	0.317	0.002	-0.3160	10.337	10.337	0.000	03N9002
03N9000	Bollard	0.004	-0.004	0.000	0.0040		10.967		Bollard

Static GPS observations were conducted in August 2008 on one tidal benchmark at each tide station. Benchmark 99B9006 was observed at tide station CHS 065 and TBM BOLLARD was observed at tide station CHS 324. The GPS data for TBM BOLLARD were processed with the National Geodetic Survey's Online Positioning User Service (OPUS). OPUS processed the GPS data in the North American Datum of 1983 (EPOCH: 2008.6171) reference frame and the International Terrestrial Reference Frame of 2000 (EPOCH: 2008.6171). The GPS data for tidal benchmark 99B9006 were post-processed using OPUS and by the UNB with the NovAtel software GrafNav. For post-processing these data UNB used the New Brunswick Active Control Station at the Saint John Port Authority (Designation: SJPA) as the base station. The ellipsoid height obtained for the tidal benchmark at CHS 065 and the TBM at CHS 324 are listed in Table 5. In Table 5, the NAD83 CSRS coordinates for tidal benchmark 99B9006 are the coordinates provided by UNB. The ITRF2000 coordinates for the 99B9006

and BOLLARD and the NAD83 CORS96 coordinates for BOLLARD are from the OPUS solutions (see appendix 0).

Table 5 - Geographic coordinates for tidal benchmark 99B9006 and TBM BOLLARD.

Tide Station	*CHS 065*		*CHS 324*	
Designation	*99B9006*		*BOLLARD*	
Refernce Frame	NAD83 CSRS	ITRF2000	NAD83 CORS96	ITRF2000
Epoch	TBD	2008.6171	2002.0000	2008.6171
Longitude (Deg. W)	66.059804	66.059805	65.757093	65.757094
Latitude (Deg. N)	45.254629	45.254639	44.660124	44.660134
Height (m)	-15.119	-16.433	-15.292	-16.460
Height Std (m)	0.005	0.192	0.035	0.035

NovAtel DL-4 GPS Data

The instrument configuration for the *Princess of Acadia* GPS Project consisted of two GPS base stations; one on the roof of the Canadian Coast Guard building in Saint John, NB (CGSJ) and the other on the roof of the Digby Regional High School in Digby, NS (DRHS). The GPS antenna for the base station CGSJ was moved once (Wells et. al., 2004). Both of the locations at which the GPS antenna was mounted were located on the roof of the Canadian Coast Guard building. These locations are shown in Figure 22. Figure 23 shows the GPS antenna for the base station DRHS. Both GPS base stations were installed by 16 October 2003 and data collection began on 28 November 2003 (Wells et. al., 2004). The coordinates for these base stations were adjusted in ITRF2000 using permanent base stations in Fredericton, NB and Halifax, NS (Kim and Langley, 2005).

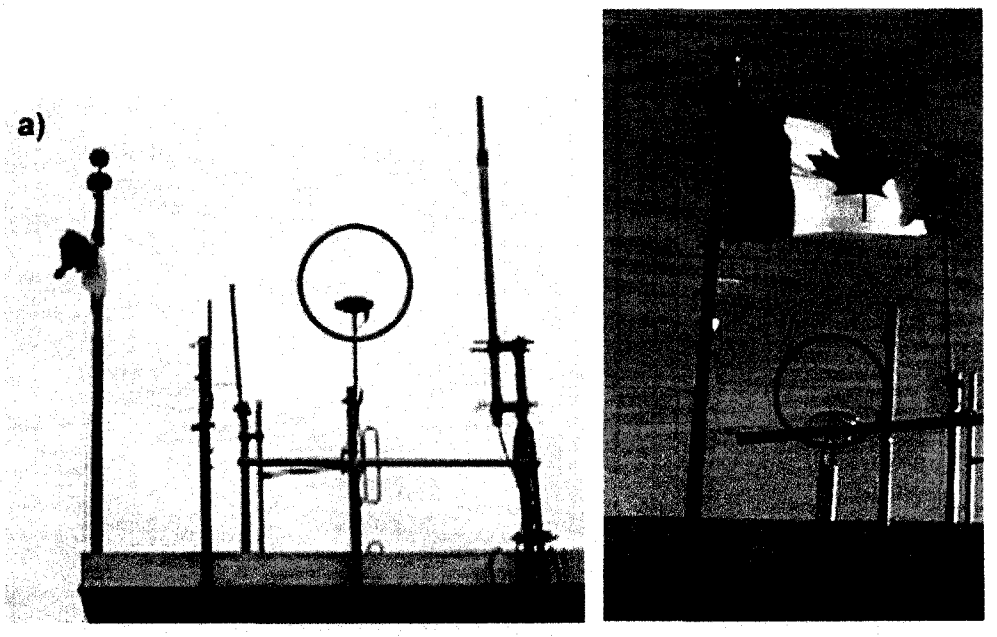

Figure 22 – a) First location of the GPS antenna for base station CGSJ mounted on the roof of the Canadian Coast Guard building in Saint John, NB. b) Second location of the GPS antenna for base station CGSJ mounted on the roof of the Canadian Coast Guard building in Saint John, NB (Modified from Wells et. al., 2004).

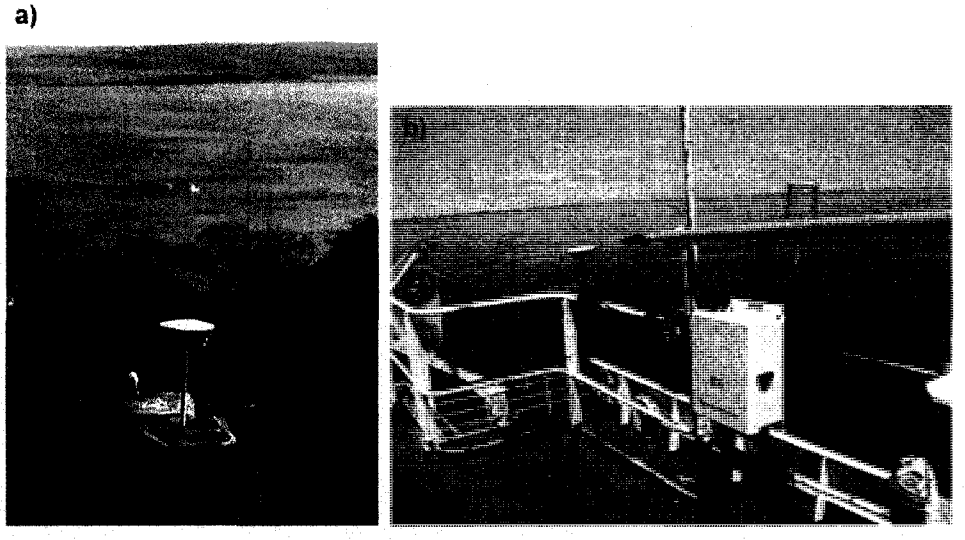

Figure 23 – a) Location of the GPS antenna for base station DRHS mounted on the roof of the Digby Regional High School in Digby, NS (From Wells et. al., 2004). b) GPS antenna and meteorological sensor mounted on the portside of the *Princess of Acadia's* navigating bridge deck.

A third receiver was installed on the *Princess of Acadia* ferry. The antenna for this receiver was installed on the portside rail of the ferry's navigation deck (Figure 23-b). The *Princess of Acadia* is a cargo ferry that transits between Saint John, NB and Digby, NS 1 to 3 times a day. The frequency of the crossings varies from season-to-season with more daily crossing during the summer months than there are in the winter months.

The three GPS receivers were NovAtel dual-frequency high-accuracy geodetic receivers that were programmed to log a position every second. The location and coordinates of the two base stations are shown in Table 6. The type of GPS receiver and antenna used at the two base stations and on the ferry are listed in Table 7.

Table 6 - Information about the location of the three GPS receivers used during the *Princess of Acadia* GPS project.

				ITRF2000 (EPOCH: November 2003)		
Designation	**Location**	**Town**	**Province**	**Longitude (Deg. W)**	**Latitude (Deg. N)**	**Antenna Height (m)**
CGSJ	Canadian Coast Guard Building	Saint John	New Brunswick	66.0630	45.2715	4.568
DRHS	Digby Regional High School	Digby	Nova Scotia	65.7597	44.6205	37.469
BOAT	Portside of the navigation deck on Princess of Acadia	-	-	-	-	-

Table 7 - Information about the type of GPS receivers and GPS antennas used during the *Princess of Acadia* GPS project.

Designation	Station Type	Manufacturer	Receiver Type/ Serial Number	Antenna Type/ Serial number
CGSJ	Base station	NovAtel	DL-4 OEM4 SNJ02210002	GPS-600 series NPM02190069
DRHS	Base station	NovAtel	DL-4 OEM4 NSJ02210035	GPS-600 series NPM02190036
BOAT	Rover	NovAtel	DL-4 OEM4 NVS03340018	GPS-702 series NVH03280042

GrafNav Processing of Raw GPS Data

The PPK heights for the GPS antenna on the ferry were post-processed in 2005 by a graduate student at the University of New Brunswick (Santos, 2005). All of the data were processed using NovAtel's GrafNav Batch version 7.01. The parameters used for the GrafNav processing are included in the Option output file. The option file for the parameters used to process the data from GPS week 1248 (7 Dec 2003 to 13 Dec 2003) is shown in the "GrafNav Option output file (*.opt)" appendix. The same parameters were used to process all of the GPS data.

UNB used an elevation cutoff angle of 5° during GrafNav post-processing of the GPS data. This low cutoff angle was used because the loss of a position during kinematic applications is more detrimental then using signals with some tropospheric contamination (Wells, 2008b).

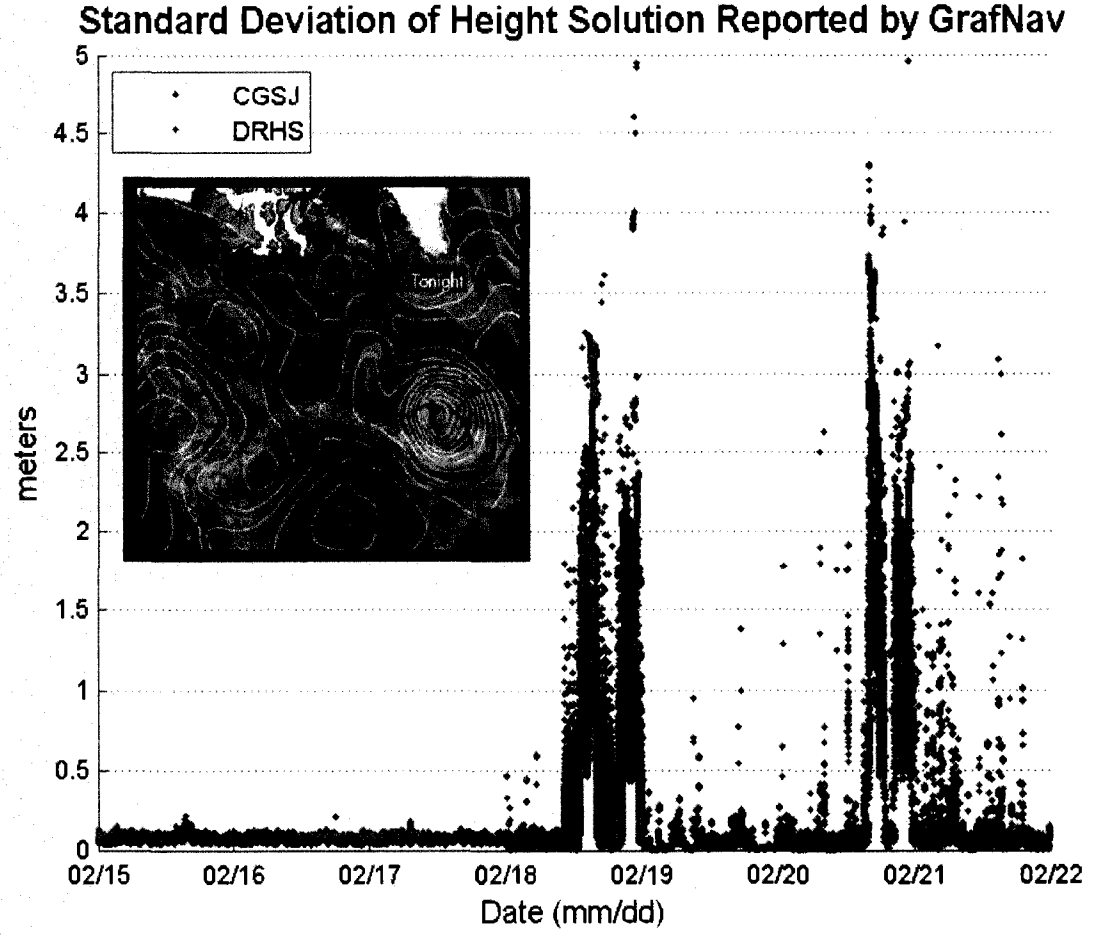

Figure 24 - Height standard deviations for CGSJ and DRHS reported by GrafNav. The inset is modified from Santos et. al. 2005.

Two sets of single-baseline PPK solutions were provided by UNB as ASCII text files. One set of solutions is the GPS data collected on the ferry post-processed with data from GPS base station CGSJ. The other set is the GPS data collected in the ferry post-processed with data from GPS base station DRHS. Table 8 shows the GrafNav parameters provided in each of the ASCII text files.

Table 8 - GrafNav parameters provided in the single-baseline solution files (Waypoint, 2004).

Parameter	Example	Definition
Station	1-S	User defined sequency number for data epochs
GPSTime (HMS)	00:00:01.00	GPS time of solution in hours, minutes, seconds and decimal seconds
Date (MDY)	12/7/2003	Date of solution in Month, Day Year format
GPSTime (sec)	1.00	GPS time of solution in second of the GPS week
Longitude (+/-D M S)	-66 03 40.04046	Longitude of solution in degrees, minutes, seconds E
Latitude (+/-D M S)	45 15 17.20028	Latitude of solution in degrees, minutes, seconds N
H-Ell (m)	-3.563	Ellipsoid height in meters
SDNorth (m)	0.054	Estimated error along the north axis in meters
SDEast (m)	0.041	Estimated error along the east axis in meters
SDHoriz (m)	0.068	Estimated position standard deviaton along the east and north axes
SDHeigh (m)	0.087	Estimated error along the vertical axis in meters
HorizDist (m)	1867.958	Horizondtal distance from the base station in meters
Vnorth (m/s)	-0.089	Velocity north in m/s
Veast (m/s)	-0.02	Velocity east in m/s
PDOP (dop)	1.51	Position Dillution of Precision
L1Rms (m)	0.011	Root mean square of the L1 carrier phase signal
GP	7	Number of satellites
Q	2	Quality factor from GrafNav; 1 (best) to 6 (worst)

Six parameters in Table 8 were used to characterize the water-level during a ferry crossing. The ellipsoid heights (H-Ell) were used to estimate the water level height. The ellipsoid heights were time stamped using the GPS time (HMS) and Date parameters. The longitude and latitude of the solutions were used when the solutions were aggregated into spatial zones. The vertical uncertainties for the ellipsoid height (SDHeigh) were used to filter out heights with uncertainties larger than 15 cm. This 15 cm threshold is larger than the uncertainty level (10 cm) of kinematic surveying (Seeber, 2003). Table 9 shows the number of single-baseline solutions, the percentage of the solutions that had

a vertical uncertainty less than 15 cm and percentage of those with a vertical uncertainty less than 10 cm.

Table 9 - Statistics for the number of single-baseline solutions used in this research.

Station	Number of solutions	Number of solutions with vertical uncertainty		Percent of solutions with vertical uncertainty	
		<=15cm	<=10cm	<=15cm	<=10cm
CGSJ	19564898	19211740	16767580	98.19%	85.70%
DRHS	20614242	19211740	16767580	93.20%	81.34%
Total	40179140	38423480	33535160	95.63%	83.46%

Combining PPK heights from CGSJ and DRHS

The distance between the GPS base stations CGSJ and DRHS was 74 km. The CGSJ base station was 1.8 km from the ferry terminal in Saint John, NB (Figure 14). The DRHS base station was 4.4 km from the ferry terminal in Digby, NS (Figure 15). While the ferry was moored to the terminals the errors in the GPS signals received by the GPS on the ferry are more strongly correlated with the GPS signals received by the nearest base station than the signals received by the base station farther away (Figure 25).

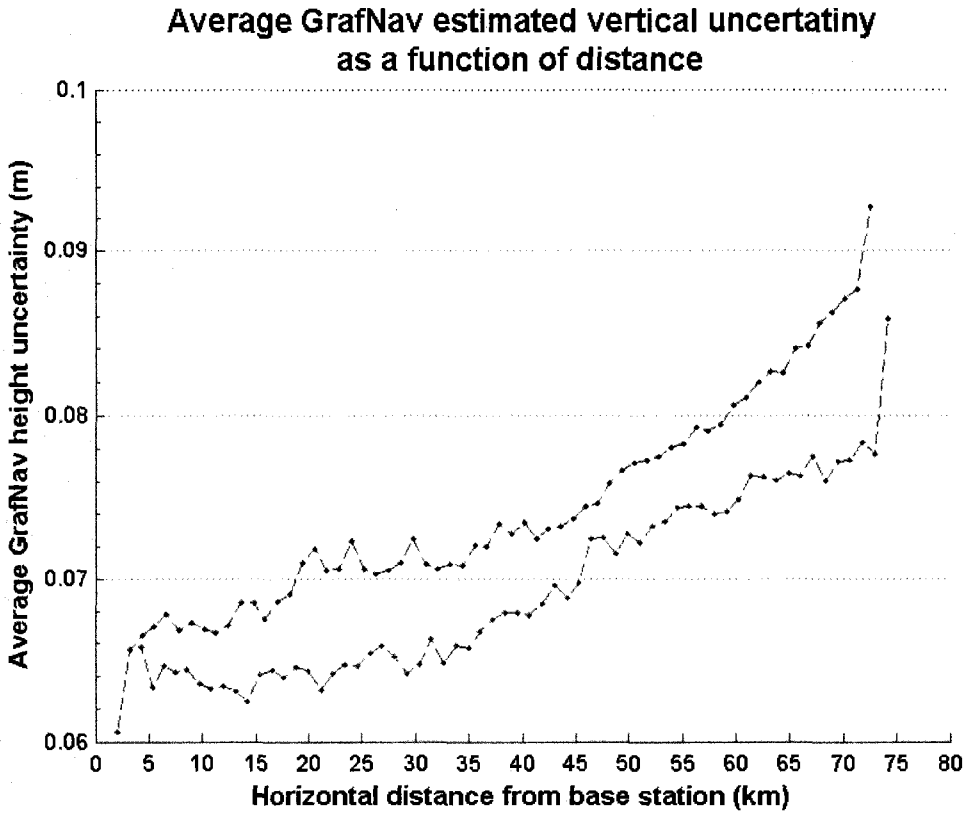

Figure 25 - Average uncertainty in PPK solutions as a function of distance from CGSJ (blue) and from DRHS (red).

Figure 25 shows the average vertical uncertainty of all the single-baseline solutions in a VTGZ as a function of distance from the GPS base-stations. The average vertical uncertainties were computed using all the solutions from 7 Dec 2003 to 25 September 2004. The average vertical uncertainties for the VTGZ at the ferry terminal in Saint John, NB were computed from more than 7200000 1-sec single-baseline solutions. The average vertical uncertainties for the VTGZ at the ferry terminal in Digby, NS were computed from more than 5020000 1-sec single-baseline solutions. For the VTGZs between the two terminals the average vertical uncertainties were computed from less than 185000 1-sec single-

baseline solutions. On average, solutions processed using data from CGSJ have a larger vertical uncertainty than solutions processed with data from DRHS. The average uncertainty for the solutions between 72 and 75 km from CGSJ or DRHS is less than 10 cm.

The two sets of single-baseline solutions were combined using the GrafNav estimated vertical uncertainties. The expressions for combining the solutions are as follows:

$$w = \frac{1}{\sigma^2} \tag{6}$$

where: w = weighting factor

σ = single-baseline GrafNav height uncertainty

and:

$$ht_{dual} = \frac{w_{CGSJ} ht_{CGSJ} + w_{DRHS} ht_{DRHS}}{w_{CGSJ} + w_{DRHS}} \tag{7}$$

where: ht_{dual} = dual-baseline solution (DBLS)

ht_{CGSJ} = CGSJ single-baseline solution

ht_{DRHS} = DRHS single-baseline solution

w_{CGSJ} = weight factor for CGSJ single-baseline solution

w_{DRHS} = weight factor for DRHS single-baseline solution

For epochs that data was available from only one GPS base station the single-baseline solutions were used to estimate the water-level height. This resulted in a combination of single- and dual-baseline solutions, which are referred to as the

h_{mix} solutions. The statistics for the number of single- and dual- baseline solutions used are shown in Table 10.

Table 10 - Statistics of the PPK solution types used to characterize the water-level height.

Solution type	Number of Solutions	Percent of total solutions
single-baseline	16259527	33%
dual-baseline	32519054	67%
total	48778581	

Example of Long-Baseline High-Uncertainty Solutions

This section uses a time period while the ferry was docked at the ferry terminal in Digby, NS to show the behavior of the single-baseline solutions, their vertical uncertainty and the resulting h_{mix} solutions. This behavior occurred several times, but is not typical. Figure 26 shows the long-baseline solutions (CGSJ), the short baseline solutions (DRHS), the water-level measurements from the conventional tide gauge in Saint John, NB (CHS 065), the water-level estimates from the conventional tide gauge in Digby, NS (CHS 324) and the distance the ferry was from the CGSJ base station (dist). The mean was removed from the single baseline solutions and the conventional water-level measurements for comparison purposes. There are two features of interest in Figure 26: the phase difference between the tide signals measured at Saint John, NB (CHS 065) and Digby, NS (CHS 324) and the discrepancy between the CGSJ and DRHS heights around the 9th hour of 16 May 2004.

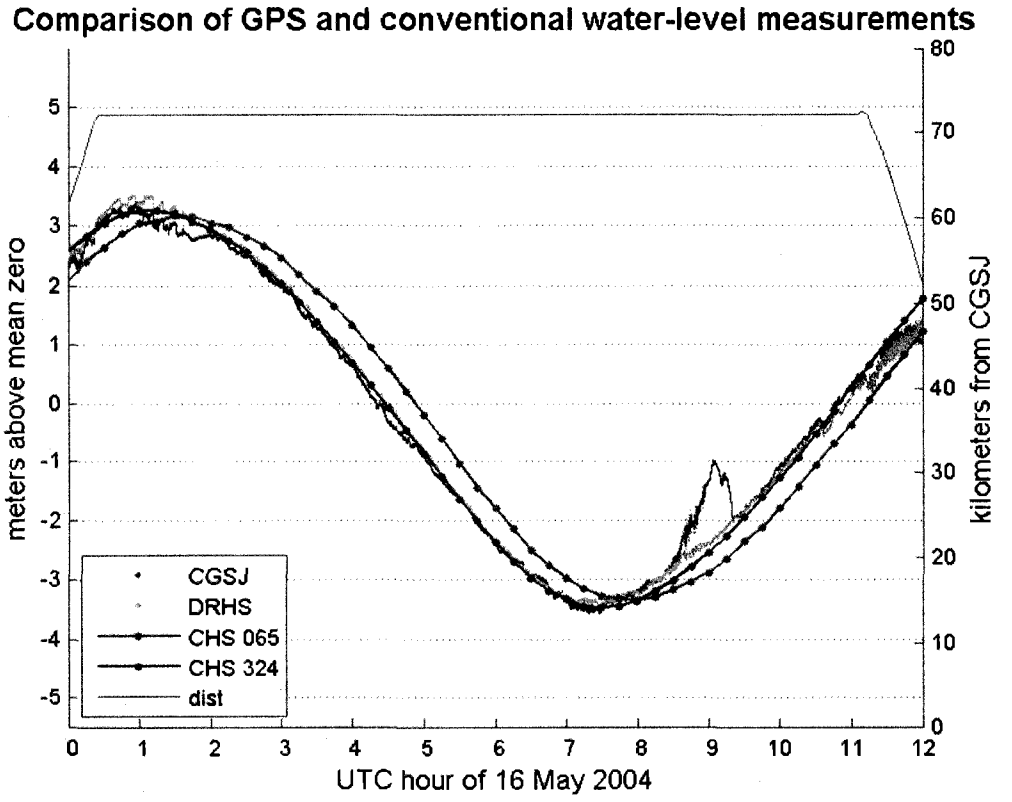

Figure 26 - PPK heights from both base stations, with conventional tide data from both tide stations and the distance the ferry was from the GPS base station CGSJ.

Figure 27 shows the long and short single-baseline solutions and the CHS 065 water-level measurements with the tide signal removed. The tide signal was removed by subtracting the CHS 324 water-level measurements. This figure shows the phase difference between the tide signal at CHS 065 and CHS 324. It also shows that between the 2nd and the 7th hours the short-baseline solutions agree better with the CHS 324 water-level measurements than the long-baseline solutions do. This is expected as a result from the average uncertainties shown in Figure 25. This figure also shows that shortly after the 8th hour the long-baseline solutions diverge from the short-baseline solutions and the CHS 324

water-level measurements. The divergence reaches a maximum of 1.42 m at 09:03 on 16 May 2004.

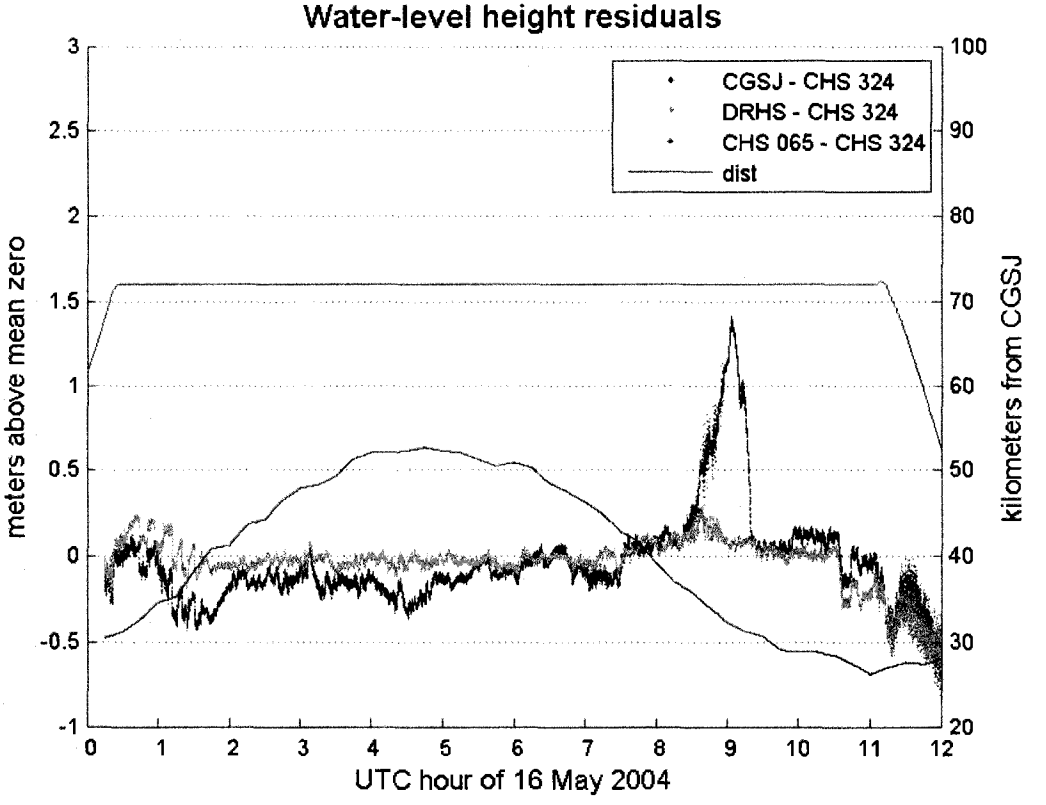

Figure 27 - The long-baseline solutions, short-baseline solutions, and the CHS 065 water-level measurements after the CHS 324 water-level measurements have been removed from each of the signals.

Figure 28 shows the GrafNav estimated vertical uncertainties for the single-baseline solutions shown in Figure 26. During this time period the vertical uncertainty was relatively high, rarely improving to less than 10 cm. The black dashed-line marks the 15 cm vertical uncertainty threshold that was used in this research. The uncertainty of the long baseline solutions exceeded the 15 cm threshold more often than the short baseline solutions. Also, there were times when both solutions exceeded the 15 cm threshold. The most obvious times that

this occurred was at the beginning of the day as the ferry was approaching the terminal and then 8.5 hours later while the ferry was moored to the dock. During the time that the long-baseline solutions diverge from the short-baseline solutions the maximum vertical uncertainty of the long baseline solutions is 30.7 cm, which is 21.6% of the difference in height between the long-baseline solutions and the CHS 324 water-level measurements. The vertical uncertainties of the short-baseline solutions increase to 29.7 cm around the 9th hour, which is larger than the difference between the short-baseline solutions and CHS 324 water-level measurements during that time. The GrafNav estimated vertical uncertainty is smaller than the differences between the long-baseline solutions and the CHS 324 water-level measurements that were observed around the 9th hour of May 2004.

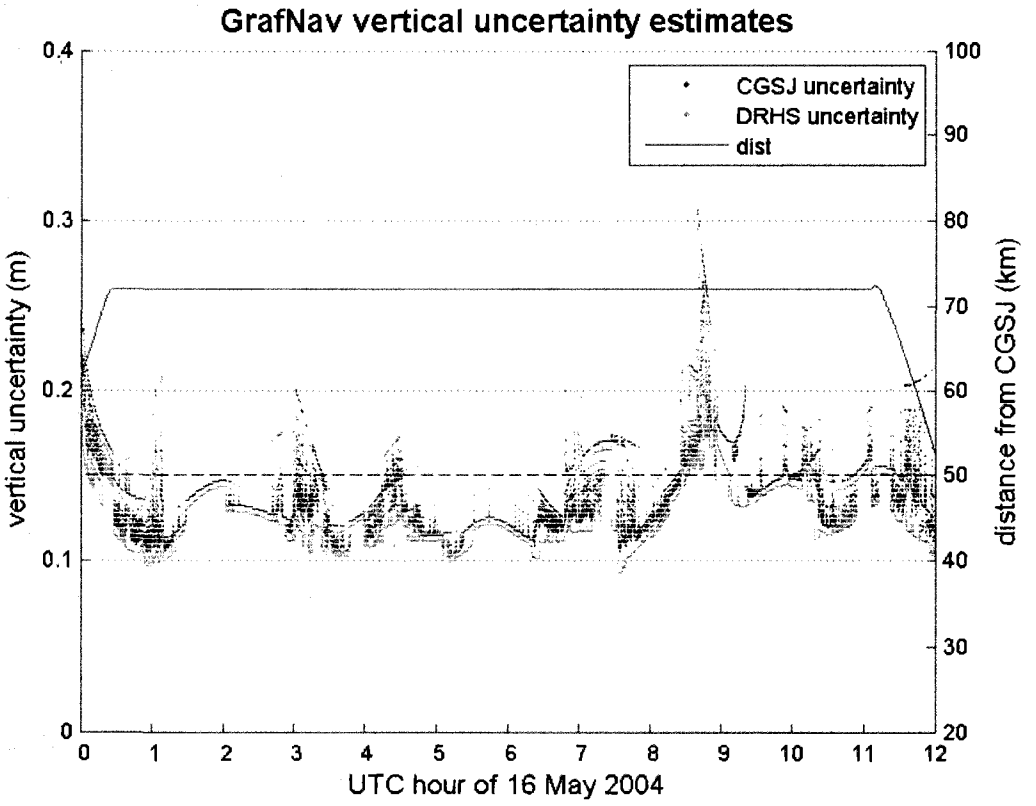

Figure 28 - The GrafNav estimated vertical uncertainty for the single-baseline solutions while the ferry was docked at the Digby, NS terminal.

Figure 29 compares the two sets of single baseline solutions to the set of h_{mix} solutions, after the tide signal was removed. The solutions between the 1st and 2nd hour that are outlined in red are an example of a time period when there are single-baseline solutions from both the CGSJ and DRHS GPS base stations. The h_{mix} solutions during this time period are dual-baseline solutions. The differences between these h_{mix} solutions and the CHS 324 water-level measurements (black dots) are larger than the differences between the short-baseline solutions and the CHS 324 water-level measurements (green dots) during this time period.

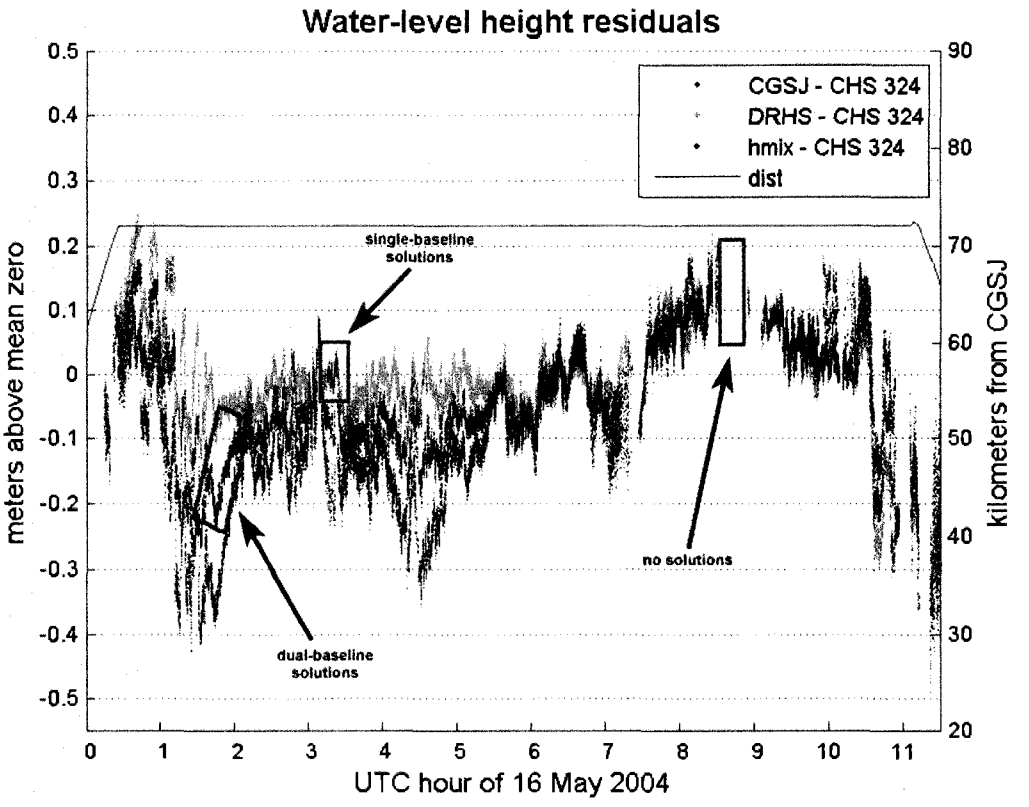

Figure 29 – Differences between the CHS 324 water level measurements, the two sets of single-baseline solutions and the h_{mix} solutions.

Some of the long-baseline solutions between the 3rd and 4th hour have vertical uncertainties that exceed the 15 cm vertical uncertainty threshold, thus the h_{mix} solutions at those epochs are single-baseline solutions. The time period outlined between the 8th and 9th hours shows a time period when the vertical uncertainties for both the long- and short- baseline solutions exceeded the 15 cm threshold thus no solutions were available for analysis during that time.

Virtual Tide Gauge Zones (VTGZ)

One of the challenges of using a ferry as a moving GPS buoy is that the ferry rarely crosses the same location twice. Thus, in order to develop a time series of water-level estimates for a harmonic analysis, h_{mix} solutions within spatial regions were aggregated together. These spatial regions are called Virtual Tide Gauge Zones (VTGZ).

The area over which the ferry traveled while it was transiting between Saint John, NB and Digby, NS was divided into 62 VTGZ. VTGZ number 1 is at Saint John, NB and VTGZ number 62 is at Digby, NS. The coordinates for these zones are in the 'Virtual Tide Gauge Zone Coordinates' appendix.. All of the 62 VTGZs had an east/west width of 5km and a north/south width of 1.2 km. These widths were based on achieving an optimal balance between the spatial density and the variability of the data.

A literature search showed that the recommended sampling period for estimating water-level heights in the US is at least 180 sec (CO-OPS, 2008). The width of the VTGZs was based on this sampling period. The maximum rate of change in the water-level height was used to estimate the uncertainty introduced by this sampling period. The frequency of the ferry's motions identified in a power spectrum of single-baseline PPK heights were used to verify that this averaging period was long enough to average out the ferry's roll, pitch and heave.

Because of the 1 Hz logging rate of the GPS receivers and the north/south route of the ferry the spatial density of the data in the north/south direction was

primarily controlled by the speed of the ferry. The speed of the ferry varies from crossing-to-crossing and from VTGZ-to-VTGZ. For example, the average speed of the ferry for all of the ferry crossings of VTGZ 15 and 35 are shown in Figure 30. In each of these histograms there are two peaks, one large peak at 7.5 m/s and another much smaller peak at 9.8 m/s. The reason for these two peaks is that under most conditions the ferry operates using two engines; however when the ferry is behind schedule and needs to travel faster the ferry operates using 4 engines. When the ferry was operating with 2 engines it took an average of 160 sec for the ferry to cross from one end of the VTGZ to the other. When the ferry was operating with 4 engines it took an average of 122 sec. Because the path of the ferry through a VTGZ also varies from crossing-to-crossing and VTGZ-to-VTGZ these 160 and 122 sec time spans are representative of direct straight-line crossings when the ferry was operating with 2 or 4 engines.

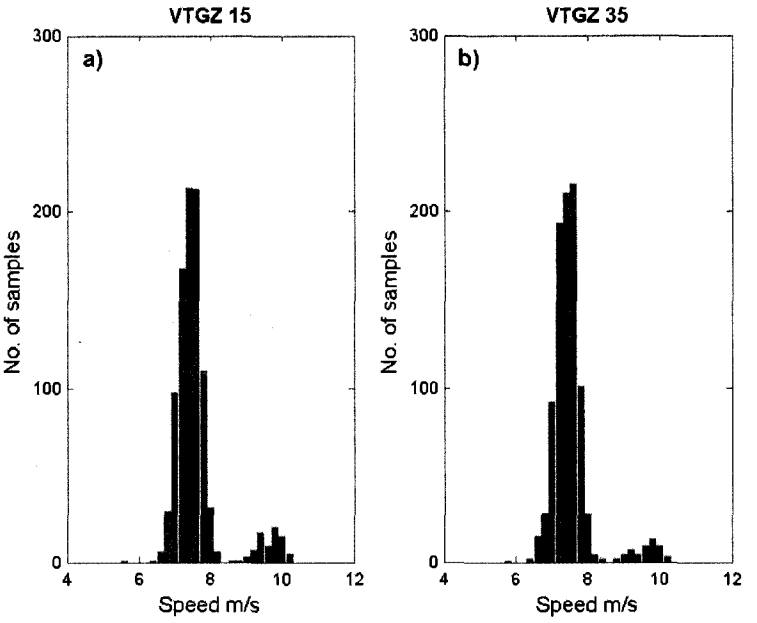

Figure 30 – Average speed of the ferry during each crossing of VTGZ 15 (a) and VTGZ 35 (b).

The spatial density of the data in the east/west direction was controlled by the weather conditions under which the ferry was capable of operating. Under good conditions the ferry takes the most direct path between the terminals at Saint John, NB and Digby, NS. However, when the sea-state increases and a large swell propagates out of the Atlantic Ocean and up the Bay of Fundy the ferry deviates from a direct path between the terminals and travels so its path has more of a perpendicular orientation to the swell (Figure 31). This is done to minimize the roll of the vessel, which provides a safer more enjoyable ride for the passengers, crew and cargo.

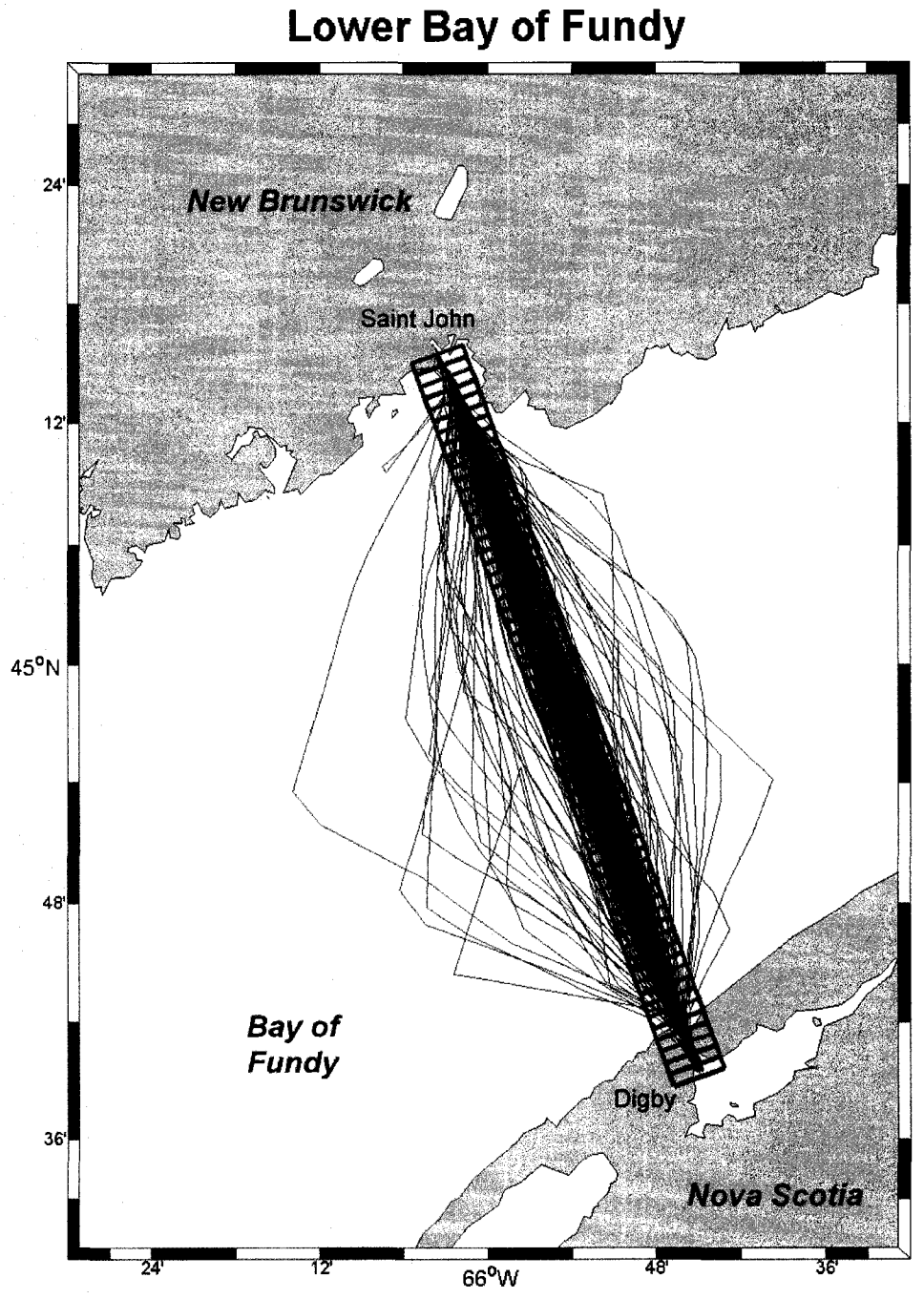

Figure 31 - All of the ferry crossings during the project are in blue. The individual tide regions are in red. Data outside the tide regions were not used in the analysis to estimate the height of the water-level.

The 5 km east/west width was used because it encompassed the spatial area along the ferry's route with the highest density of crossings. A larger width would have encompassed more ferry crossings, which are valuable from a time-series analysis point of view because the ferry's crossing schedule provides a sparse record of the tide in each of the VTGZ. However, the width needs to be limited to allow the assumption that the water-surface in a VTGZ moves up and down as a horizontal surface without a slope.

Figure 32 is a co-amplitude map of the Bay of Fundy. The tidal amplitude along a line crossing the bay is the same. For example Saint John, NB and Digby, NS are at the ends of a co-amplitude line. Thus, the amplitude of the tide between Saint John, NB and Digby, NS is 3 m. This co-amplitude map shows that the amplitude of the tide progressively increases from 2.1 m near the mouth to more than 5 m at the upper regions of the bay.

Figure 32 also shows the rate of change for the tidal height at Saint John, NB, Digby, NS and Herring Cove, NB. The rate of change for Saint John, NB was computed from CHS 065 water-level measurements from 1 October 2003 to 31 Dec 2004. The rate of change for Digby, NS was computed from CHS 324 water-level measurements from 2 October 2003 to 10 December 2004. The rate of change for Herring Cove, NB was computed from CHS 140 water-level measurements from 24 August 1960 to 22 September 1960. The sample interval for the water-level measurements at CHS 065 and for CHS 324 is 15 minutes. The sample interval for the water-level measurements at CHS 140 is 1 hour.

Based on the co-amplitude map and the maximum rates of change for the three tide stations it is apparent that there is spatial variability of the tidal characteristics in the bay. Thus, the larger a VTGZ is the more variability there will be within a zone. Assuming a maximum 3.5 cm/min rate of change along the co-amplitude line between Saint John, NB and Digby, NS, during a crossing of a VTGZ that takes 160 sec the water-level within the VTGZ will have changed 10 cm.

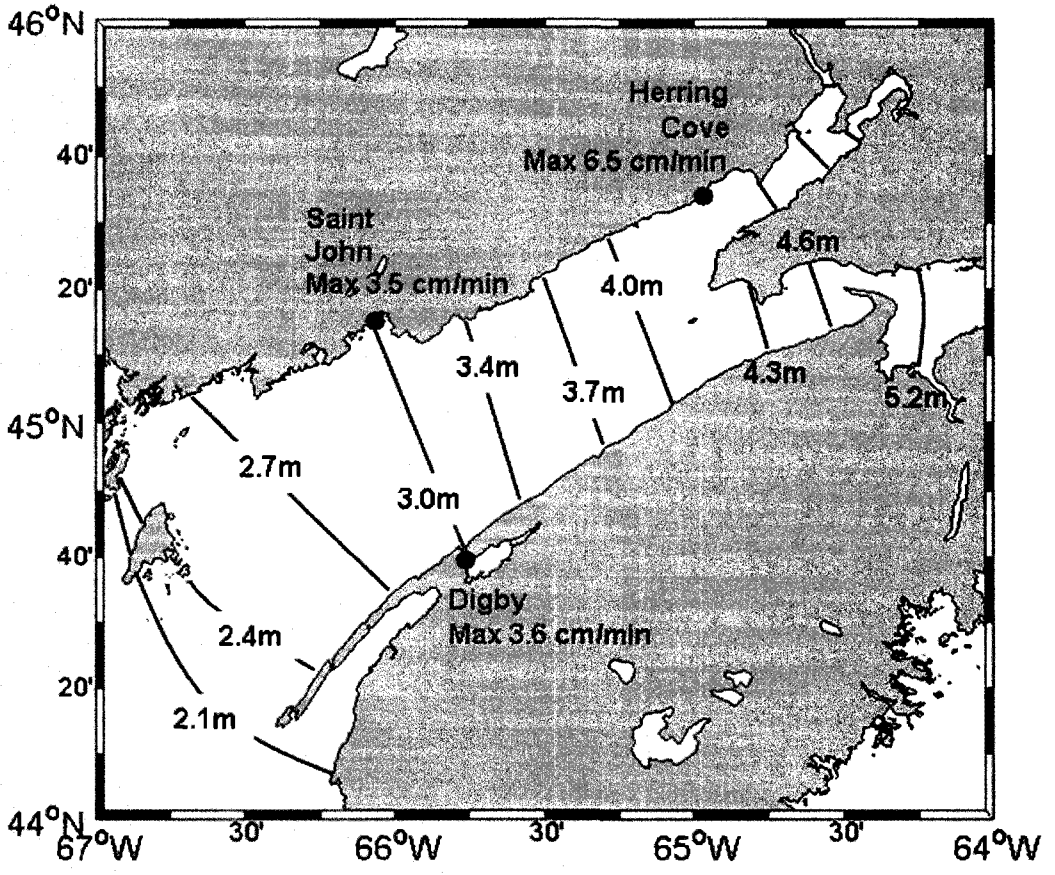

Figure 32 - Map of the co-tidal lines in the Bay of Fundy (Modified from Forrester, 1983)

If the size of the VTGZ is too small, then the estimated height of the water surface in that VTGZ could potentially be biased by the high-frequency motion of the ferry. Figure 33 is a power spectrum of the single-baseline PPK heights from 14 December 2003 to 17 December 2003. This figure shows a clear increase in signal power over the frequency range between 0.05 Hz and 0.25 Hz.

Figure 34 shows the single-baseline PPK heights (blue) during a crossing on 14 December 2003. These single-baseline heights were post-processed using the CGSJ base station. The distance of the ferry from base station CGSJ is shown in green. The red and black boxes outline the 1-minute time spans of single-baseline PPK heights that are shown in Figure 35. These 1-minute windows are snapshots of the PPK height behavior during a crossing of the bay (Figure 35-a) and while the ferry was docked (Figure 35-b). The period of the peak-to-peak cycles shown in Figure 35-a varies from 5 sec to 10 sec. The peak-to-trough range of these cycles varies from 39 to 11 cm. The behavior of the PPK heights shown in Figure 35-b do not display the same cyclical pattern that appears in the heights as the ferry is crossing the bay. The period of the peak-to-peak cycles shown in Figure 35-a verify that the frequencies identified in the power spectrum (Figure 33) are a result of motions induced by the roll, pitch and heave of the vessel as it crosses the bay. Because the average amount of time it takes the ferry to cross through the middle of the 1.25 km wide VTGZ is longer than the longer period motions of the ferry identified in the power spectrum, averaging the PPK heights during the crossings of the VTGZ will

reduce the noise from the high-frequency motions of the vessel without biasing the averages.

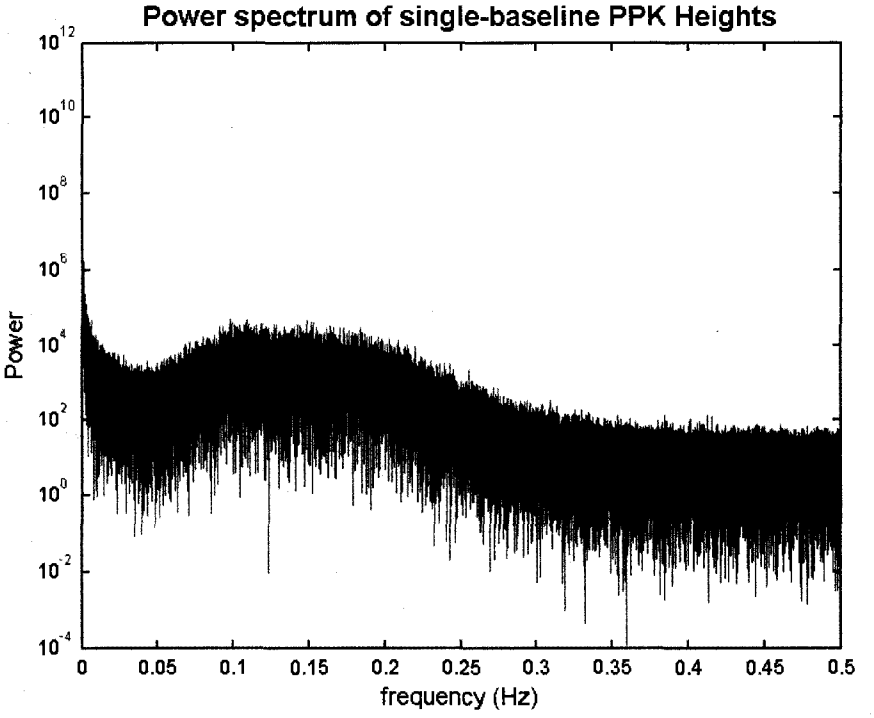

Figure 33 - Power spectrum of single-baseline PPK height observed along the ferry's route from 14 December 2003 to 17 December 2003. Note the significant power increase from 0.05 to 0.25 Hz.

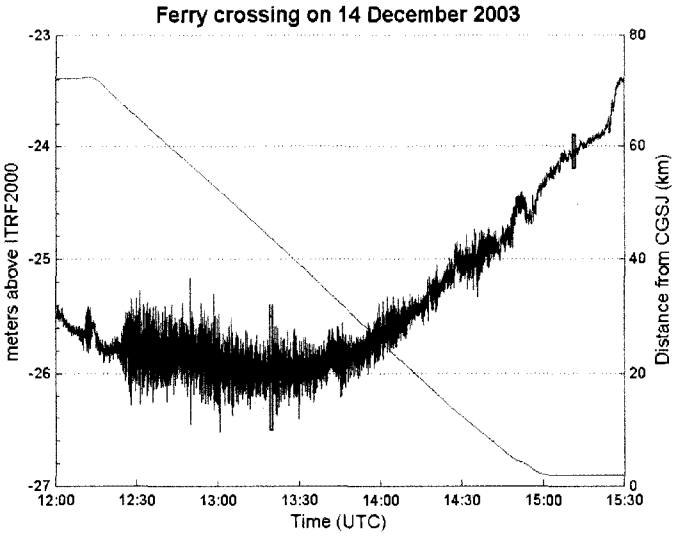

Figure 34 - Single-baseline PPK heights during a ferry crossing from Digby, NS to Saint John, NB on 14 December 2003 (blue). The distance the ferry was from the GPS base station CGSJ is shown in green.

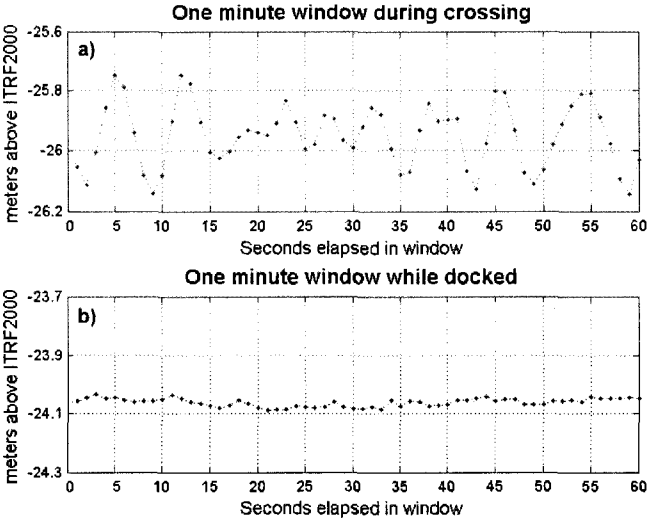

Figure 35 – a) A one-minute snapshot of the single-baseline PPK heights (from CGSJ) during a crossing on 14 December of 2003. b) A one-minute snapshot of the single-baseline PPK heights (from CGSJ) while the ferry was docked at the terminal at Saint John, NB on 14 December 2003.

Water-Level Height Estimates and their Uncertainty

The water surface in each VTGZ during each crossing is characterized by a height and height uncertainty estimate. These parameters are computed using the h_{mix} solutions. These solutions are evaluated on a VTGZ-by-VTGZ and crossing-by-crossing basis. Each VTGZ has a reference location which is its center point (see last appendix). This reference point does not change from crossing-to-crossing. For each crossing a time tag is attached to the water-level and uncertainty estimates from equations (8) and (9), which is the time at which the ferry crossed the center of the VTGZ. The height of the water surface in a VTGZ during a crossing is the average of the h_{mix} solutions during that crossing of that VTGZ:

$$h_{wl}^{vtgz} = \frac{1}{nmix} \sum_{i=1}^{nmix} h_{mix}^{i} \qquad \textbf{(8)}$$

where: h_{wl} = water-level height estimate

$vtgz$ = 1, 2, ..., 62 and represents which VTGZ is being characterized

$nmix$ = number of mixed solutions in the VTGZ being characterized during the crossing

i = 1, 2, ..., $nmix$

The uncertainty in the water-level height is estimated by the sum of the squares of the residuals between the h_{mix} solutions and the average computed from them:

$$\sigma^{2}_{wl^{vtgz}} = \frac{1}{nmix-1}\sum_{i=1}^{nmix}\left(h^{i}_{mix} - h^{vtgz}_{wl}\right)^{2} \quad (9)$$

where: $\sigma^{2}_{h_{wl}}$ = uncertainty of h_{wl}

Equations (8) and (9) result in a vector of water-level height estimates ($\vec{h}_{wl}$) and a vector of water-level height uncertainly estimates ($\vec{\sigma}^{2}_{h_{wl}}$) for each of the 62 VTGZs.

Harmonic Analysis of Weighted Least-Squares (HAMWLS)

The vector of water-level height estimates for each VTGZ was independently fit to the tide model:

$$\hat{h}_i = h_0 + \sum_{j=1}^{nk} A_j \cos(2\pi f_j t_i) + B_j \sin(2\pi f_j t_i) \quad (1)$$

using a weighted least-squares solution. The normal equations for the water-level estimates in each VTGZ are

$$\left(A^{t}_{\vec{h}_{wl}} Q^{-1}_{\vec{h}_{wl}} A_{\vec{h}_{wl}}\right)\vec{x} = \left(A^{t}_{\vec{h}_{wl}} Q^{-1}_{\vec{h}_{wl}}\right)\vec{h}_{wl} \quad (10)$$

where $A_{\vec{h}_{wl}}$ is the design matrix containing the partial derivatives of equation (1) evaluated at the time of each water-level estimate. The covariance matrix for the water-level estimates (Q_{wl}) is

$$Q_{\vec{h}_{wl}} = \begin{bmatrix} \sigma^{2}_{\vec{h}_{wl_1}} & 0 & \cdots & 0 \\ 0 & \sigma^{2}_{\vec{h}_{wl_2}} & \cdots & 0 \\ \vdots & \vdots & \ddots & \vdots \\ 0 & 0 & \cdots & \sigma^{2}_{\vec{h}_{wl_{nc}}} \end{bmatrix} \quad (11)$$

where $\sigma^2_{\bar{h}_{wl_i}}$ is the uncertainty of water-level estimate (h_{wl_i}) computed for crossings *i* through *nc*. For VTGZ 1 and 62 nc is 2250 and 1547, respectively. For VTGZs 2 though 61 nc ranged from 983 to 905 (see the 'MLLW and MSL for Virtual Tide Gauge Zones' appendix).

The vector of coefficients for the tide model is:

$$\bar{x} = \begin{bmatrix} h_0 \\ A_1 \\ \vdots \\ A_{nk} \\ B_1 \\ \vdots \\ B_{nk} \end{bmatrix}. \quad \textbf{(12)}$$

where *nk* is the number of tidal frequencies used to model the water-level estimates. The amplitude and phase of tidal constituent *j* are computed from the vector of coefficients using equations (2) and (3):

$$R_j = \sqrt{A_j^2 + B_j^2} \quad \textbf{(2)}$$

$$\phi_j = \tan\left(\frac{B_j}{A_j}\right)^{-1} \quad \textbf{(3)}$$

The variance of coefficient *j* is

$$\sigma^2_{\bar{x}_j} = Q_{\bar{x}_{jj}} \quad \textbf{(13)}$$

where $Q_{\bar{x}}$ is the covariance matrix of the coefficients and *j* = 1, 2, ..., 1 + *nk*. Covariance matrix $Q_{\bar{x}}$ is computed by combining $A_{h_{wl}}$ and $Q_{h_{wl}}$

$$Q_{\bar{x}} = \left(A_{\bar{h}_{wl}}^{t} Q_{\bar{h}_{wl}}^{-1} A_{\bar{h}_{wl}} \right)^{-1} \quad \textbf{(14)}$$

The coefficients unique to each VTGZ were used to predict hourly water-levels ($\hat{h}_{wl}$) spanning the period from 1 January 2004 to 31 August 2004 in each VTGZ

$$\hat{h}_{wl} = A_{\hat{h}_{wl}} \bar{x}. \quad \textbf{(15)}$$

The design matrix $A_{\hat{h}_{wl}}$ in equation (15) contains the partial derivatives of equation (1) evaluated at the prediction epochs. The variances for $\bar{x}$ are propagated through the model as follows

$$Q_{\hat{h}_{wl}} = A_{\hat{h}_{wl}} Q_{\hat{x}} A_{\hat{h}_{wl}}^{t}. \quad \textbf{(16)}$$

The variance of the water-level predicted at time *i* is

$$\sigma_{\hat{h}_{wl_i}}^{2} = Q_{\hat{h}_{wl_{ii}}}. \quad \textbf{(17)}$$

The vector of predictions ($\hat{h}_{wl}$) and their variances ($\vec{\sigma}_{\hat{h}_{wl}}^{2}$) are revisited during the discussion of tidal datum computations.

Tidal Harmonic Constituents used to Model each VTGZ

The primary parameters for computing tidal datums are high and low water-levels. Because of the non-uniform sampling by the ferry and the large sampling intervals, few high and low water-levels were sampled. Therefore, the high and low water-levels had to be predicted.

Two sets of tidal constituents were used to independently model the water-level estimates in each VTGZ. One set consists of a combination of the tidal constituents in the CHS models for tide stations 065 and 324. The other set

of constituents consisted of the same constituents that are used by the DFO tidal prediction software WebTide (Wert, 2006). These two sets of constituents were used because one set provides a comparison with the WebTide predictions for VTGZs in the middle of the bay and the other set is used under the assumption that the amplitudes of constituents, which did not contribute to the tide signal, would approach zero in the least-squares solution. The constituents in each set are shown in Table 11 and Table 12. The remainder of this thesis will refer to computations and analysis using the 61 constituents listed in Table 11 as freq-61 and to computations and analysis using the 5 constituents listed in Table 12 as freq-5.

Table 11 – Water-level height estimates were modeled using the 61 constituents shown. The constituents are ordered by decreasing amplitude at Saint John, NB (CHS 065).

all amplitudes are in meters

Name	Amplitue	Name	Amplitue	Name	Amplitue	Name	Amplitue
M2	3.0577	MF	0.0175	OO1	0.0067	SO3	0.0022
N2	0.6549	Q1	0.0173	CHI1	0.0061	MSK6	0.0019
S2	0.4799	MSN2	0.0167	M3	0.0059	2MK5	0.0018
L2	0.1935	EPS2	0.0163	2MK6	0.0054	2SM6	0.0017
K1	0.1577	SSA	0.0158	TAU1	0.0049	SN4	0.0014
NU2	0.1505	2MS6	0.0157	ETA2	0.0048	SK4	0.0012
K2	0.1373	MN4	0.0152	MK3	0.0048	SK3	0.0011
O1	0.1198	OQ2	0.0144	THE1	0.0042	3MK7	0.0011
2N2	0.0792	MSM	0.0122	ALP1	0.0040	M8	0.0010
LDA2	0.0609	MO3	0.0117	PHI1	0.0040	RHO1	0.0005
M4	0.0399	NO1	0.0110	SIG1	0.0035	S4	0.0003
M6	0.0384	MSF	0.0099	BET1	0.0035	SO1	0.0002
2MN6	0.0228	MU2	0.0094	2Q1	0.0034	2SK5	0.0002
MM	0.0210	MS4	0.0088	MK4	0.0028	OP2	0.0000
MKS2	0.0200	J1	0.0080	UPS1	0.0027	2MS2	0.0000
						MSN6	0.0000

Table 12 –WebTide uses the five tidal constituents shown for tidal predictions in the Bay of Fundy region. These five constituents were also used to model the water-level estimates in each VTGZ for validation purposes. The amplitude for the constituents are from the Saint John, NB and Digby, NS tide models.

	Amplitude (m)	
Name	Saint John	Digby
M2	3.058	3.146
N2	0.655	0.622
S2	0.480	0.505
K1	0.158	0.149
O1	0.120	0.115

Computation of Tidal Datums and Their Uncertainties

For computing tidal datums in each VTGZ the coefficients for the prediction that were unique to it are used to predict water-levels from January 2004 to August 2004. Monthly means were then computed from the predicted high and low water-levels. The monthly means are then reduced and corrected to the 1983 to 2001 NTDE using the methods described in NOAA Special Publication NOS CO-OPS 2 (CO-OPS, 2003). The specific reduction and correction methods used from NOAA Special Publication NOS CO-OPS 2 (CO-OPS, 2003) are the Comparison of Monthly Means (CMM) and the Modified Range Ratio methods. NOAA station 8410140 in Eastport, ME was used as the control station in the simultaneous comparisons. The following sections will describe the tabulation of Monthly Means using the CMM method and the

reduction of MSL and MLLW to the 1983 to 2001 NTDE. Each section will also include a discussion of how the variances ($\sigma^2_{\hat{h}_{wl}}$) of the predictions ($\hat{h}_{wl}$) in each region were propagated through the datum computations. All of the calculations used to determine the variance of a tidal datum were based on the "General Formula for Error Propagation" as described by John R. Taylor (1997).

Tabulation of Monthly Means

Tidal-datum computations start with the tabulation of monthly means. Monthly means are surfaces defined by the range of the tide. The tides in the Bay of Fundy region are semi-diurnal, which requires each of the high and low water-levels in a day to be designated as the higher or lower water-level. For example a month with 30 days typically has 60 high and low water-levels, 2 high and 2 low water-levels a day. These high (low) water-levels are paired starting with the first set of high (low) water-levels in the month to give 30 pairs of high (low) water-levels. Then each individual high water-level in a pair of high water-levels is designated as higher high-water (*hhw*) or lower high-water (*lhw*). Similarly, the individual low water-level in a pair of low water-levels are designated as higher low-water (*hlw*) and lower low-water (*llw*). These designations then result in 4 categories of tide with each category containing 30 tide values (high or low water-levels). The tides in each category are reduced to mean *hhw* (*mhhw*), mean *lhw* (*mlhw*), mean *hlw* (*mhlw*) and mean *llw* (*mllw*). The form of the reduction for the tides in each category is the same as the example given for *mhhw*

$$mhhw = \frac{1}{nw}\sum_{i=1}^{nw} hhw(i) \tag{18}$$

where *nw* is the number of *hhw* in the month, which in the case of a 30 day month *nw* would typically equal 30. The variance of *mhhw* (σ^2_{mhhw}) is

$$\sigma^2_{mhhw} = \frac{1}{nw}\sum_{i=1}^{nw} \sigma^2_{hhw}(i). \tag{19}$$

where σ^2_{hhw} is the variance of predicted *hhw*. This variance is based on the propagation of the uncertainty of the water-level estimate through the HAMWLS and is obtained directly from equation (17) as are those for all the predicted high and low water-levels used to compute the monthly means. The monthly means described above are then used to tabulate monthly means for the diurnal tide level (*dtl*), the great diurnal range (*gt*), mean high-water (*mhw*), mean low-water (*mlw*), and the mean range (*mn*). The *dtl* is the average of *mhhw* and *mllw*

$$dtl = \frac{mhhw + mllw}{2} \tag{20}$$

and its variance is

$$\sigma^2_{dtl} = \frac{1}{4}\left(\sigma^2_{mhhw} + \sigma^2_{mllw}\right). \tag{21}$$

where σ^2_{mhhw} is the variance of *mhhw* and σ^2_{mllw} is the variance of *mllw*. The *gt* is the difference between *mhhw* and *mllw*

$$gt = mhhw - mllw \tag{22}$$

and its variance is

$$\sigma^2_{gt} = \sigma^2_{mhhw} + \sigma^2_{mllw}. \tag{23}$$

Mean high-water (*mhw*) is the difference between *mhhw* and *mlhw*

$$mhw = mhhw - mlhw . \tag{24}$$

The variance of *mhw* (σ^2_{mhw}) is

$$\sigma^2_{mhw} = \sigma^2_{mhhw} + \sigma^2_{mlhw} . \tag{25}$$

where σ^2_{mlhw} is the variance for *mlhw*. Similarly, mean low-water (*mlw*) is the difference between the two low-water monthly means *mhlw* and *mllw*

$$mlw = mhlw - mllw \tag{26}$$

The variance of *mlw* is

$$\sigma^2_{mlw} = \sigma^2_{mhlw} + \sigma^2_{mllw} . \tag{27}$$

where σ^2_{mhlw} is the variance for *mhlw*.

The computation of Monthly mean sea level (*msl*) has a different form than the computation for the four high and low water monthly means. Instead of averaging individual high or low water-levels, msl_k is the average of all the hourly water-level heights in month *k*

$$msl_k = \frac{1}{n}\sum_{i=1}^{n} \hat{b}_k(i) \tag{28}$$

where *n* is the number of hourly heights in month *k* and $\hat{b}_k$ is a vector of all the hourly predictions for the k^{th} month. The variance of *msl* (σ^2_{msl}) is computed from the vector of variances for the predictions ($\sigma^2_{\hat{b}_k}$) in the k^{th} month

$$\sigma^2_{msl} = \frac{1}{n}\sum_{i=1}^{n} \sigma^2_{\hat{b}_k}(i) \tag{29}$$

Reduction of MLLW Monthly Means to the NTDE Equivalent

The monthly means for *dtl* are corrected to the current NTDE by adding the average difference between the monthly means for the VTGZ (DTL^A_{mm}) and Eastport, ME (DTL^B_{mm}) to the accepted DTL datum at Eastport, ME (DTL^B_{ntde})

$$DTL^A_{ntde} = DTL^B_{ntde} + \frac{1}{m}\sum_{k=1}^{m}\left(dtl^A(k) - dtl^B(k)\right) \tag{30}$$

where dtl^A and dtl^B are the VTGZ and Eastport, ME monthly means, respectively. $k = 1,2,\ldots,m$ where m is the number of monthly means being evaluated. The calculation for reducing the monthly means for *gt* and correcting to the current NTDE is

$$Gt^A_{ntde} = Gt^B_{ntde} \times \frac{1}{m}\sum_{k=1}^{m}\left(\frac{gt^A(k)}{gt^B(k)}\right) \tag{31}$$

where gt^A is the monthly mean for the tide region, gt^B is the monthly mean for Eastport, ME and Gt^B_{ntde} is the accepted value of *Gt* for Eastport, ME during the 1983 to 2001 NTDE.

The variance of DTL^A_{ntde} and Gt^A_{ntde} are computed based on the law of the propagation of variances (Taylor, 1997). These calculations start with the development of the vector of partial derivatives for the stochastic variables used to compute DTL^A_{ntde}

$$\Phi_{DTL} = \left[\frac{\partial DTL^A_{ntde}}{\partial DTL^B_{ntde}} \quad \frac{\partial DTL^A_{ntde}}{\partial dtl^A} \quad \frac{\partial DTL^A_{ntde}}{\partial dtl^B}\right] \tag{32}$$

and Gt^A_{ntde}

$$\Phi_{Gt} = \left[\frac{\partial Gt^{A}_{ntde}}{\partial Gt^{B}_{ntde}} \quad \frac{\partial Gt^{A}_{ntde}}{\partial gt^{A}} \quad \frac{\partial Gt^{A}_{ntde}}{\partial gt^{B}} \right] \tag{33}$$

The DTL^{B}_{ntde} and Gt^{B}_{ntde} values used in the calculations for DTL^{A}_{ntde} and Gt^{A}_{ntde} are published NOAA values that were computed from 19 yrs of data collected at Eastport, ME. The 19 yrs of data spans the 1983 to 2001 NTDE. Because all of the tidal datums computed in this research were corrected to the 1983 to 2001 NTDE DTL^{B}_{ntde} and Gt^{B}_{ntde} are not considered stochastic variables. Therefore, the vectors Φ_{DTL} and Φ_{Gt} simplify to

$$\Phi_{DTL} = \left[\frac{\partial DTL^{A}_{ntde}}{\partial dtl^{A}} \quad \frac{\partial DTL^{A}_{ntde}}{\partial dtl^{B}} \right] \tag{34}$$

and

$$\Phi_{Gt} = \left[\frac{\partial Gt^{A}_{ntde}}{\partial gt^{A}} \quad \frac{\partial Gt^{A}_{ntde}}{\partial gt^{B}} \right]. \tag{35}$$

If tidal datums computed from 19 yrs of data spanning a period other than the 1983 to 2001 NTDE are used then the values for DTL^{B}_{ntde} and Gt^{B}_{ntde} would be different. Thus, the assumption that they are not stochastic is no longer valid and they must be included when developing Φ_{DTL} and Φ_{Gt}.

The Φ_{DTL} and Φ_{Gt} vectors have one row with 2 times the number of monthly means being evaluated. Because 8 monthly means are used to compute the datums, vectors Φ_{DTL} and Φ_{Gt} have one row with 16 columns.

The diagonal elements in the covariance matrix for DTL^{A}_{ntde} and Gt^{A}_{ntde} are the variances of the monthly means for the VTGZ and for Eastport, ME.

Assuming DTL^{A}_{ntde} and Gt^{A}_{ntde} are independent the covariance terms (off diagonal elements) are zero. These matrices are shown below

$$Q_{DTL} = \begin{bmatrix} \sigma^2_{dtl^A} & 0 \\ 0 & \sigma^2_{dtl^B} \end{bmatrix} \tag{36}$$

$$Q_{Gt} = \begin{bmatrix} \sigma^2_{gt^A} & 0 \\ 0 & \sigma^2_{gt^B} \end{bmatrix} \tag{37}$$

The variance of each monthly mean computed in a VTGZ is obtained from equations (21) and (23) for *dtl* and *gt,* respectively. The variance of each monthly mean for Eastport was held constant as the variance of the eight monthly means used in the calculation. The final calculation for the variance of DTL^{A}_{ntde} and Gt^{A}_{ntde} is

$$\sigma^2_{DTL^{A}_{ntde}} = \Phi_{DTL} Q_{DTL} \Phi^{t}_{DTL} \tag{38}$$

and

$$\sigma^2_{Gt^{A}_{ntde}} = \Phi_{Gt} Q_{Gt} \Phi^{t}_{Gt} \tag{39}$$

The final step in computing MLLW corrected to the current NTDE and its variance is

$$MLLW^{A}_{ntde} = DTL^{A}_{ntde} - 0.5 * Gt^{A}_{ntde} \tag{40}$$

and

$$\sigma^2_{MLLW^{A}_{ntde}} = \sigma^2_{DTL^{A}_{ntde}} + \frac{1}{4}\sigma^2_{Gt^{A}_{ntde}} \tag{41}$$

Reduction of MSL Monthly Means to NTDE Equivalent

The *msl* values are reduced and corrected to the 1983 to 2001 NTDE using equation (42)

$$MSL^{A}_{ntde} = MSL^{B}_{ntde} + \frac{1}{m}\sum_{k=1}^{m}\left(msl^{A}(k) - msl^{B}(k)\right) \quad \textbf{(42)}$$

where MSL^{B}_{ntde} is the accepted datum for Eastport, ME, msl^{B} are the NOAA accepted monthly means for Eastport, ME and msl^{A} are the monthly means for the VTGZ, computed from the water-level prediction using equation (28). The variance of MSL^{A}_{ntde} is computed using the same expression that was used to compute the variance of DTL^{A}_{ntde} and Gt^{A}_{ntde}.

CHAPTER 3

TIDAL DATUMS THAT RESULT FROM HARMONIC ANALYSES OF NON-UNIFORM WATER-LEVEL RECORDS

This chapter outlines the significant results gained from this research. These results are the samples of the tidal signal in each VTGZ; the analysis used to overcome not having independent measurements of vessel motion to correct for roll, pitch, settlement and squat; the decomposition of the tidal signals using HAMWLS; and the computed tidal datums in each VTGZ. These results are presented in 5 sections.

The first section emphasizes the non-uniform sampling interval introduced by using the ferry as a sampling platform.

The second section includes the results from modeling the water-level estimates with two sets of tidal frequencies using the least-squares procedure. This section also includes the prediction uncertainties resulting from propagating the original measurement uncertainties through the least-squares procedure.

The third section compares amplitudes and phases computed using HAMWLS to the amplitudes and phases determined by the CHS. This section also includes an analysis of the correlation between the signals predicted by WebTide and HAMWLS for VTGZs 1 through 54. This analysis was not done for

VTGZs 55 through 62 because WebTide does not make predictions for them. The correlation analysis is followed by a comparison of the amplitudes and phases that result from the HAMWLS of the non-uniform time series in VTGZ 35.

The fourth section shows the match between the MSL tidal datums extracted from the h_{mix} solutions and the Geoid-to-ellipsoid separations obtained using Natural Resources Canada's transformation software GPS-Hv2.0. Also, this section identifies the VTGZs for which the assumptions made to address the lack of roll, pitch and heave measurements are not valid.

The last section includes MLLW tidal datums resulting from the analysis of the non-uniform time series of water-level estimates in each VTGZ. These MLLW tidal datums are compared to MLLW at Saint John, NB and Digby, NS.

Sampling Intervals Achieved by the Ferry

A typical record used in a traditional harmonic analysis would have a water-level sample at least every hour. Thus, there would be ~7200 observations for a 10-month record, which is the time span of the data from the *Princess of Acadia* GPS project that was used in this research (7 December 2003 to 25 September 2004). Because it takes the *Princess of Acadia* ferry 3 hours to transit between Saint John, NB and Digby, NS and the ferry makes 1 to 3 round trip crossings a day, the period of time between crossings of a VTGZ not only exceeds the sample interval for a traditional water-level record but it varies from crossing-to-crossing. However, the ferry's route is along a co-amplitude line with similar tidal characteristics at each end. Thus, it is safe to assume that the

tidal characteristics along the ferry's route are similar and *a priori* knowledge of the tidal constituents contributing to the tidal signals at Saint John, NB and Digby, NS are used as *a priori* knowledge to model the tides in each of the VTGZs. The non-uniform sampling interval of the water-level record in each VTGZ allows for tidal frequencies higher than the Nyquist frequency to be resolved (Scargle, 1982).

In the 2008 specifications and deliverables for water-level stations the CO-OPS recommends that water-level measurements should be computed from an average of at least 180 one-second water-level measurements (CO-OPS, 2008). Because the ferry follows different paths at different speeds through each of the VTGZs each water-level estimate (h_{wl}) in each VTGZ is computed from a different number of h_{mix} solutions.

The water-level estimates in VTGZs 2 through 61 were computed differently than the water-level estimates in VTGZ 1 and 62. This is done because VTGZ 1 and 62 encompass the ferry terminals and to avoid averaging over long time spans (the ferry could be moored for anywhere between 1 to 24 hours depending on the ferry schedule), the averaging period in VTGZ 1 and 62 is held constant at 181 sec.

Because the amount of time the ferry spent in a VTGZ varied from crossing-to-crossing minimum and maximum time constraints were established to restrict which crossings are used to characterize the height of the water-surface in a VTGZ. The minimum number of h_{mix} solutions used to compute a water-level estimate is at least 30 sec (Figure 36-a and Figure 36-b). This

constraint is based on the high-frequency motions of the ferry, as identified in a power spectrum of the single-baseline solutions from CGSJ from 14 December 2003 to 20 Dec 2003 (Figure 33). The maximum number of h_{mix} solutions used to compute a water-level estimate is constrained to consist of h_{mix} solutions spanning no more than 240 sec (Figure 36-a and Figure 36-b). This constraint is based on the number of ferry crossings and the CO-OPS recommended averaging period of water-level measurements.

Figure 36 shows the distribution of the number of h_{mix} solutions per water-level estimate in VTGZ 15 (Figure 36-a) and 35 (Figure 36-b). There is an obvious bimodal structure to both of the distributions with a peak at 155 sec and another at 120 sec. The reason for the two peaks is explained by the distribution of the average speed of the ferry for all of the crossings of VTGZ 15 (Figure 36-c) and VTGZ 35 (Figure 36-d). These two distributions show that the ferry usually crosses these zones at an average speed of 7.5 m/s, however there is a group of crossings of each VTGZ at 9.8 m/s. The two different peaks in the distributions of the average crossing speed is a result of the ferry using 2 engines under most conditions, but when the ferry is behind schedule two more engines are engaged, increasing the maximum cruising speed.

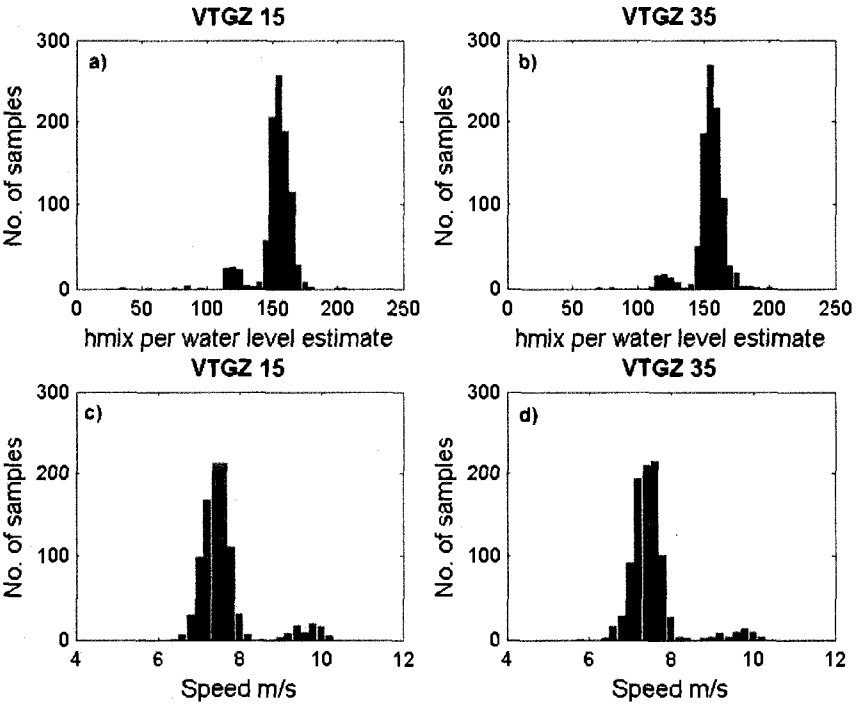

Figure 36 – Distribution of the number of h_{mix} solutions used to compute the water-level estimates in VTGZ 15 (a) and VTGZ 35 (b). Distribution of the average speed of the ferry during the crossings of VTGZ 15 (c) and VTGZ 35 (d).

The time when the water-level was sampled in each VTGZ was controlled by the ferry crossing schedule. Consequently, the time series used in the harmonic analyses were not equally spaced. Figure 37 shows the distribution of sample intervals for the time series of water-level estimates in VTGZs 2 through 61. The average sample interval between water-level estimates (ferry crossings) in each VTGZ was 7.26 hrs +/- 9.5 hrs (1σ). There are some samples that are separated by more than 4.5 days as a result of the ferry traveling outside the VTGZs (Figure 31). Sixty-five percent of the samples are separated by a period of time smaller than the Nyquist equal sampling interval for the M2 tide. The other 35% exceed the Nyquist sampling interval for M2.

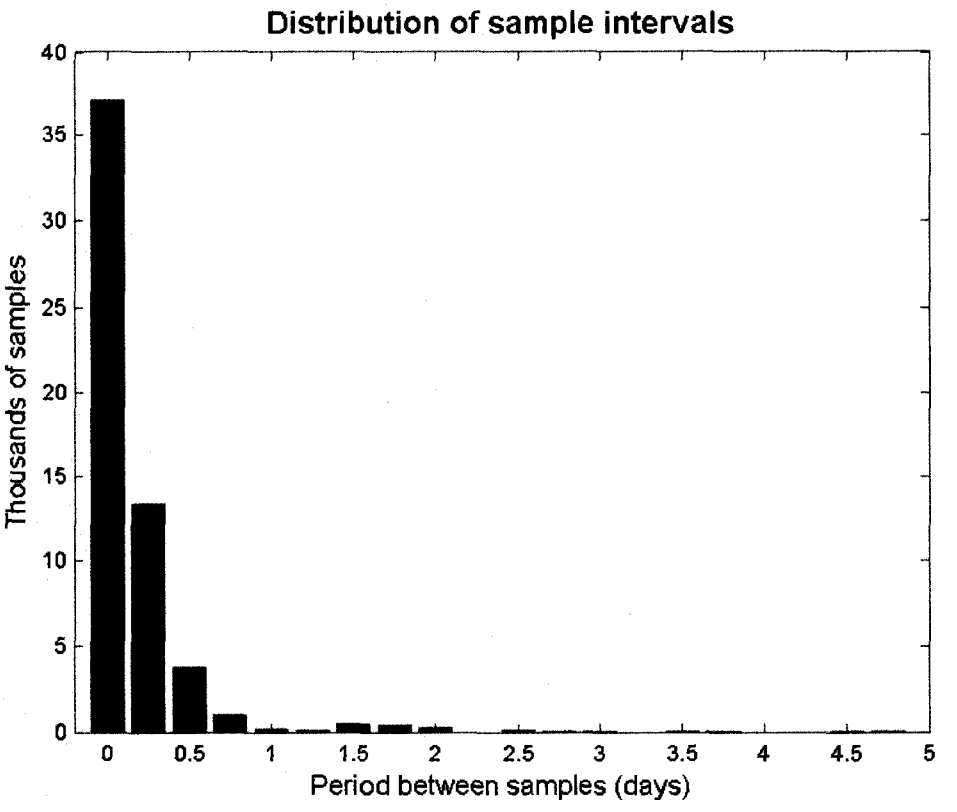

Figure 37 - Distribution of water-level estimate sample intervals.

Least-squares fit to Water-Level Estimates

The water-level estimates were weighted in the HAMWLS by the inverse of the uncertainty of the water-level estimate. The distribution of these standard deviations follows a Rayleigh distribution (Figure 38). This is expected because there is a lower limit of zero for the standard deviation. This distribution also shows there are few estimates with large standard deviations. The standard deviation of the distribution was estimated using a Rayleigh distribution to be 0.04 m. The mode, median and mean of this distribution is 4.8 cm, 5.2 cm and 6.9 cm, respectively.

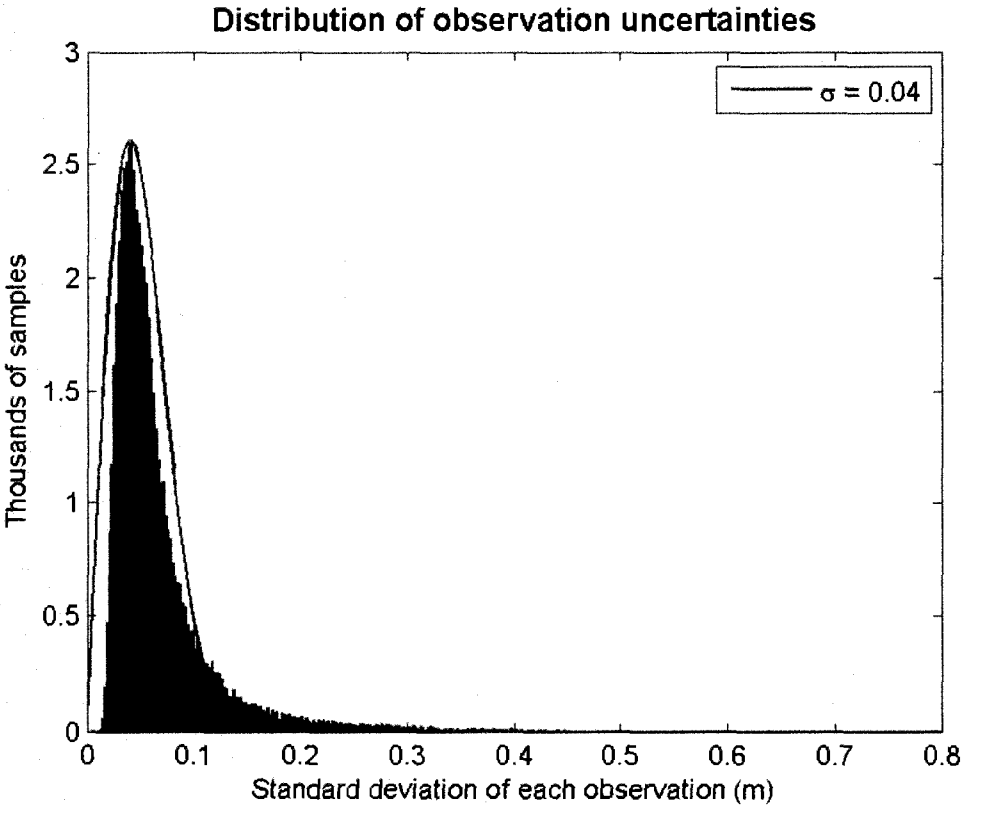

Figure 38 - Standard deviation of each computed water-level estimate.

The difference between the water-level estimates and the least-squares prediction using the two different sets of constituents are shown in Figure 39. The standard deviation of the differences when the water-level estimates are modeled using the freq-61 and freq-5 sets of constituents is 17.2 cm and 30.2 cm, respectively.

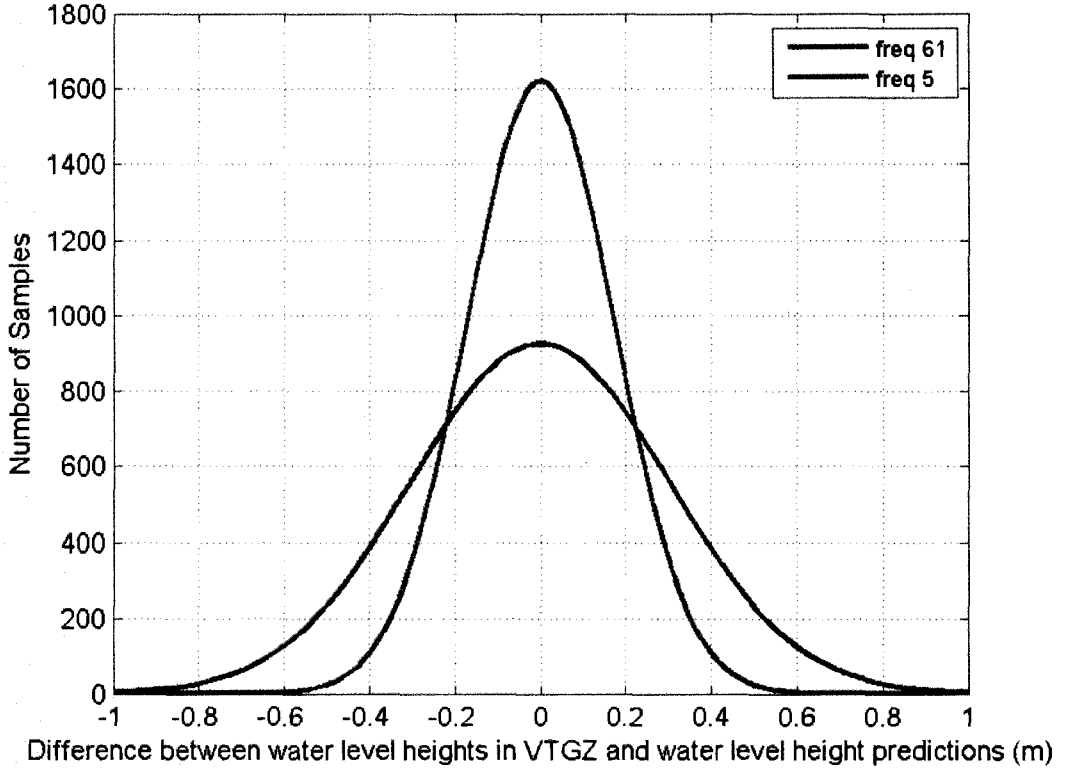

Figure 39 - Residuals after modeling the water-level estimates using the freq-61 (red) and freq-5 (blue) set of constituents.

The measurement uncertainties used to derive the weighted least-squares solution for both sets of constituents resulted in standard deviations for the predicted values that were much smaller than the residuals between the observation and the predictions. Figure 40 shows the distribution of the uncertainties produced from equation (17) using the two different sets of constituents. The uncertainties from the freq-61 set are in red and the uncertainties from the freq-5 set are in blue. The two distributions clearly have two different central tendencies and widths. The central tendency for the freq-5 uncertainties is smaller than that of the freq-61 uncertainties by a factor of 3. The

average uncertainty in the predictions using the freq-5 set of constituents is 65 times smaller than the standard deviation of the residuals when using the freq-5 set to model the water-level estimates. The average uncertainty in the predictions using the freq-61 set of constituents is 10 times smaller than the standard deviation of the residuals when using the freq-61 set of constituents.

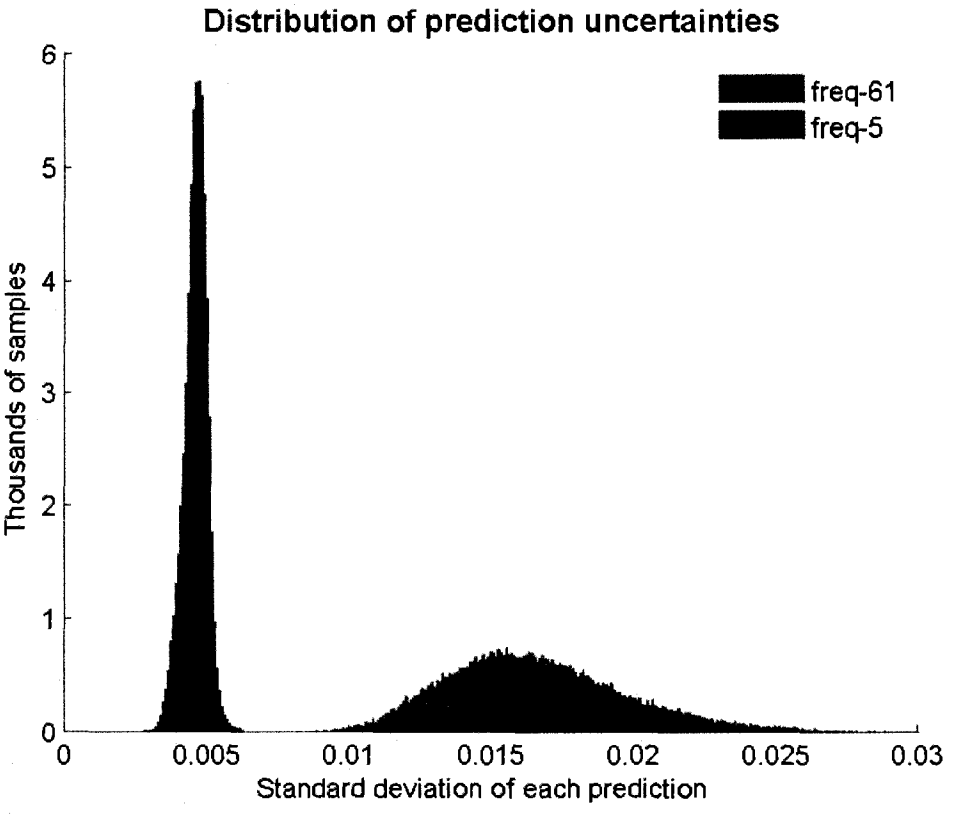

Figure 40 - Standard deviations of the predictions from the least-squares fit using the two different sets of harmonic functions.

The difference between the distribution of the least-squares predictions uncertainties using 61 and 5 tidal constituents is a result of the number of frequencies used in each model. For example, the magnitudes of the uncertainties of the coefficients, from VTGZ 35, that are in common between the

two models are shown in Table 13. The first column shows the name of the tidal constituent. Each tidal constituent has two coefficients, one for cosine (A_j) and one for sine (B_j). The least-squares estimated standard deviation of A_j and B_j are σ_{Aj} and σ_{Bj}, respectively. The standard deviations for the coefficients in the model with 61 tidal constituents are in the columns labeled 'freq-61'. The columns labeled 'freq-5' show the standard deviations of the coefficients in the model with 5 tidal constituents. The columns labeled 'diff' show the differences between the estimated standard deviations of the coefficients in the two models.

Table 13 – These are the standard deviations of the coefficients that are in common between the two different models. These standard deviations were estimated using the least-squares procedure.

Coefficient uncertainties						
	σ_{Aj} (m)			σ_{Bj} (m)		
Name	freq-61	freq-5	diff	freq-61	freq-5	diff
O1	0.0026	0.0021	0.0005	0.0026	0.0022	0.0004
K1	0.0027	0.0021	0.0006	0.0027	0.0022	0.0005
N2	0.0026	0.0021	0.0005	0.0027	0.0021	0.0006
M2	0.0027	0.0022	0.0005	0.0029	0.0021	0.0008
S2	0.0028	0.0023	0.0005	0.0028	0.0021	0.0007

Table 13 shows that the uncertainties for the coefficients in both models are similar in magnitude. Thus, the uncertainty, at any epoch, estimated using the "General Formula for Error Propagation" as described by John R. Taylor (1997) and the coefficient uncertainties listed in Table 13, will also be similar in magnitude. The estimated standard deviations of the coefficients for the other 56 tidal constituents used in VTGZ 35 range from 0.0006 to 0.0054 with an average standard deviation of 0.0023 m +/-0.0028 (1σ). This means that the magnitude of the uncertainty of an individual coefficient estimated through the least-squares

procedure is independent of the number of tidal constituents used. Consequently, as the number of tidal constituents used to predict the water-level estimate increases the uncertainty in the least-squares prediction also increases.

Amplitude and Phase Computed using HAMWLS

The least-squares procedure used in this research was validated by comparing constituent amplitudes and the time of predicted high and low water-levels to values published by the CHS. This section refers to two types of least-squares procedures HAMELS and HAMWLS. There are two differences between the two procedures. One difference is that in the HAMWLS the water-level estimates are weighted by the inverse of water-level estimate uncertainty, whereas in the HAMELS they are weighed equally with unit weight. The second difference is that the covariance matrix for model coefficients, for which the errors in amplitude and phase are computed, is not computed using equation (14) because there is no original uncertainty estimates. Instead, the covariance matrix for the coefficients ($Q_{\bar{x}}$) is computed as

$$Q_{\bar{x}} = mse * (A_{\overline{wl}}^{t} A_{\overline{wl}})^{-1} \quad \textbf{(43)}$$

where *mse* is the quotient of the sum of squares of the residuals and the degrees of freedom.

Table 14 compares the amplitude and phase resulting from the HAMELS to the amplitude and phase for the Saint John, NB tide station determined by the CHS. The amplitude and phase resulting from the HAMELS differ from those

reported by the CHS for two reasons. First, the CHS amplitudes and phases are corrected for the variations of their mean caused by the regression of the Moon's nodes (Pugh, 2004), whereas the amplitudes and phases from HAMELS are not corrected for nodal regression. Second, the CHS uses a phase epoch of Atlantic Standard Time, whereas the phase epoch for the solutions from HAMELS is the start time of the record used in the analysis. Consequently, inferences made from comparing amplitudes and phases between columns are limited. However, the percent difference between the amplitudes in the two columns gives insight to the accuracies of the amplitudes in the HAMELS column. Pugh (2004) reported that the amplitude variation due to nodal regression is 3.7% for M2, 11.5% for K1, and 28.6% for K2. The lunar declination constituents K1 and K2 have the largest amplitude changes (Pugh, 2004). The un-corrected amplitudes for M2, K1, and K2 in the HAMELS column are 1.0%, 8.2%, and 27.0% different from the corrected amplitudes in the CHS column. These percent differences are within the expected amplitude variation for these tide constituents.

Because of the different epochs for the phases in the two different columns of Table 14, the times of the predicted high and low water-levels were used to assess the accuracy of the HAMELS predictions. Four months of high and low water-levels predicted using HAMELS were compared to highs and lows for the same 4 months predicted using the CHS model. The times of the two different sets of predicted high and low water-levels agree to within +/- 9.6 min (1σ).

Table 14 - Tidal harmonic constants obtained from the Canadian Hydrographic Service and amplitude and phase computed using the HAMELS least-squares procedure.

Amplitude and Phase for Saint John				
	CHS Saint John Gauge Data		HAMELS Saint John Gauge Data	
	amp (m)	phase (°)	amp (m)	phase (°)
M2	3.058	342.54	3.027	262.61
			0.002	0.36
N2	0.655	312.2	0.614	169.27
			0.002	0.07
S2	0.480	17.75	0.476	143.10
			0.002	0.06
L2	0.194	30.42	0.175	179.14
			0.002	0.02
K1	0.158	134.22	0.171	189.89
			0.002	0.02
NU2	0.151	318.17	0.141	100.51
			0.002	0.02
K2	0.137	18.2	0.174	314.09
			0.002	0.02
O1	0.120	119.93	0.136	341.29
			0.002	0.02
2N2	0.079	304.5	0.111	72.84
			0.002	0.01
LDA2	0.061	9.73	0.061	247.52
			0.002	0.01
P1	0.052	134.28	0.054	205.46
			0.002	0.01

The HAMWLS predictions for each of the VTGZs were compared to predictions from WebTide for the midpoint of the same VTGZs. The covariance of the two predictions and their correlation are used to measure how well the two predicted signals agree. The covariance (σ_{xy}) is computed as

$$\sigma_{xy} = \frac{1}{n-1}\sum_{i=1}^{n}\left(x(i)-\bar{x}\right)\left(y(i)-\bar{y}\right). \quad \textbf{(44)}$$

where *x* is the predictions from WebTide, *y* is the predictions from the HAMWLS, *x(i)* and *y(i)* denote the WebTide and HAMWLS prediction at time *i*, respectively.

n is the total number of predictions. The correlation (r) between the two signals is computed as

$$r = \frac{\sigma_{xy}}{\sqrt{\sigma_x^2 \sigma_y^2}} \tag{45}$$

where σ_x^2 is the variance of x and σ_y^2 is the variance of y. When the two predicted signals are equal in amplitude and exactly in phase, they are perfectly correlated (r =1) and

$$\sigma_{xy} = \sigma_x^2 = \sigma_y^2 . \tag{46}$$

If the signals are equal in amplitude, but out of phase by 180°, the signals are negatively correlated (r = -1) and

$$\sigma_{xy} = -\sigma_x^2 = -\sigma_y^2 . \tag{47}$$

If the signals are equal in amplitude and out of phase by 90°, they are not correlated (r = 0),

$$\sigma_{xy} = 0 \tag{48}$$

and

$$0 \neq \sigma_x^2 \neq \sigma_y^2 . \tag{49}$$

If the signals are in phase, but not equal in amplitude, they will still be perfectly correlated (r = 1); however, the covariance of the two signals will no longer equal the variance of each set of predictions and equation (46) will no longer be true.

The variance of the WebTide predictions for VTGZ 35 is 4.45 m. The covariance of the WebTide and the HAMWLS predictions is 4.65 m. The correlation between the two predicted signals is 0.9967. Based on the definitions above, this strong correlation suggests the two signals are near to being in

Table 15 - Comparison of amplitude and phase resulting from harmonic analysis of water-level estimates from the ferry and predictions from WebTide.

Virtual Tide Gauge Zone 35						
	HAMWLS Non-Uniform Time Series				HAMELS Uniform Time Series	
	freq-61		freq-5		WebTide	
	amp (m)	phase (°)	amp (m)	phase (°)	amp (m)	phase (°)
M2	3.022	254.78	3.025	255.19	2.926	254.52
	0.003	0.53	0.002	0.39	0.000	0.02
N2	0.611	163.61	0.590	160.21	0.593	166.85
	0.003	0.09	0.002	0.07	0.000	0.00
S2	0.483	142.80	0.466	138.45	0.489	136.78
	0.004	0.14	0.002	0.06	0.000	0.00
K1	0.200	194.01	0.209	193.02	0.164	182.85
	0.003	0.03	0.002	0.03	0.000	0.00
O1	0.147	323.44	0.129	325.52	0.127	335.11
	0.003	0.02	0.002	0.02	0.000	0.00

phase. The fact that the covariance of the two signals is slightly larger than the variance of the WebTide predictions suggest that the amplitude of the signal predicted from the least-squares fit to the water-level estimates is larger than the amplitude of the signal predicted by WebTide. The average correlation between the WebTide and HAMWLS predictions for VTGZs 1 through 54 is 0.996 +/- 0.003 (1σ) with the two predictions de-correlating as a function of distance offshore from Saint John, NB.

The results from modeling the water-level estimates in VTGZ 35 using the two different sets of constituents are compared to the amplitude and phase computed from the WebTide predictions for VTGZ 35 using HAMELS. The comparisons are shown in Table 15. The two rows for each constituent show the computed amplitude/phase in the top row and the uncertainty in the amplitude/phase in the bottom row.

The high water-levels predicted from the HAMWLS of the non-uniform time series in VTGZ 35 are within +/-11 min (1σ) of the high water-levels predicted by WebTide. The low water-levels are +/-11.5 min (1σ) of low water-levels predicted by WebTide. The height differences between the two predictions are larger during the rise and fall of the tide than they are at the high and low water-levels as expected by the time differences. The maximum height difference between the two predictions is 27 cm.

The accuracy of the WebTide predictions was assessed by comparing the times of 364 high and low water-levels measured at CHS 065 to the times of those same high and low water-levels predicted by WebTide. The high and low water-levels predicted by WebTide are within +/-12.6 min (1σ) of the measured high and low water-levels. Therefore, the uncertainty in the times of the predictions from the non-uniform time series with respect to the WebTide predictions are within the uncertainty of the times of the WebTide predictions with respect to the measured water-levels at Saint John, NB.

Profiles of MSL Computed from the Ferry Data

Tidal datums for each VTGZ are computed from the HAMWLS predictions in each VTGZ using the two different sets of constituents described previously. Figure 41 compares the Geoid, an equipotential surface that approximates global mean sea level, to MSL computed for each VTGZ using the two different sets of HAMWLS predictions. The solid blue line in Figure 41 is the heights from the

Natural Resources Canada Geoid-to-ellipsoid separation model GPS-Hv2.0. This software package transforms between orthometric CGVD28 and ellipsoidal (NAD83(CSRS) or ITRF97) heights using the Canadian Geoid model CGG2000 and a corrector surface. The corrector surface distorts the Geoid heights to fit the errors in the CGVD28 and ellipsoid heights (Veronneau, 2000).

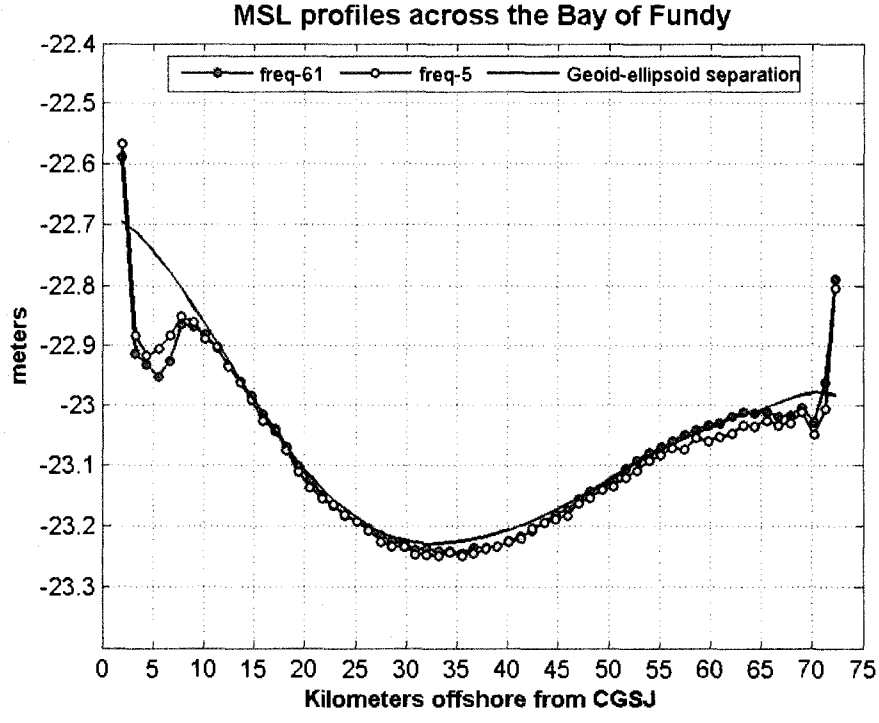

Figure 41 - MSL profiles computed from the predictions made using the two different sets of constituents. The freq-61 profile was computed using 61 constituents. The freq-5 profile was computed using M2, N2, S2, K1, and O1.

The differences between the Geoid and MSL derived from the h_{mix} solutions are shown in Figure 42. This figure shows a very good match between the Geoid and the MSL for the VTGZs between 13.61 and 64.38 offshore from the GPS base station in Saint John, NB. The maximum difference for those VTGZs is 2.2 and 2.5 cm for freq-61 and freq-5, respectively.

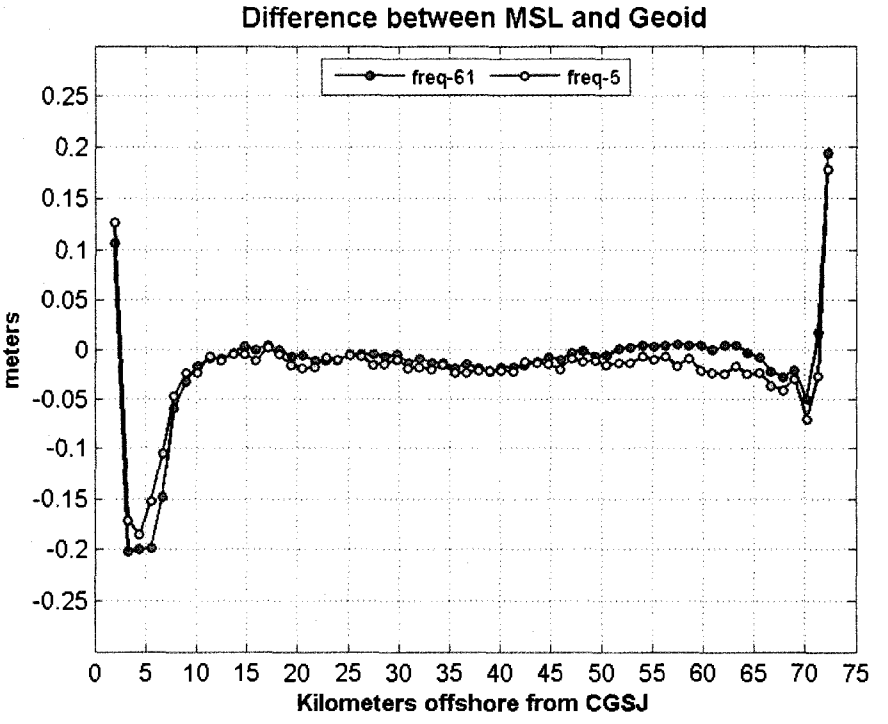

Figure 42 - Difference between the Geoid and the MSL profiles computed using the two different sets of tidal constituents.

Figure 43 shows 5 hrs of h_{mix} solutions (black line) and the distance the ferry was from Saint John, NB (green line) during that time. The scale for the h_{mix} solutions is on the left of the figure and the scale for the distances is on the right. There are two features in the h_{mix} solutions that are of interest. The first feature is the 'dip' of ~50 cm in the h_{mix} solutions that occurred while the ferry was leaving the terminal in Saint John, NB. The second feature is another 'dip' in the h_{mix} solutions, similar in magnitude to the first 'dip', that occurred when the ferry was approaching the terminal at Digby, NS.

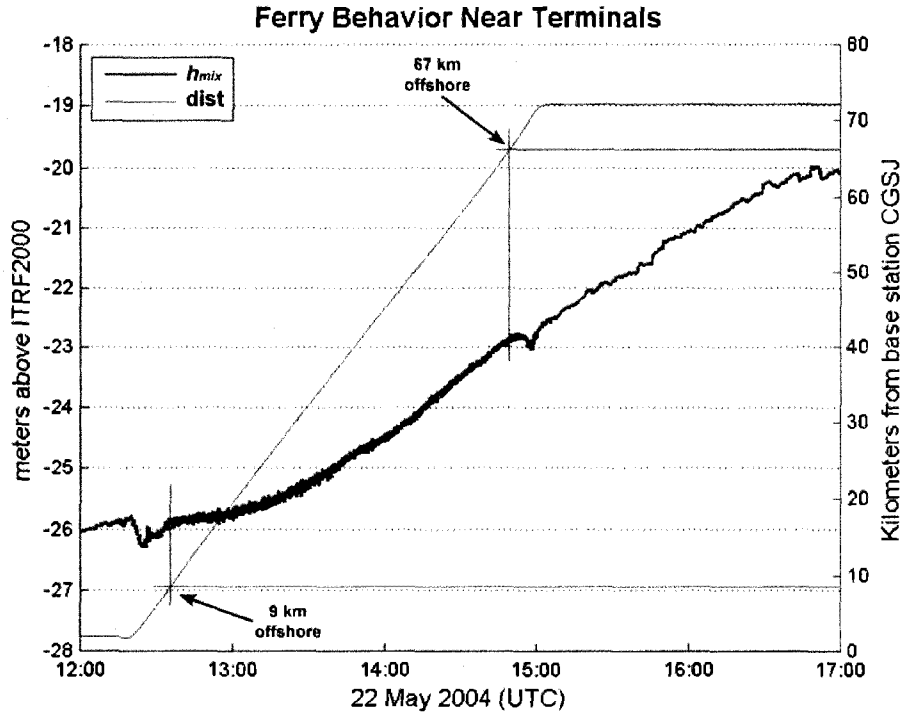

Figure 43 – The h_{mix} are shown in black and the distance the ferry was from base station CGSJ is shown in green.

The reason for the two 'dips' identified in Figure 43 is shown in Figure 44, which shows the h_{mix} solutions that are in Figure 43. Figure 44 also shows the speed of the ferry. Immediately one notices that the dips occur when the ferry is accelerating as it leaves the terminal at Saint John, NB and when the ferry is decelerating as it approaches the terminal at Digby, NS. It takes the ferry about 8 minutes to reach a speed 7.8 m/s then it takes 10 minutes for the h_{mix} solutions to stabilize (i.e. the ferry has come out of the 'dip'). Ten minutes after the h_{mix} solutions have stabilized the speed of the ferry is decreased to 7.2 m/s and remains at about that speed for the next 2 hours. When the speed of the ferry was reduced to 7.2 m/s after leaving the terminal at Saint John, NB it was 13 km

offshore from the CGSJ base station. Two hours later when the speed of the ferry increased rapidly it was 65 km offshore from the CGSJ base station and 7 km from the terminal at Digby, NS.

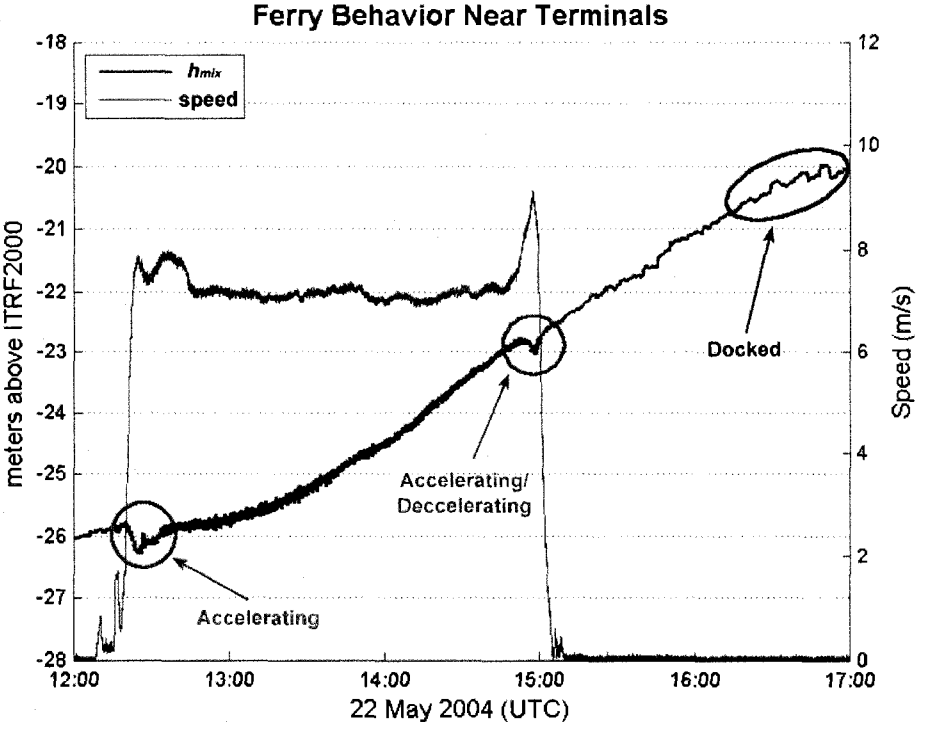

Figure 44 – Single- and dual-baseline PPK heights are shown in black and the speed of the ferry is shown in green.

Figure 44 also shows that while the ferry was moored to the dock at the Digby, NS terminal there was a lot of irregular noise in the h_{mix} solutions. For example, at 16:29 (UTC) the heights rapidly increased by 13 cm then 14 minutes later the heights rapidly decreased by 14 cm. Then again, 5 minutes later, the heights increased rapidly by 11 cm and 3 minutes later they decreased by 17 cm. The exact cause of these rapid height changes is not known but they are

believed to be a combination of cargo being unloaded and loaded, and restrictions from the mooring lines holding the ferry to the dock.

Figure 45 shows three different sets of residuals. The black curve with the red dots is the difference between the Geoid and MSL computed using 61 tidal constituents. The black curve with the green dots is the difference between the Geoid and MSL computed using 5 tidal constituents. The h_{mix} curve is the difference between all the h_{mix} solutions from 16 May 2004 to 22 May 2004 (GPS week 1271) smoothed using two running-average filters. The h_{mix} solutions are smoothed with a 30-sec running-average filter to remove the high-frequency noise in the solutions. The h_{mix} solutions are also smoothed with a 20-min running-average filter to remove the features identified in Figure 44. The results from the 30-sec filter contain both the tide signal and the acceleration/deceleration signals. The results from the 20-min filter contain the tide signal. Differencing the results form the two filters removes the tide signal and isolates the acceleration/deceleration events. The blue curve in Figure 45 shows these events as a function of distance offshore from the GPS base station CGSJ.

Figure 45 shows that the locations that the acceleration/deceleration events occur are the same locations that the larger differences between MSL and the Geoid occur. Thus, the larger differences between MSL and the Geoid that occur on both sides of the bay are a result of the h_{mix} solutions being contaminated by the behavior of the ferry in those VTGZs, which in turn bias the HAMWLS of the water-level estimates in those VTGZs.

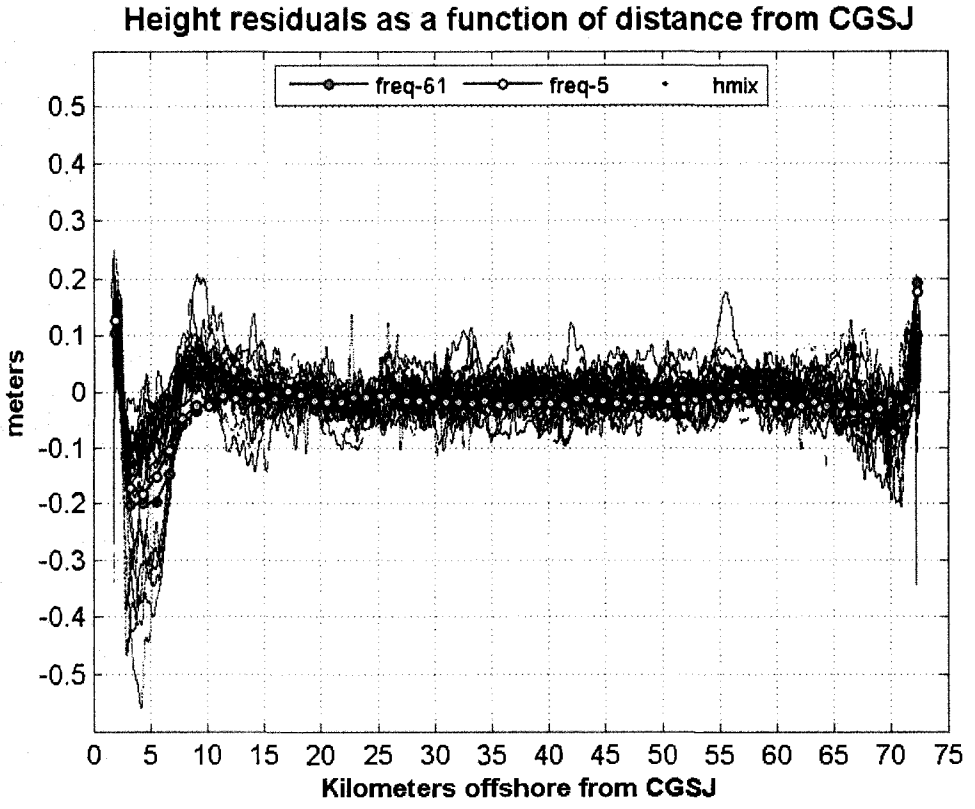

Figure 45 - Height residuals for h_{mix} solutions from 16 May 2004 to 22 May 2004 (GPS week 1271). The blue line is the differences between h_{mix} smoothed with a 30-sec running average and h_{mix} smoothed with a 20-min running average.

Similar 'dips' to those identified in Figure 43 and Figure 44 occur on most of the crossings during the *Princess of Acadia* GPS Project, thus the differences shown by the blue curve in Figure 45 are representative of the 9 months of data. Based on Figure 45, the locations that acceleration and deceleration of the ferry has the largest apparent effect on the h_{mix} solutions are from 0 to 13.61 km and from 64.38 to 72.25 km offshore from GPS base station CGSJ. The maximum difference between the Geoid and the two MSL profiles for the VTGZs that are not within those ranges is 2.5 cm (Figure 42). The uncertainties estimated for the tidal datums in each profile from the water-level estimates uncertainties

propagated through the least-squares procedure, the predictions, and the tidal datum computations are 1.2 cm and 0.9 cm for the freq-61 and freq-5 profiles.

Profiles of MLLW Computed from the Ferry Data

There are a limited number of sources to compare with the MLLW heights computed from the ferry data. This research used MLLW heights for Saint John, NB and Digby, NS computed from published tidal benchmark elevations, the height of MLLW above CD, and ITRF2000 Online Positioning User Service (OPUS) solutions. The OPUS solutions are based on static observations of tidal benchmark 99B9006 at tide station CHS 065 and TBM BOLLARD at tide station CHS 324 (Table 5). The transformation from CD to MLLW was necessary because the tidal datums computed in this research follow the NOAA Special Publication NOS CO-OPS 2 (CO-OPS, 2003), which does not define LLWLT.

The height of MLLW above CD at Saint John, NB and Digby, NS was computed using the same methods as were used to compute MLLW from the predicted water-levels in all of the tide regions, although using conventional gauge data instead of predictions. Monthly means for March 2004 through August 2004 were computed for Saint John, NB (Table 16). Monthly means for May 2004 through August 2004 were computed for Digby, NS (Table 17). Data from these periods of time are used because they are the longest continuous records during the *Princess of Acadia* GPS Project for the respective stations. The monthly means for each station were corrected to the 1983 to 2003 NTDE using NOAA station 8410140 in Eastport, ME. The Eastport, ME monthly means used in the tidal datum computation for tide stations CHS 065 and CHS 324 are

shown in Table 18. Table 19 shows the corrected tidal datums for tide stations CHS 065 and CHS 324 in columns 2 and 3, respectively. Column 3 contains the accepted 1983 to 2001 NTDE tidal datums for Eastport, ME that were used to compute the tidal datums for tide stations CHS 065 and CHS 324. The difference in the definition of CD used at the CHS and NOAA stations shown in Table 19 is caused by the fact that the height of MLLW above chart datum at NOAA 8410140 is zero whereas the height of MLLW above CD at CHS 065 and CHS 324 is 1.10 m and 1.14 m, respectively.

Table 16 - Monthly means from March 2004 to August 2004 for Saint John, NB (CHS 065).

Saint John, NB (CHS 065) monthly means *(data are in meters above CD at Saint John)*				
Year	**Mo**	**DTL**	**MSL**	**Gt**
2004	3	4.32	4.35	6.32
2004	4	4.37	4.41	6.46
2004	5	4.38	4.42	6.50
2004	6	4.40	4.44	6.61
2004	7	4.36	4.40	6.68
2004	8	4.35	4.39	6.62

Table 17 - Monthly means from May 2004 to August 2004 for Digby, NS (CHS 324).

Digby, NS (CHS 324) monthly means *(data are in meters above CD at Digby)*				
Year	**Mo**	**DTL**	**MSL**	**MN**
2004	5	4.53	4.57	6.45
2004	6	4.57	4.60	6.52
2004	7	4.56	4.58	6.59
2004	8	4.57	4.59	6.58

Table 18 - Monthly means from March 2004 to August 2004 for Eastport, ME (NOAA 841040).

Eastport, ME (NOAA 8410140) monthly means *(data are in meters above CD at Eastport)*				
Year	**Mo**	**DTL**	**MSL**	**Gt**
2004	3	2.907	2.910	5.661
2004	4	2.912	2.933	5.785
2004	5	2.903	2.938	5.824
2004	6	2.948	2.979	5.932
2004	7	2.935	2.955	5.981
2004	8	2.949	2.969	5.918

Table 19 – These are tidal datums for CHS 065, CHS 324 and NOAA 841040. The datums for CHS 065 and CHS 324 are corrected to the 1983 to 2001 NTDE using the accepted datums for NOAA 8410140.

Tidal Datums Corrected to 1983 to 2001 NTDE *(data are in meters above CD)*			
	Saint John CHS 065	**Digby CHS 324**	**Eastport, ME NOAA 8410140**
DTL	4.38	4.56	2.937
Gt	6.56	6.83	5.874
MSL	4.41	4.58	2.958
MLLW	1.10	1.14	0.000

Figure 46 shows the MLLW profiles for freq-61 and freq-5. The vertical offset between the two MLLW profiles is easily explained by the fact that MLLW was computed using the diurnal tide level (*DTL*) for VTGZ *A* corrected to the 1983 to 2001 NTDE and the great diurnal range (*Gt*) for VTGZ *A* corrected to the 1983 to 2001 NTDE

$$MLLW^{A}_{ntde} = DTL^{A}_{ntde} - 0.5 * Gt^{A}_{ntde} \quad \textbf{(50)}$$

The average difference between *Gt* used to compute the two profiles was 17 cm. The average difference between the freq-61 and freq-5 MLLW profiles was 8 cm,

which is approximately half of the average difference for *Gt*. Figure 46 also shows the height of MLLW above ITRF2000 at the Saint John, NB and Digby, NS ferry terminals computed from the OPUS solutions and the height of MLLW above CD. The error bars for the MLLW heights at Saint John, NB and Digby, NS have a length equal to 2 times the peak-to-peak vertical accuracy reported by OPUS. The uncertainties estimated for the tidal datums in each profile from the propagation of the original water-level estimates uncertainties through the least-squares procedure, the predictions, and the tidal-datum computations are 3.3 cm and 3.1 cm for the freq- 61 and freq-5 profiles.

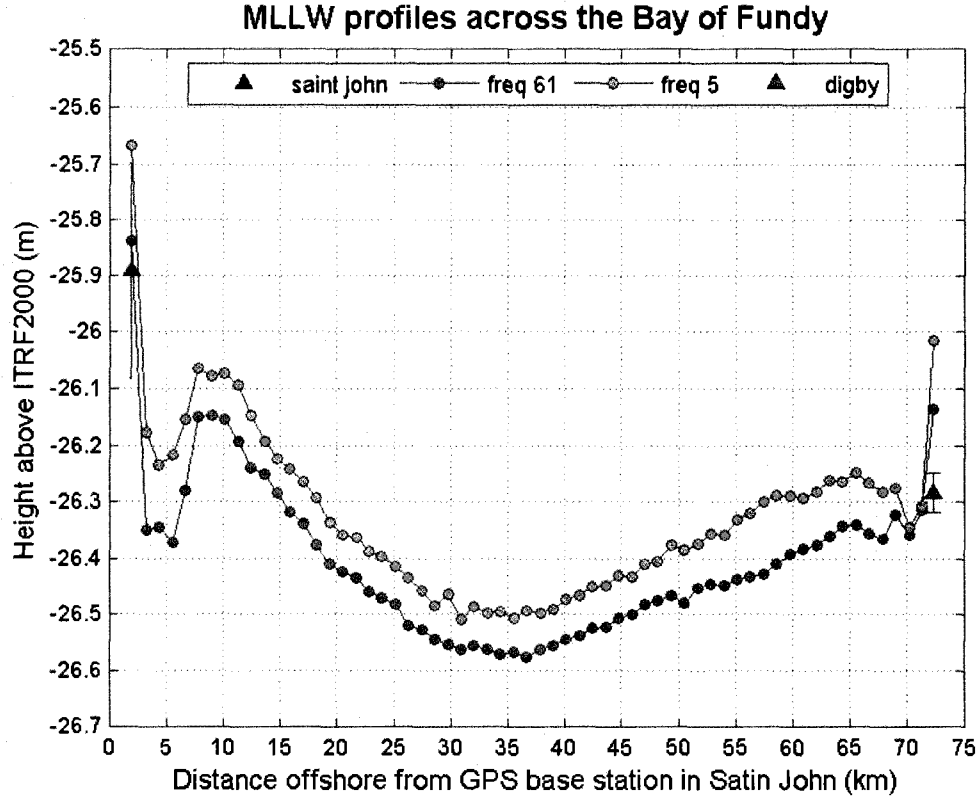

Figure 46 - Profiles of MLLW across the Bay of Fundy computed using the freq-61 and freq-5 sets of constituents.

CHAPTER 4

CONCLUSIONS AND RECOMMENDATIONS

Conclusions

This work resulted in a procedure to extract tidal datums from GPS observations obtained on a moving platform. The validity of these results is confirmed by the close match of the extracted MSL to the local Geoid that was established through independent means. In this work two challenges became immediately apparent: The first is due to the use of a ferry as the measurement platform which results in a non-uniform sampling interval for discrete VTGZs and that the intervals are relatively large. The second challenge is to use a dataset that lacks vessel roll, pitch, heave and draft measurements for correcting changes in the measured water-level, resulting from the GPS antenna not being at the roll/pitch center of the ferry. The magnitude of theses changes due to roll, pitch and heave are shown in the 'Virtual Tide Gauge Zone' section to reach more than 1 m. The magnitude of these changes due to constraints from the mooring lines holding the ferry to the dock, loading and unloading while the ferry was moored to the terminals was shown in to be on the order of 15 cm for an individual docking event.

The method that was developed to overcome the first challenge is composed of 5 primary steps. The first step consists of dividing a portion of the region over which the ferry travels into discrete VTGZs. The second step consists of compiling water-level records for each VTGZ. These water-level records consist of estimates of the height of the water-level in the VTGZ. These estimates are computed by averaging all the h_{mix} solutions in a VTGZ during a ferry crossing. The uncertainty in the estimated water-level height is estimated by the sum of the squares of the residuals between the h_{mix} solutions and the average computed from them. The third step employs *a priori* knowledge of the significant constituents at shore-based tide stations. This knowledge is used in a least-squares procedure to define coefficients for the model in equation (1) that are unique to each VTGZ. The fourth step consists of using these model coefficients to predict 8 months of high and low water-levels. The fifth step employs the techniques in the NOAA Special Publications NOS CO-OPS 2 (CO-OPS, 2003) to compute tidal datums in each VTGZ from the predicted high and low water-levels (see the 'Processing Flow Chart' section).

The 'Least Squares Fit to Water-Level Estimates' section shows that the results from modeling the non-uniform water-level estimates with 61 constituents agree to within +/-17.2 cm (1σ) of the water-level estimates. When only 5 constituents are used the standard deviation of the differences between the water-level estimates and the least-squares predictions increases to 30.2 cm. The 'Profiles of MSL Computed from the Ferry Data' section shows that the propagation of the original uncertainty estimates through the least-squares

procedure, the predictions, and the tidal-datum computation results in uncertainty estimates between 0.9 and 1.2 cm for MSL when using 5 and 61 tidal constituents, respectively. The 'Profiles of MLLW Computed from the Ferry Data' section shows that for the MLLW tidal datums the original uncertainty estimates resulted in datum uncertainties of 3.1 to 3.3 cm when using 5 and 61 tidal constituents, respectively. The uncertainty in the MSL and MLLW tidal datums estimated using the original uncertainty estimates are at least 10 times smaller than the difference between the water-level estimates and the least-squares predictions, which ranged from -86.2 to 76.3 cm when using 61 tidal constituents and from -110.1 to 107.3 cm when using 5 tidal constituents. The section with the MSL profiles and the section with the MLLW profiles also show that propagation of the original uncertainties results in less uncertainty in the tidal datums computed from the model using 5 constituents than the tidal datums computed from the model using 61 constituents. Based on the results in the 'Profiles of MLLW Computed from the Ferry Data' section, the uncertainties in the tidal datums computed for each VTGZ are underestimated by the propagation of the original uncertainty estimates. Therefore, a more appropriate estimate of uncertainty is the standard deviation of the residuals between the water-level estimates and the predictions.

The 'Profiles of MSL Computed from the Ferry Data' section shows that tidal datums computed using the Comparison of Monthly Means and Modified Range Ratio methods from the predicted high and low water-levels agree with the Geoid-to-ellipsoid separations to within 2.2 cm and 2.5 cm when using 61

constituents and 5 constituents, respectively. The uncertainty in the Geoid model used to compute the Htv2.0 heights is between 3 and 6 cm for the Bay of Fundy region (Veronneau, 2000). Also, uncertainties in the MSL heights computed in this research are estimated to be 17.2 cm for profiles computed using 61 constituents and 30.2 cm for the profiles computed using 5 constituents. Thus, the difference between the MSL-to-ellipsoid separations and the Geoid-to-ellipsoid are not significant. The significant result is that the MSL-to-ellipsoid separations computed from the non-uniform times series closely follow the same trend as the Geoid-to-ellipsoid separations.

Although the MSL profiles show that MSL computed from water-levels predicted using 5 and 61 tidal constituents differ from the Geoid-to-ellipsoid separation by no more than 2.5 cm, the MLLW profiles shows that MLLW is underestimated when 5 tidal constituents are used. The trend of the two MLLW profiles is similar, however at 8 km offshore from the Digby, NS terminal the height of MLLW computed from water-level predictions based on 5 tidal constituents is -26.26 m above ITRF2000, which is 2.3 cm higher than MLLW computed for TBM BOLLARD at the Digby, NS ferry terminal. The height of MLLW 8 km offshore from the Digby, NS terminal computed from water-level predictions based on 61 tidal constituents is -26.34 m above ITRF2000, which is 5.7 cm lower than MLLW computed for TBM BOLLARD.

In conclusion, this research shows that by employing *a priori* knowledge during the harmonic analysis useful information can be extracted from a non-uniform times series. This research also shows that applying these techniques to

the *Princess of Acadia* GPS Project dataset MSL and MLLW can be computed to within +/-17.2 cm at the 1σ level using water-levels predicted from a model with 61 constituents.

Recommendations for Future Work

The future recommendations fall into three categories. One is a group of suggestions for improving the accuracy of water-level measurements made using a ferry. The second category suggests a validation of the method developed in this research. The third category involves two suggestions for alternative methods of estimating the uncertainty in the model coefficients obtained from the least-squares procedure.

Category 1 - To get the full potential out of water-level measurements from a ferry settlement and squat should be modeled using a controlled experiment. Also, accurate measurements of the ferry's rotation around its center of gravity (roll and pitch) should be made to improve the results when the ferry is maneuvering. Similarly, measurements should be made to correct for the changes in draft introduced by the loading and unloading of ferry cargo.

Category 2 - It is recommended that offshore MLLW heights computed using the method developed in this research be validated by deploying one or more GPS buoys along the *Princess of Acadia* route. The buoys should be strategically deployed in one of the VTGZs used during this research that resulted in unbiased

tidal datums. Tidal datums should be computed using the water-level heights observed by the GPS buoy and from predictions based on the water-level measurements.

Category 3 - The final recommendation is to develop a more robust method, such as a Monte Carlo (Brennan, 2005) or bootstrapping (Pawlowicz, 2002) method, for estimations of the uncertainty in the amplitude and phase of the tidal constituents. More robust uncertainty estimates could then be propagated through the predictions and datum computation to better estimate the uncertainty in the tidal datums.

REFERENCES

Adams, R., 2004, *Seamless data and vertical datums – Reconciling chart datum with a global reference frame*: The Hydrographic Journal, no. 113, p. 9-14

Andreasen, C., 2008, *Vertical datum issues for data continuity from the land to the seafloor*: Proceedings of the Canadian Hydrographic Conference, Victoria, BC, May 5-8, 2008

Arroyo-Suarez, E.N., Mabey, D.L., Hsiao, V. and Phillips, R., 2005, *Implementation of a Positioning and telemetry buoy to determine chart datum for hydrographic survey applications*: ION GNSS 18th International Technical Meeting of the Satellite Division, Long Beach, CA p. 801-804.

Brennan, R. T., 2005, *An uncertainty model for the Tidal Constituent and Residual Interpolation (TCARI) method of water level correction*: University of New Hampshire, Masters Thesis 90p

Boon, J.D., 2004, *Secrets of the tide: Tide and tidal current analysis and predictions, storm surges and sea level trends*: Horwood Publishing, Chichester, UK, 212p.

Cartwright, D.E. 2000, *Tides a scientific history*: Cambridge University Press, Cambridge, UK, 292p

Craymer, M., 2006, *The evolution of NAD83 in Canada*: Geomatica, v. 60, p. 151-164

Chen, W., Hu, C., Li, Z., Chen, Y., Ding, X., Gao, S., and Ji, S., 2004, *Kinematic GPS precise point positioning for sea level monitoring*: Journal of Global Positioning Systems, v. 3, p. 302-307

Church, I., Hughes-Clarke, J.E., Haigh, S., Santos, M., Lamplugh, M., Griffin, J., and Parrott, R., 2008, *Using globally-corrected GPS solutions to assess the viability of hydrodynamic modeling in the Bay of Fundy*: Proceedings of the Canadian Hydrographic Conference, Victoria, BC, May 5-8, 2008

CO-OPS, 2003, *Computational techniques for tidal datums handbook*: NOAA Special Publication NOS CO-OPS 2, NOAA, National Ocean Service, Center for Operational Oceanographic Products and Services, Silver Spring, MD, 113p

CO-OPS, 2008, *CO-OPS specifications and deliverables for installation, operation, and removal of water level stations*: NOAA National Ocean Service

Center for Operational Oceanographic Products and Services, Silver Spring, MD 43p

Cove, K., Santos, M., Wells, D., and Bisnath, S., 2004, *Improved tropospheric delay estimation for long baseline, carrier-phase differential GPS positioning in a coastal environment*: Proceedings of the Institute of Navigation GNSS Conference, Long Beach, CA, September 21-24, 2004

Cove, K., 2005, *Improvements in GPS tropospheric delay estimation with numerical weather prediction*: University of New Brunswick, Masters Thesis, 114p

DeLoach, S.R, 1995, *GPS tides: A project to determine tidal datums with the global positioning system*: U.S. Army Corps of Engineers Topographic Engineering Center, Technical Report TEC-0071, 111p.

Eble, M.C. and Gonzalez, F.I., 1991, *Deep-ocean bottom pressure measurements in the northeast pacific*: Journal of Atmospheric and Oceanic Technology, v. 8, p. 221-233

El-Rabbany, A., 2006, *Introduction to GPS the global positioning system 2nd edition*: Artech House Inc., Boston, MA, 210p.

FIG, 2006, *FIG guide on the development of a vertical reference surface for hydrography*: Publication NO 37, International Federation of Surveyors Copenhagen, DK, 30p

Forrester, W.D., 1983, *Canadian tidal manual*: Department of Fisheries and Ocean, Ottawa, 138p.

Gill, G.K., and Schultz, J.R., 2001, *Tidal datums and their applications*: NOAA Special Publication NOS CO-OPS 1, NOAA, National Ocean Service, Center for Operational Oceanographic Products and Services, Silver Spring, MD, 132p

Hess, K., R. Schmalz, C. Zervas, and W. Collier, 1999, *Tidal Constituent and Residual Interpolation (TCARI): A new method for tidal correction of bathymetric data*: NOAA Technical Report NOS CS 4, NOAA, National Ocean Service, Silver Spring, MD, 112p

Hess, K. W., Milbert, D. G., Gill, S. K., Roman, D. R., 2003, *Vertical Datum transformations for kinematic GPS hydrographic surveys*: Proceedings or the U.S. Hydrographic Conference, Biloxi, MS, March 24-27, 2003

Hicks, S., 2006, *Understanding tides*: NOAA, National Ocean Service, Center for Operational Oceanographic Products and Services, Silver Spring, MD 83p.

Hughes Clarke, J., Dare, P., Beaudoin, J. and Bartlett, J., 2005, *A stable vertical reference for bathymetric surveying and tidal analysis in the high Arctic*: Proceedings of the U.S. Hydrographic Conference, San Diego, CA, March 29-31, 2005

Huff, L., and Remondi, B., 2000, *GPS Expedition to Tangier Island*: Proceedings of the ION NTM, Anaheim, CA, January 26-28, 2000

IHO, 1998, *IHO standards for hydrographic surveys*: International Hydrographic Organization, Special Publication No. 44, 4th edition, April, 23p.

Iliffe, J.C., Ziebart, M. K., and Turner, J. F., 2007, *A new methodology for incorporating tide gauge data in sea surface topography models*: Marine Geodesy, v. 30, p. 271-296

Kim, D., Bisnath, S., Langley, R.B., and Dare, P., 2004, *Performance of long-baseline real-time kinematic applications by improving tropospheric delay modeling*: Proceedings of the ION GNSS 17th International Technical meeting of the Satellite Division, Long Beach, CA, September 21-24, 2004

Kim, D., Langley, R.B., 2005, *Nullification of differential ionospheric delay for long-baseline real-time kinematic applications*: Proceedings of the ION 61st Annual Meeting, Cambridge, MA, June 27-29, 2005

Myers, E., 2005, *Review of progress on VDATUM, a vertical datum transformation tool*: Proceedings of the Marine Technology Society/IEEE OCEANS Conference, Washington, DC, September 19-23, 2005

MacAulay, P., O'Reilly, C., and Thompson, K., 2008, *Atlantic Canada's real-time water level observations, predictions, forecasts and datums on the web*: Proceedings of the Canadian Hydrographic Conference, Victoria, BC, May 5-8, 2008

CO-OPS, 2000, *Tide and Current Glossary*: NOAA, National Ocean Service, Center for Operational Oceanographic Products and Services, Silver Spring, MD, 113p

Nievinski, F., Cove, K., Santos, M., Wells, and D., Kingdon, R., 2005, *Range-extended GPS kinematic positioning using numerical weather prediction model*: Proceedings of the ION 61st Annual Technical Meeting, Cambridge, MA, June 27-29, 2005

Van Norden, M.F., Arroyo-Suarez, E.N., and Najjar, A.S., 2005, *Hydrographic surveys to IHO standards without shore stations using Real-Time Gipsy (RTG) Global Positioning System (GPS)*: Proceedings of the U.S. Hydrographic Conference, San Diego, CA, March 29-31, 2005

Pawlowicz, R., Beardsley, B., and Lentz, S., 2002, *Classical tidal harmonic analysis including error estimates in MATLAB using T_TIDE*: Computers & Geosciences, v. 28, p. 929-937

Parker, B.B., 2007, *Tidal analysis and prediction*: NOAA Special Publication NOS CO-OPS 3, NOAA, National Ocean Service, Center for Operational Oceanographic Products and Services, Silver Spring, MD, 378p

Press, W.H., Teukolsky, S.A., Vetterling, W.T., and Flannery, B.P., 1992, *Numerical recipes in C the art of scientific computing second edition*: Cambridge University Press, New York, 994p.

Pugh, D., 2004, *Changing Sea levels*: Cambridge University Press, New York, 265p.

O'Reilly, C., Parsons, S., and Langelier, D., 1996, *A seamless vertical reference surface for hydrographic data acquisition and information management*: Proceedings of the Canadian Hydrographic Conference, Halifax, NS, June 3-5, 1996

Santos, M., Wells, D., Cove, K. and Bisnath, S., 2004, *The Princess of Acadia GPS project: description and scientific challenges*: Proceedings of the Canadian Hydrographic Conference, Ottawa, ON, May 25-27, 2004

Santos, M., Nievinski, F., Cove, K., Kingdon, R., and Wells, D., 2005, *Range-extended post-processing kinematic (PPK) in a marine environment*: Proceedings of the ION GNSS 18th International Technical Meeting of the Satellite Division, Long Beach, CA, September 13-16, 2005

Santos, M., 2007, *Personal Communication*: University of New Brunswick, Fredericton, NB, Canada, July 31, 2007

Scargle, J.D., 1982, *Studies in astronomical time series analysis. II. Statistical aspects of spectral analysis of unevenly spaced data*: The Astrophysical Journal, v. 263, p. 835-853.

Seeber, G., 2003, *Satellite geodesy 2nd edition*: Walter de Gruyter, Berlin, DE, 589p.

Taylor, J.R., 1997, *An introduction to error analysis: The study of uncertainties in physical measurements second edition*: University Science Books, CA, 327p.

Torge, W., 2001, *Geodesy 3rd edition*: Walter de Gruyter, Berlin, DE, 416p.

Veronneau, M., 2000, *The Canadian gravimetric geoid model of 2000 (CGG2000)*: Geodetic Survey Division, Natural Resources Canada 17p

Waypoint, 2004, *GrafNav/GrafNet, GrafNav Lite, GrafMov, Inertial Explorer for Windows 95™, 98™, 2000™, XP™ & NT™ operating manual version 7.01*: Waypoint Consulting Inc, Calgary, AL, 431p:

Wells, D., 1987, *Guide to GPS positioning*: Canadian GPS Associates, Fredericton, NB

Wells, D., 2008a, *Personal communication*: 11 October 2008.

Wells, D., 2008b, *Personal communication*: 14 November 2008.

Wells, D., Bisnath, S., Howden, S., Dodd, D., Santos, M., and Cove, K., 2004, *Prospects for extended-range marine PPK*: Proceeding of the International Navigation Conference MELAHA, Cairo, Egypt, April 13-15, 2004

Wert, T., Dare, P., and Hughes-Clarke, J., 2004, *Tidal height retrieval using globally corrected GPS in the Amundsen Gulf region of the Canadian Arctic*: Proceedings of the ION GNSS 17th International Technical Meeting of the Satellite Division, Long Beach, CA, September 21-24, 2004

Wert, T.D., 2006, *Tidal height retrieval using globally corrected GPS in the Amundsen Gulf region of the Canadian Arctic*: University of New Brunswick, Masters Thesis, 142p

Yang, M., Lo, C., 2000, *Real-time kinematic GPS positioning for centimeter level ocean surface monitoring*: Proceedings of the National Science Council ROC(A), v. 24, p. 79-85

Zilkoski, D.B. et al., 1999, *Centimeter-level positioning of a U.S. Coast Guard buoy tender*: GPS Solutions, v. 3, p. 53-65

APPENDICES

GrafNav Option output file (*.opt)

```
;   PROJECT:    D:\Rokus_GPS\data\wk1248\wk1248.opt
;
;   DATE:       Feb  4/5  (date/time of processing)
;   TIME:       12:51:24
;   CREATED BY  GrafNav Batch Version 7.0)
;

PROCESS_MODE = TRK LOG LIB LSQ  ; Processing modes (GrafNav Batch only)

DATUM = WGS84 AUTO          ;  Processing Datum
INPDATUM = ON WGS84 AUTO    ;  Input Datum (ON-Use processing datum)
ELEV_MASK    = 5.0          ; Elevation mask (deg)
GRID         = UTM 1.0      ; Grid info

CYCLE_TEST   = BOTH         ; Cycle slip test method
STATIC_SLIP_TOL = 0.40      ; slip tolerance in static mode (cycles)
DOPPLER_TOL = 25.000        ; Bad doppler tolerance (m/s)
USE_DOPPLER = ON OFF        ; Use doppler meas. for phase, for code only

BASE_SAT     = 99           ; Base satellite (99 default)

TIMERANGE    = ALL 0.0 0.0 0 0 ; Processing time range
INTERVAL     = 1.00         ; Processing time interval (seconds)


PROCESS_DIR = FORWARD       ; Process direction (FORWARD/REVERSE)
BOTH_DIR = ON               ; True for processing both directions
SHOTGUN      = ON           ; Use filter reset (ON/OFF)
WRITE_BAD_EPOCHS = ON       ; Save bad data to .fwd/rev file (ON/OFF)
NOWRITE_HIGH = OFF 6 20.000 ; Don't write epoch with high statistics (q, std
OUTPUT_MODE = EXTENDED      ; Format for .fwd/rev file
DETAILED_SUM = ON           ; Detailed Static/KAR Summary Header
WRITE_SLIP_MSG = ON         ; Print cycle slips to message log
SAVE_AMB = OFF              ; Should ambiguities be saved

;Second values for KAR are Dual frequency Wide-lane values
KAR_MIN_TIME = 8.00 1.00    ; Min. time for KAR, L1 and L2 (minutes)
KAR_MIN_ADD = 1.50          ; minutes/10 Km added to KAR_MIN_TIME
KAR_MAX_TIME = 30           ; Time before first KAR epoch used (minutes)
KAR_CUBE     = 1.00   4.00  ; KAR cube size (m)
KAR_COV_L2   = ON 3.000 0.2 ; Use covariance for L2 KAR, StdDev factor, Off
KAR_MAX_DOP =    9.0        ; Cutoff DD DOP value for KAR to work
KAR_L2_NOISE = AUTO         ; L2 noise model: AUTO, ZERO, HIGH MEDIUM or LOW
KAR_ZERO_DIST = 5.0000      ; Distance for choosing between HIGH and ZERO noise
KAR_STATIC   = OFF          ; Engage KAR while in static mode
KAR_USE_PAR  = OFF          ; Allow KAR to go back in time past max. discrepancy
KAR_EPOCH_SIZE =   30.0   15.0 AUTO ; Computation interval for KAR
KAR_EPOCH_FILTER =    5.0           ; KAR data storage interval
KAR_DISTANCE = 7.500 30.000         ; KAR cutoff distance (Km)
KAR_EXACT_INTERVAL = OFF              ; ON if KAR to restrict data to KAR_EPOCH_
ISSUE_KAR_DOP = OFF  25.0           ; Issue KAR when DOP drops below value
ISSUE_KAR_TIME = OFF   15.000       ; Issue KAR when DOP drops below value
KAR_DIST_WEIGHT = ON        ; ON if distance weighting to be used
KAR_STRICT_TOL = OFF ON     ; RMS(ON/OFF), RES(ON/OFF) -- ON if stricter tolera
KAR_PASS = OFF OFF            ; Past KAR search, second param for 5 satellites
KAR_REFINE = ON             ; Refine L1/L2 KAR search

RAPID_TIME   = 0.0          ; Quick Static time (min)
RAPID_CUBE   = 1.50   2.50  ; Quick Static cube size (m)

;Fixed static solution options
FIX_CUBE = AUTOPERDOP 0.500 1.500 -1    ; Fixed solution search area options
FIX_L2_NOISE = AUTO -1          ; Fixed solution L2 noise mode)
FIX_ZERO_DIST = 5.000 -1        ; Distance for switching to Zero model for AUTO L2
FIX_REFINE   = OFF              ; Refine L1/L2 fixed solution
FIX_STRICT   = OFF OFF          ; Stricter RMS and reliability tolerances

FIX_INTERVAL = 15.0         ; Fixed static interval (s)
SPLIT_SS = OFF 120.0        ; Break static sessions if gap larger than value
FIX_AUTO = 180 0 40.000     ; Min(mins), Max(dist(Km) for automatic fixed sol
```

```
; new FCODE, L2 for sub. res., L2 for cono.(OFF/RELATIVE/FREE), correct C/A to
DUAL FREQUENCY = OFF ON FREE OFF
CONO DIST    = 4.0              ; Engage Relative cono after this dist. (km)
L2 SLIP TOL  = 0.500            ; Small cycle slip tolerance on L2 (cycles)
L2 LOCKTIME  = OFF              ; ON if L2 lock time variable to be used
USR PCODE = OFF OFF           ; Use P1 and use P2 flags (ON,OFF)
SF_CONO_MODE = OFF              ; ON if CONREX or CCD cono model to be used for SF

; Standard dev.at zero and tolerances
RANGE SD     = 2.00             ; C/A code stdev (m)
PHASE SD     = 0.050            ; L1 phase stdev (m)
PHASE RATE SD = 0.250           ; L1 phase rate stdev (m)
AUTO DOP_SD = ON                ; On for auto doppler standard dev.
PCODE SD     = 2.00             ; P code stdev (m)
RMS TOL      = 9.10 25.0 10.0 1.0; L1, CA, P RMS tolerance (m)  PPM scale
LOCKTIME_CUTOFF = 4.0      ; Carrier Lock time cutoff (seconds)

;Miscellaneous options
WRITE RESIDUALS = ON            ; Create .fil#/.lc# or .fil#/.rs# (# b/l number)
DYNAMICS = AUTO HIGH              ; Constraint on vehicle dynamics

; Single point processing options
SP PROC MODE = 0                ; 0 auto, 1 st, 2 df
SP CA VALUES =    5.00   15.00 ; C/A SD (m), C/A Req Tol (m)
SP AVG STATIC = ON               ; ON/OFF
SP SF_CONO    = 1               ; SF cono mode 0 off, 1 broadcast
SP WTH APPORX = ON               ; Increase meas. stdev for other errors (ON/OFF)
SP P1 OVRP CA = OFF              ; ON if P1 to be used instead of CA if available
SP CLK MODE   = ON               ; ON=Use Clockshift for time, OFF=use corrtime

; Combine settings (only used in ASC)
WRITE CMB = OFF


; Glonass Options
GLN TOFF = ON 0.0000 1000.0000 0.000000


; The following are Additional User Items


; End of file
```

Calculation of Vertical Offset for the GPS Antenna on the Ferry

Typically, the position of the antenna in the vessel reference frame is surveyed while the vessel is in dry dock, from which the X, Y, and Z lever-arm offsets can be calculated from the vessels pitch point. Because the *Princess of Acadia* was a vessel of opportunity, the precise position of the antenna in the vessel reference frame was not established. Instead, the average height above the water line of the GPS antenna on the ferry was computed using equation (51)

$$Z_{offset} = N - CD_{wl} + EH_{ant} \quad \textbf{(51)}$$

where N is the separation between ITRF2000 and CD, CD_{wl} is the height of the water relative to CD measured by the conventional gauges, and EH_{ant} is the height of the GPS antenna on the ferry relative to ITRF2000.

The N at Saint John, NB was computed from the CD height for 99B9006 and the OPUS solution from a 10 hour observation of that benchmark. The N at Digby, NS was established for TBM BOLLARD (Figure 47) at the ferry terminal because larger portions of the horizon were blocked when the GPS antenna was set up over the existing CHS tidal benchmarks.

Figure 47 - GPS observation on TBM BOLLARD at CHS 324. Benchmark 03N9002 is at the base of the flag pole.

A Z_{offset} is computed for every epoch that the ferry was docked at the ferry terminals and there were simultaneous PPK and conventional tide-gauge water-level measurements. The distribution of all the Z_{offset} values computed is shown in Figure 48. The average Z_{offset} is -17.96 +/-0.15 (1σ).

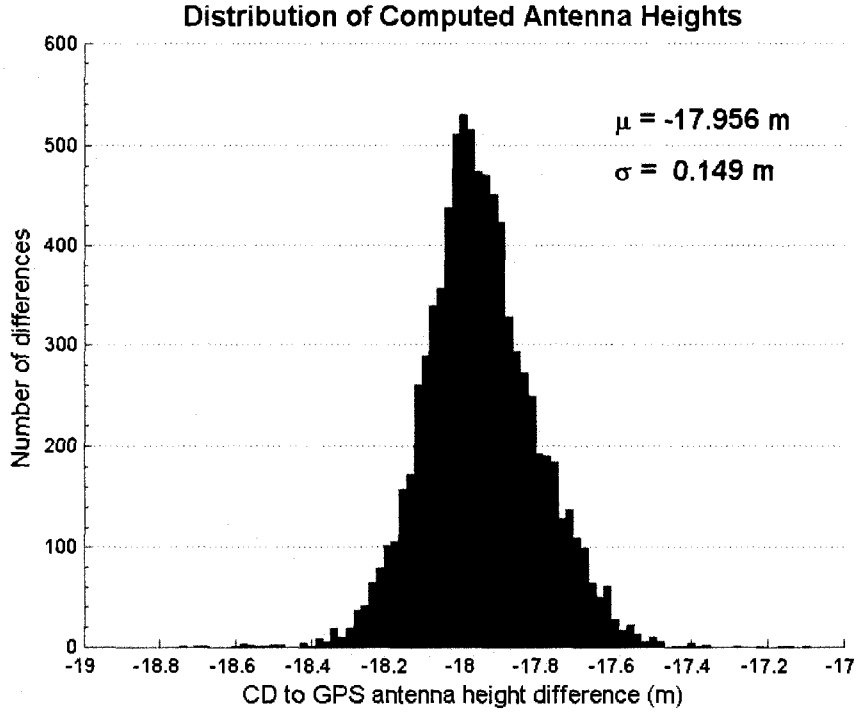

Figure 48 - Antenna height offsets computed using the conventional tide-gauge data, measured *N* values, and the GrafNav PPK heights solved to the L1 phase center of the GPS antenna on the ferry.

OPUS Solutions

TBM BOLLARD (DIGBY, NS)

```
FILE: BOLL2260.DAT 000413538

                        NGS OPUS SOLUTION REPORT
                        ========================

All computed coordinate accuracies are listed as peak-to-peak values.
For additional information: www.ngs.noaa.gov/OPUS/Using_OPUS.html#accuracy

      USER: nwardwell@ccom.unh.edu                DATE: August 14, 2008
RINEX FILE: BOLL226s.08o                          TIME: 22:26:02 UTC


  SOFTWARE: page5  0612.06 master23.pl            START: 2008/08/13  18:03:00
 EPHEMERIS: igr14923.eph [rapid]                   STOP: 2008/08/13  23:59:00
  NAV FILE: brdc2260.08n                      OBS USED: 13992 / 14608    :  9
  ANT NAME: TRM41249.00      NONE          # FIXED AMB:    56 /    57    :  9
ARP HEIGHT: 0.919                          OVERALL RMS: 0.016(m)


 REF FRAME: NAD_83(CORS96)(EPOCH:2002.0000)          ITRF00 (EPOCH:2008.6171

         X:       1865878.980(m)    0.024(m)          1865878.225(m)    0.024(m)
         Y:       4143467.407(m)    0.025(m)          4143465.978(m)    0.025(m)
         Z:       4460551.218(m)    0.032(m)          4460551.188(m)    0.032(m)

       LAT:    44 39 36.44470       0.021(m)       44 39 36.48074       0.021(m)
     E LON:   294 14 34.46558       0.024(m)      294 14 34.46096       0.024(m)
     W LON:    65 45 25.53442       0.024(m)       65 45 25.53904       0.024(m)
    EL HGT:           -15.292(m)    0.035(m)             -16.460(m)    0.035(m)
 ORTHO HGT:             6.360(m)    0.035(m) [NAVD88 (Computed using GEOID03)]

                       UTM COORDINATES     STATE PLANE COORDINATES
                        UTM (Zone 20)           *** NOTE ***
Northing (Y) [meters]     4948893.657       Please manually select
Easting (X)  [meters]      281416.953       SPC zone.
Convergence  [degrees]      -1.93872486
Point Scale                  1.00018758
Combined Factor              0.00000000

US NATIONAL GRID DESIGNATOR: 20TKQ8141748894(NAD 83)


                              BASE STATIONS USED
PID        DESIGNATION                    LATITUDE     LONGITUDE DISTANCE(m)
DF9215 ZBW1 BOSTON WAAS 1 CORS ARP     N424408.559 W0712849.518  508215.6
DJ7831 BRU5 BRUNSWICK 5 CORS ARP       N435323.306 W0695647.662  345158.6
DK4177 PNB5 PENOBSCOT 5 CORS ARP       N442706.177 W0684620.162  240655.0

                    NEAREST NGS PUBLISHED CONTROL POINT
PD0675       GANNET ROCK LH 1887       N443037.791 W0664653.729   82914.3

This position and the above vector components were computed without any
knowledge by the National Geodetic Survey regarding the equipment or
field operating procedures used.
```

BM 99B9006 (Saint John, NB)

```
FILE: 90062250.DAT 000413534

                        NGS OPUS SOLUTION REPORT
                        ========================

All computed coordinate accuracies are listed as peak-to-peak values.
For additional information: www.ngs.noaa.gov/OPUS/Using_OPUS.html#accuracy

      USER: nwardwell@ccom.unh.edu                DATE: August 14, 2008
RINEX FILE: 9006225o.08o                          TIME: 22:04:56 UTC


  SOFTWARE: page5  0612.06 master23.pl            START: 2008/08/12  14:24:00
 EPHEMERIS: igr14922.eph [rapid]                   STOP: 2008/08/13  00:41:00
  NAV FILE: brdc2250.08n                      OBS USED:  2857 /  3040   :  9
  ANT NAME: TRM41249.00      NONE          # FIXED AMB:    16 /    21   :  7
ARP HEIGHT: 1.651                         OVERALL RMS: 0.017(m)


 REF FRAME: NAD_83(CORS96)(EPOCH:2002.0000)          ITRF00 (EPOCH:2008.6143

         X:      1825019.086(m)    0.523(m)          1825018.330(m)    0.523(m)
         Y:     -4110601.597(m)    0.016(m)         -4110600.176(m)    0.016(m)
         Z:      4507302.743(m)    0.106(m)          4507302.717(m)    0.106(m)

       LAT:   45 15 16.66468       0.109(m)       45 15 16.70102       0.109(m)
     E LON:  293 56 24.70622       0.478(m)      293 56 24.70098       0.478(m)
     W LON:   66  3 35.29378       0.478(m)       66  3 35.29902       0.478(m)
    EL HGT:           -15.284(m)    0.192(m)           -16.433(m)    0.192(m)
 ORTHO HGT:             6.044(m)    0.192(m)  [NAVD88 (Computed using GEOID03)]

                      UTM COORDINATES     STATE PLANE COORDINATES
                       UTM (Zone 19)           *** NOTE ***
Northing (Y) [meters]     5015443.145      Please manually select
Easting (X)  [meters]      730702.972      SPC zone.
Convergence  [degrees]       2.08916927
Point Scale                  1.00025446
Combined Factor              0.00000000

US NATIONAL GRID DESIGNATOR: 19TGL3070315443(NAD 83)


                          BASE STATIONS USED
PID       DESIGNATION                      LATITUDE     LONGITUDE DISTANCE(m)
AH5044 BARH BAR HARBOR CORS ARP          N442342.137 W0681318.080  195834.3
       UNBJ                                                         89650.8
       SHE2                                                        159049.4

                  NEAREST NGS PUBLISHED CONTROL POINT
PD0792      HANNABURY                    N445618.430 W0665509.228   76156.1

This position and the above vector components were computed without any
knowledge by the National Geodetic Survey regarding the equipment or
field operating procedures used.
```

Tidal Constituents in Order of Increasing Frequency

The table in this appendix is a list of the tidal constituents that were used to model the water-level estimates in each of the VTGZ. The values in this table are from Bruce B. Parker's book "Tidal Analysis and Prediction" (2007). The first column is the name of the tidal constituent. The second column is the origin of the tidal constituent defines if the constituent is derived from the Moon (lunar), the Sun (solar), a combination of the moon and sun (luni-solar), meteorological influence (*met), or shallow-water non-linear effects (shallow). The shallow-water constituents are both overtides and compound tides. Columns 3 through 8 define the Cartwright numbers that are used with the 6 fundamental frequencies to compute the speed of the constituent. Column 9 shows the name, if there is one, of the shallow-water constituent that is equivalent. Column 10 is the angular speed in degrees per hour of the constituents. The angular speed (Ω) is derived from the Cartwright numbers of the constituent. Column 11 is the frequency (*f*) of the constituent in cycles per day (cpd). The angular speed is converted to frequency in cpd by dividing by 360 and multiplying by 24 ($f = \Omega/360 * 24$). Column 12 is the period (*T*) in hours of the tidal constituent. The period equals 360 divided by the angular speed ($T = 360/\Omega$).

Tidal Harmonic Constituent	Origin of Constituent	Cartwright No						Shallow-water equivalent	Angular Speed (deg/hr)	Freq (cpd)	Period (hours)
Ssa	solar (*met)	0	0	2	0	0	0		0.0821373	0.0055	4382.9052
MSM		0	1	-2	1	0	0		0.4715521	0.0314	763.4363
Mm	lunar (*met)	0	1	0	-1	0	0	MN4	0.5443747	0.0363	661.3092
MSf	lunar (*met)	0	2	-2	0	0	0	MS	1.0158958	0.0677	354.3671
Mf	lunar (*met)	0	2	0	0	0	0	KO	1.0903310	0.0727	330.1750
ALP1 (α1)		1	-4	2	1	0	0		12.3827652	0.8255	29.0727
2Q1	lunar	1	-3	0	2	0	0		12.8542862	0.8570	28.0062
SIG1 (σ1)	lunar	1	-3	2	0	0	0		12.9271398	0.8618	27.8484
Q1	lunar	1	-2	0	1	0	0		13.3986609	0.8932	26.8684
RHO1 (ρ1)	lunar	1	-2	2	-1	0	0		13.4715145	0.8981	26.7231
O1	lunar	1	-1	0	0	0	0	MK1	13.9430356	0.9295	25.8193
TAU1 (τ1)	lunar	1	-1	2	0	0	0	MP1	14.0251729	0.9350	25.6681
BET1 (β1)		1	0	-2	1	0	0		14.4145548	0.9610	24.9748
NO1									14.4967221	0.9664	24.8332
CHI1	lunar	1	0	2	-1	0	0		14.5695476	0.9713	24.7091
K1	luni-solar	1	1	0	0	0	0	MO1	15.0410686	1.0027	23.9345
PHI1(φ1)	solar	1	1	2	0	0	0	2KP1	15.1232058	1.0082	23.8045
THE1 (θ1)	lunar	1	2	-2	1	0	0		15.5125897	1.0342	23.2070
J1	lunar	1	2	0	-1	0	0		15.5854433	1.0390	23.0985
SO1	lunar	-1	3	-2	0	0	0	SO1	16.0569644	1.0705	22.4202
OO1	lunar	1	3	0	0	0	0		16.1391017	1.0759	22.3061
UPS1 (υ1)		1	4	0	-1	0	0		16.6834764	1.1122	21.5782
OQ2	shallow							OQ2	27.3416965	1.8228	13.1667
EPS2 (ε2)		2	-3	2	1	0	0	MNS2	27.4238337	1.8283	13.1273
2N2	lunar	2	-2	0	2	0	0	2NM2	27.8953548	1.8597	12.9054
MU2 (μ2)	lunar	2	-2	2	0	0	0	2MS2	27.9682084	1.8645	12.8718
N2	lunar	2	-1	0	1	0	0		28.4397295	1.8960	12.6583
NU2 (ν2)	lunar	2	-1	2	-1	0	0		28.5125831	1.9008	12.6260
OP2	shallow							OP2	28.9019669	1.9268	12.4559
M2	lunar	2	0	0	0	0	0	KO2	28.9841042	1.9323	12.4206
MKS2	shallow							MKS2	29.0662415	1.9377	12.3855
LDA2 (λ2)	lunar	2	1	-2	1	0	0		29.4556253	1.9637	12.2218
L2	lunar	2	1	0	-1	0	0	2MN2	29.5284789	1.9686	12.1916
S2	solar	2	2	-2	0	0	0	KP2	30.0000000	2.0000	12.0000
K2	luni-solar	2	2	0	0	0	0		30.0821373	2.0055	11.9672
MSN2	shallow							MSN2	30.5443747	2.0363	11.7861
ETA2 (η2)	lunar	2	3	0	-1	0	0	KJ2	30.6265119	2.0418	11.7545
2SM2	shallow	2	4	-4	0	0	0	2SM2	31.0158958	2.0677	11.6070
MO3 (2MK3)	shallow	3	-1	0	0	0	0	2MK3 (MO3)	42.9271398	2.8618	8.3863
M3	lunar	3	0	0	0	0	0		43.4761563	2.8984	8.2804
SO3	shallow							SO3	43.9430356	2.9295	8.1924
MK3 (2MO3)	shallow	3	1	0	0	0	0	MK3 (2MO3)	44.0251729	2.9350	8.1771
SK3	shallow							SK3	45.0410686	3.0027	7.9927
MN4	shallow	4	-1	0	1	0	0	MN4	57.4238337	3.8283	6.2692
M4	shallow	4	0	0	0	0	0	M4	57.9682084	3.8645	6.2103
SN4	shallow							SN4	58.4397295	3.8960	6.1602
MS4	shallow	4	2	-2	0	0	0	MS4	58.9841041	3.9323	6.1033
MK4	shallow							MK4	59.0662415	3.9377	6.0949
S4	shallow	4	4	-4	0	0	0	S4	60.0000000	4.0000	6.0000
SK4	shallow							SK4	60.0821122	4.0055	5.9918
2MK5 (3MO5)	shallow							2MK5 (3MO5)	73.0092770	4.8673	4.9309
2SK5								2SK5	75.0406470	5.0027	4.7974
2MN6	shallow							2NMKS6	86.4079380	5.7605	4.1663
M6	shallow	6	0	0	0	0	0	M6	86.9523127	5.7968	4.1402
MSN6	shallow							MSN6	87.4238337	5.8283	4.1179
2MS6	shallow							2MS6	87.9682084	5.8645	4.0924
2MK6	shallow							2MK6	88.0503457	5.8700	4.0886
2SM6	shallow							2SM6	88.9841042	5.9323	4.0457
MSK6	shallow							MSK6	89.0662415	5.9377	4.0419
3MK7	shallow							3MK7	101.9933600	6.7996	3.5296
M8	shallow	8	0	0	0	0	0	M8	115.9364169	7.7291	3.1052

Map of VTGZ 1 through 62

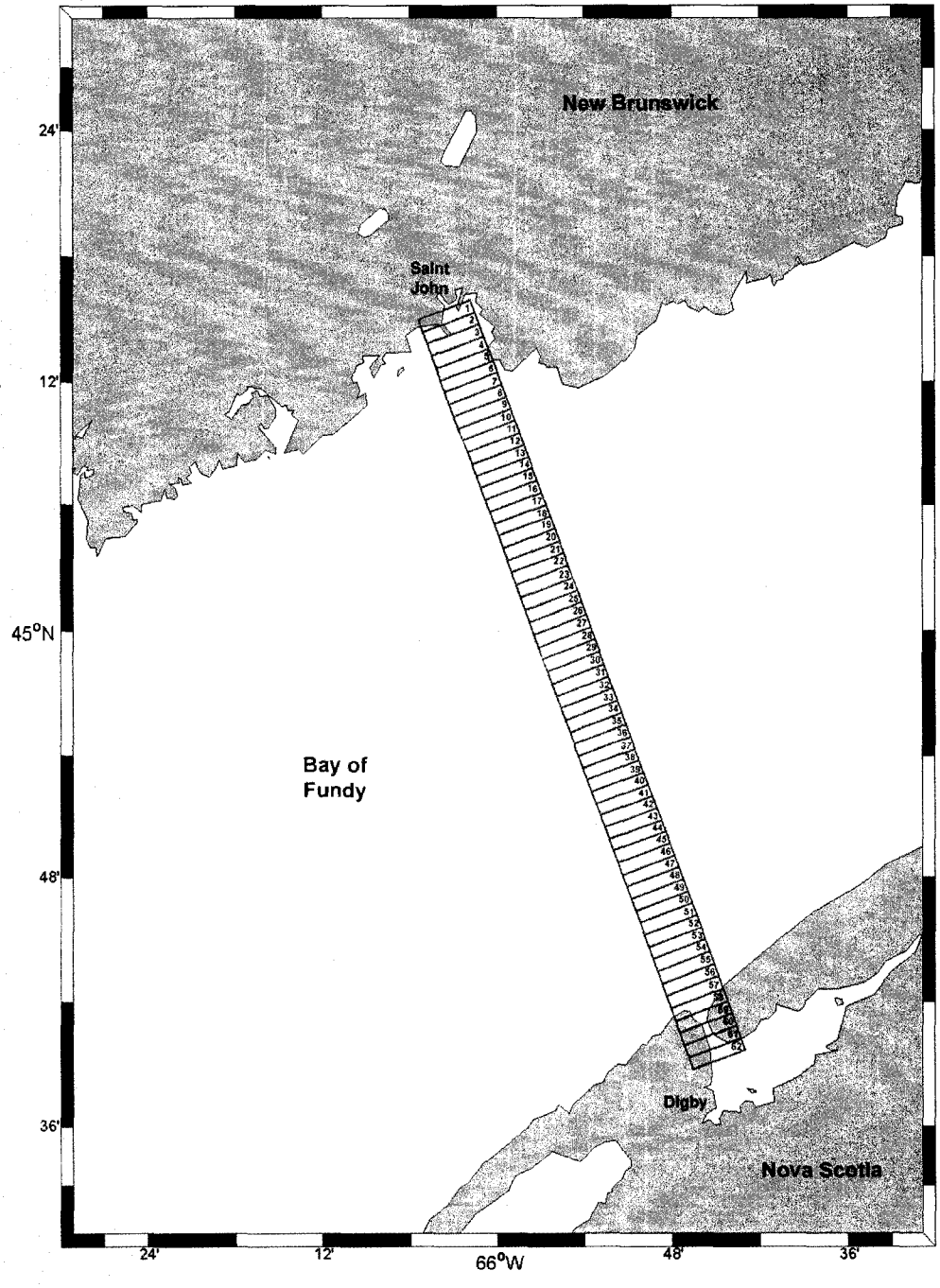

Virtual Tide Gauge Zone Coordinates

This appendix includes a table with the coordinates for the vertices of 62 VTGZ. Column 1 of the table in this appendix is the identification number of the VTGZ. These numbers can be cross referenced with the map in the previous appendix. The first and second columns are the latitude and longitude of the northeast vertices. The third and fourth columns are the latitude and longitude of the southeast vertices. The fifth and sixth columns are the latitude and longitude of the southwest vertices. The seventh and eight columns are the latitude and longitude of the northwest vertices. All of the latitude coordinates are in decimal degrees north. All of the longitude coordinates are in decimal degrees west.

	NE-Vertice		SE-Vertice		SW-Vertice		NW-Vertice	
VTGZ	lat (N)	lon (W)	lat (N)	lon (W)	lat (N)	lon (W)	lat (N)	lon (W)
1	45.26572	293.96949	45.25598	293.97459	45.24035	293.91487	45.25008	293.90976
2	45.25598	293.97459	45.24625	293.97969	45.23061	293.91998	45.24035	293.91487
3	45.24625	293.97969	45.23651	293.98479	45.22087	293.92509	45.23061	293.91998
4	45.23651	293.98479	45.22677	293.98989	45.21114	293.93020	45.22087	293.92509
5	45.22677	293.98989	45.21703	293.99499	45.20140	293.93531	45.21114	293.93020
6	45.21703	293.99499	45.20730	294.00008	45.19166	293.94041	45.20140	293.93531
7	45.20730	294.00008	45.19756	294.00518	45.18192	293.94552	45.19166	293.94041
8	45.19756	294.00518	45.18782	294.01027	45.17218	293.95062	45.18192	293.94552
9	45.18782	294.01027	45.17808	294.01536	45.16245	293.95572	45.17218	293.95062
10	45.17808	294.01536	45.16834	294.02044	45.15271	293.96082	45.16245	293.95572
11	45.16834	294.02044	45.15861	294.02553	45.14297	293.96591	45.15271	293.96082
12	45.15861	294.02553	45.14887	294.03062	45.13323	293.97101	45.14297	293.96591
13	45.14887	294.03062	45.13913	294.03570	45.12349	293.97610	45.13323	293.97101
14	45.13913	294.03570	45.12939	294.04078	45.11375	293.98119	45.12349	293.97610
15	45.12939	294.04078	45.11965	294.04586	45.10401	293.98628	45.11375	293.98119
16	45.11965	294.04586	45.10991	294.05094	45.09427	293.99137	45.10401	293.98628
17	45.10991	294.05094	45.10017	294.05601	45.08453	293.99646	45.09427	293.99137
18	45.10017	294.05601	45.09043	294.06109	45.07479	294.00154	45.08453	293.99646
19	45.09043	294.06109	45.08069	294.06616	45.06505	294.00662	45.07479	294.00154
20	45.08069	294.06616	45.07094	294.07123	45.05531	294.01170	45.06505	294.00662
21	45.07094	294.07123	45.06120	294.07630	45.04557	294.01678	45.05531	294.01170
22	45.06120	294.07630	45.05146	294.08137	45.03582	294.02186	45.04557	294.01678
23	45.05146	294.08137	45.04172	294.08643	45.02608	294.02694	45.03582	294.02186
24	45.04172	294.08643	45.03198	294.09150	45.01634	294.03201	45.02608	294.02694
25	45.03198	294.09150	45.02223	294.09656	45.00660	294.03708	45.01634	294.03201
26	45.02223	294.09656	45.01249	294.10162	44.99686	294.04215	45.00660	294.03708
27	45.01249	294.10162	45.00275	294.10668	44.98711	294.04722	44.99686	294.04215
28	45.00275	294.10668	44.99301	294.11174	44.97737	294.05229	44.98711	294.04722
29	44.99301	294.11174	44.98326	294.11679	44.96763	294.05736	44.97737	294.05229
30	44.98326	294.11679	44.97352	294.12184	44.95788	294.06242	44.96763	294.05736
31	44.97352	294.12184	44.96378	294.12690	44.94814	294.06748	44.95788	294.06242
32	44.96378	294.12690	44.95403	294.13195	44.93840	294.07254	44.94814	294.06748
33	44.95403	294.13195	44.94429	294.13700	44.92865	294.07760	44.93840	294.07254
34	44.94429	294.13700	44.93454	294.14204	44.91891	294.08266	44.92865	294.07760
35	44.93454	294.14204	44.92480	294.14709	44.90916	294.08771	44.91891	294.08266
36	44.92480	294.14709	44.91505	294.15213	44.89942	294.09277	44.90916	294.08771
37	44.91505	294.15213	44.90531	294.15717	44.88967	294.09782	44.89942	294.09277
38	44.90531	294.15717	44.89556	294.16221	44.87993	294.10287	44.88967	294.09782
39	44.89556	294.16221	44.88582	294.16725	44.87018	294.10792	44.87993	294.10287
40	44.88582	294.16725	44.87607	294.17229	44.86043	294.11296	44.87018	294.10792
41	44.87607	294.17229	44.86633	294.17732	44.85069	294.11801	44.86043	294.11296
42	44.86633	294.17732	44.85658	294.18236	44.84094	294.12305	44.85069	294.11801
43	44.85658	294.18236	44.84683	294.18739	44.83120	294.12809	44.84094	294.12305
44	44.84683	294.18739	44.83709	294.19242	44.82145	294.13313	44.83120	294.12809
45	44.83709	294.19242	44.82734	294.19745	44.81170	294.13817	44.82145	294.13313
46	44.82734	294.19745	44.81759	294.20247	44.80195	294.14321	44.81170	294.13817
47	44.81759	294.20247	44.80784	294.20750	44.79221	294.14824	44.80195	294.14321
48	44.80784	294.20750	44.79810	294.21252	44.78246	294.15327	44.79221	294.14824
49	44.79810	294.21252	44.78835	294.21754	44.77271	294.15831	44.78246	294.15327
50	44.78835	294.21754	44.77860	294.22256	44.76296	294.16334	44.77271	294.15831
51	44.77860	294.22256	44.76885	294.22758	44.75321	294.16836	44.76296	294.16334
52	44.76885	294.22758	44.75910	294.23259	44.74346	294.17339	44.75321	294.16836
53	44.75910	294.23259	44.74935	294.23761	44.73372	294.17841	44.74346	294.17339
54	44.74935	294.23761	44.73960	294.24262	44.72397	294.18344	44.73372	294.17841
55	44.73960	294.24262	44.72985	294.24763	44.71422	294.18846	44.72397	294.18344
56	44.72985	294.24763	44.72010	294.25264	44.70447	294.19348	44.71422	294.18846
57	44.72010	294.25264	44.71035	294.25765	44.69472	294.19850	44.70447	294.19348
58	44.71035	294.25765	44.70060	294.26266	44.68497	294.20351	44.69472	294.19850
59	44.70060	294.26266	44.69085	294.26766	44.67522	294.20853	44.68497	294.20351
60	44.69085	294.26766	44.68110	294.27266	44.66547	294.21354	44.67522	294.20853
61	44.68110	294.27266	44.67135	294.27767	44.65571	294.21855	44.66547	294.21354
62	44.67135	294.27767	44.66160	294.28267	44.64596	294.22356	44.65571	294.21855

MLLW and MSL for the Virtual Tide Gauge Zones

The two tables in this appendix are contain the coordinates of the midpoints for each of the VTGZ, the tidal datums for the VTGZ, the uncertainties of the tidal datums, the distance the midpoint of the VTGZ is from the location of the GPS base station CGSJ in Saint John, NB, and the number of water-level estimates in each of the VTGZ. The tidal datums and the uncertainties in the first table were computed using the 61 tidal frequencies. The tidal datums and the uncertainties in the second table were computed using the same 5 tidal constituents that are used by WebTide (M2, N2, S2, K1, and O1).

For both of the tables the data in the columns are as follows. Column 1 is the identification number of the VTGZ. Column 2 is the height in meters of MLLW above ITRF2000. Column 3 is the uncertainty in meters of MLLW estimated using the least-squares procedure. Column 4 is the height in meters of MSL above ITRF2000. Column 5 is the uncertainty in meters of MSL estimated using the least-squares procedure. Column 6 is the longitude of the midpoint of the VTGZ in decimal degrees east. Column 7 is the standard deviation of the difference between the water-level estimates and the model predictions. Column 8 is the latitude of the midpoint of the VTGZ in decimal degrees north. Column 9 is the distance the midpoint is from the location of the base station CGSJ. Column 10 is the number of water-level estimates in the sparse non-uniform time series in each VTGZ.

Tidal datums for VTGZ 1 through 62 computed using 61 tidal constituents									
VTGZ	MLLW (m)	LSQ-Std (m)	MSL (m)	LSQ-Std (m)	Diff-Std (m)	Lon (E)	Lat (N)	Dist (km)	No. samples
1	-25.838	0.031	-22.589	0.011	0.216	293.9422	45.2530	1.89	2250
2	-26.348	0.034	-22.914	0.013	0.196	293.9473	45.2433	3.24	983
3	-26.345	0.034	-22.932	0.014	0.201	293.9524	45.2336	4.39	979
4	-26.372	0.033	-22.952	0.012	0.203	293.9575	45.2238	5.54	971
5	-26.279	0.033	-22.927	0.012	0.195	293.9626	45.2141	6.69	977
6	-26.150	0.032	-22.864	0.012	0.183	293.9677	45.2044	7.84	981
7	-26.148	0.032	-22.869	0.012	0.178	293.9728	45.1946	9.00	981
8	-26.153	0.033	-22.882	0.012	0.174	293.9779	45.1849	10.15	981
9	-26.192	0.033	-22.904	0.012	0.173	293.9830	45.1751	11.30	978
10	-26.240	0.033	-22.934	0.013	0.172	293.9881	45.1654	12.46	970
11	-26.250	0.033	-22.960	0.013	0.173	293.9932	45.1557	13.61	968
12	-26.263	0.033	-22.985	0.013	0.173	293.9983	45.1459	14.76	966
13	-26.318	0.033	-23.016	0.013	0.173	294.0034	45.1362	15.92	964
14	-26.338	0.033	-23.040	0.013	0.172	294.0084	45.1264	17.07	956
15	-26.376	0.033	-23.071	0.013	0.170	294.0135	45.1167	18.22	953
16	-26.410	0.033	-23.102	0.013	0.167	294.0186	45.1070	19.38	950
17	-26.423	0.033	-23.124	0.013	0.166	294.0237	45.0972	20.53	948
18	-26.434	0.033	-23.150	0.012	0.166	294.0288	45.0875	21.69	948
19	-26.458	0.033	-23.168	0.012	0.166	294.0338	45.0777	22.84	949
20	-26.470	0.033	-23.184	0.012	0.167	294.0389	45.0680	23.99	947
21	-26.482	0.033	-23.193	0.012	0.166	294.0440	45.0583	25.15	947
22	-26.519	0.033	-23.205	0.012	0.164	294.0491	45.0485	26.30	944
23	-26.527	0.033	-23.216	0.012	0.164	294.0541	45.0388	27.46	942
24	-26.544	0.033	-23.226	0.012	0.166	294.0592	45.0290	28.61	942
25	-26.553	0.033	-23.229	0.012	0.164	294.0643	45.0193	29.76	942
26	-26.562	0.033	-23.241	0.012	0.163	294.0694	45.0095	30.92	940
27	-26.555	0.033	-23.239	0.012	0.165	294.0744	44.9998	32.07	942
28	-26.562	0.033	-23.242	0.012	0.163	294.0795	44.9901	33.22	941
29	-26.571	0.033	-23.242	0.012	0.163	294.0845	44.9803	34.38	941
30	-26.567	0.033	-23.245	0.012	0.166	294.0896	44.9706	35.53	942
31	-26.575	0.033	-23.237	0.012	0.165	294.0947	44.9608	36.69	945
32	-26.563	0.033	-23.237	0.012	0.165	294.0997	44.9511	37.84	944
33	-26.555	0.033	-23.235	0.012	0.167	294.1048	44.9413	38.99	944
34	-26.544	0.033	-23.225	0.012	0.164	294.1098	44.9316	40.15	942
35	-26.537	0.033	-23.218	0.012	0.165	294.1149	44.9219	41.30	941
36	-26.524	0.033	-23.208	0.012	0.164	294.1199	44.9121	42.46	940
37	-26.522	0.033	-23.195	0.012	0.162	294.1250	44.9024	43.61	946
38	-26.506	0.033	-23.182	0.012	0.165	294.1300	44.8926	44.76	946
39	-26.500	0.033	-23.174	0.012	0.165	294.1351	44.8829	45.92	947
40	-26.482	0.033	-23.157	0.012	0.164	294.1401	44.8731	47.07	947
41	-26.475	0.033	-23.143	0.012	0.168	294.1451	44.8634	48.23	945
42	-26.466	0.033	-23.138	0.012	0.164	294.1502	44.8536	49.38	943
43	-26.479	0.033	-23.125	0.012	0.165	294.1552	44.8439	50.53	941
44	-26.453	0.033	-23.106	0.012	0.166	294.1603	44.8341	51.69	943
45	-26.445	0.033	-23.093	0.012	0.167	294.1653	44.8244	52.84	943
46	-26.447	0.033	-23.080	0.012	0.168	294.1703	44.8146	54.00	944
47	-26.436	0.033	-23.071	0.012	0.167	294.1754	44.8049	55.15	946
48	-26.432	0.033	-23.060	0.012	0.167	294.1804	44.7952	56.30	946
49	-26.429	0.033	-23.050	0.012	0.170	294.1854	44.7854	57.46	949
50	-26.410	0.033	-23.042	0.012	0.170	294.1904	44.7757	58.61	952
51	-26.392	0.033	-23.034	0.012	0.172	294.1955	44.7659	59.77	956
52	-26.383	0.033	-23.031	0.012	0.176	294.2005	44.7562	60.92	958
53	-26.376	0.033	-23.019	0.012	0.176	294.2055	44.7464	62.07	955
54	-26.360	0.033	-23.012	0.012	0.179	294.2105	44.7367	63.23	964
55	-26.343	0.033	-23.014	0.012	0.179	294.2156	44.7269	64.38	969
56	-26.341	0.033	-23.012	0.012	0.177	294.2205	44.7172	65.54	970
57	-26.356	0.033	-23.019	0.012	0.177	294.2256	44.7074	66.69	972
58	-26.365	0.033	-23.017	0.012	0.170	294.2306	44.6977	67.84	974
59	-26.322	0.033	-23.004	0.012	0.165	294.2356	44.6879	69.00	971
60	-26.359	0.033	-23.030	0.012	0.164	294.2406	44.6782	70.15	969
61	-26.312	0.033	-22.961	0.013	0.166	294.2456	44.6684	71.31	905
62	-26.137	0.033	-22.790	0.013	0.155	294.2506	44.6587	72.25	1547

Tidal datums for VTGZ 1 through 62 computed using 5 tidal constituents									
VTGZ	MLLW (m)	LSQ-Std (m)	MSL (m)	LSQ-Std (m)	Diff-Std (m)	Lon (E)	Lat (N)	Dist (km)	No. samples
1	-25.666	0.030	-22.568	0.009	0.293	293.9422	45.2530	1.89	2250
2	-26.176	0.031	-22.884	0.009	0.317	293.9473	45.2433	3.24	983
3	-26.235	0.031	-22.917	0.009	0.319	293.9524	45.2336	4.39	979
4	-26.216	0.031	-22.906	0.009	0.319	293.9575	45.2238	5.54	971
5	-26.154	0.031	-22.884	0.009	0.313	293.9626	45.2141	6.69	977
6	-26.064	0.031	-22.852	0.009	0.301	293.9677	45.2044	7.84	981
7	-26.077	0.031	-22.860	0.009	0.296	293.9728	45.1946	9.00	981
8	-26.072	0.030	-22.889	0.009	0.296	293.9779	45.1849	10.15	981
9	-26.094	0.030	-22.902	0.009	0.297	293.9830	45.1751	11.30	978
10	-26.148	0.031	-22.936	0.009	0.296	293.9881	45.1654	12.46	970
11	-26.192	0.031	-22.961	0.009	0.297	293.9932	45.1557	13.61	968
12	-26.224	0.031	-22.992	0.009	0.299	293.9983	45.1459	14.76	966
13	-26.241	0.031	-23.027	0.009	0.299	294.0034	45.1362	15.92	964
14	-26.264	0.031	-23.043	0.009	0.298	294.0084	45.1264	17.07	956
15	-26.294	0.031	-23.076	0.009	0.298	294.0135	45.1167	18.22	953
16	-26.335	0.031	-23.111	0.009	0.296	294.0186	45.1070	19.38	950
17	-26.359	0.031	-23.137	0.009	0.297	294.0237	45.0972	20.53	948
18	-26.363	0.031	-23.157	0.009	0.298	294.0288	45.0875	21.69	948
19	-26.388	0.031	-23.165	0.009	0.296	294.0338	45.0777	22.84	949
20	-26.395	0.031	-23.183	0.009	0.296	294.0389	45.0680	23.99	947
21	-26.415	0.031	-23.194	0.009	0.299	294.0440	45.0583	25.15	947
22	-26.434	0.031	-23.208	0.009	0.297	294.0491	45.0485	26.30	944
23	-26.456	0.031	-23.227	0.009	0.297	294.0541	45.0388	27.46	942
24	-26.464	0.031	-23.234	0.009	0.298	294.0592	45.0290	28.61	942
25	-26.463	0.031	-23.234	0.009	0.299	294.0643	45.0193	29.76	942
26	-26.509	0.031	-23.247	0.009	0.299	294.0694	45.0095	30.92	940
27	-26.486	0.031	-23.248	0.009	0.299	294.0744	44.9998	32.07	942
28	-26.497	0.031	-23.249	0.009	0.300	294.0795	44.9901	33.22	941
29	-26.495	0.031	-23.244	0.009	0.300	294.0845	44.9803	34.38	941
30	-26.506	0.031	-23.249	0.009	0.303	294.0896	44.9706	35.53	942
31	-26.492	0.031	-23.246	0.009	0.302	294.0947	44.9608	36.69	945
32	-26.498	0.031	-23.239	0.009	0.304	294.0997	44.9511	37.84	944
33	-26.491	0.031	-23.234	0.009	0.302	294.1048	44.9413	38.99	944
34	-26.472	0.031	-23.228	0.009	0.302	294.1098	44.9316	40.15	942
35	-26.465	0.031	-23.222	0.009	0.302	294.1149	44.9219	41.30	941
36	-26.449	0.031	-23.204	0.009	0.300	294.1199	44.9121	42.46	940
37	-26.447	0.031	-23.196	0.009	0.300	294.1250	44.9024	43.61	946
38	-26.430	0.031	-23.189	0.009	0.299	294.1300	44.8926	44.76	946
39	-26.431	0.031	-23.184	0.009	0.300	294.1351	44.8829	45.92	947
40	-26.410	0.031	-23.163	0.009	0.300	294.1401	44.8731	47.07	947
41	-26.404	0.031	-23.154	0.009	0.302	294.1451	44.8634	48.23	945
42	-26.375	0.031	-23.142	0.009	0.300	294.1502	44.8536	49.38	943
43	-26.385	0.031	-23.135	0.009	0.301	294.1552	44.8439	50.53	941
44	-26.373	0.031	-23.120	0.009	0.303	294.1603	44.8341	51.69	943
45	-26.356	0.031	-23.109	0.009	0.305	294.1653	44.8244	52.84	943
46	-26.357	0.031	-23.092	0.009	0.303	294.1703	44.8146	54.00	944
47	-26.332	0.031	-23.084	0.009	0.303	294.1754	44.8049	55.15	946
48	-26.319	0.031	-23.072	0.009	0.305	294.1804	44.7952	56.30	946
49	-26.300	0.031	-23.073	0.009	0.305	294.1854	44.7854	57.46	949
50	-26.289	0.031	-23.056	0.009	0.306	294.1904	44.7757	58.61	952
51	-26.289	0.031	-23.060	0.009	0.305	294.1955	44.7659	59.77	956
52	-26.292	0.031	-23.054	0.009	0.305	294.2005	44.7562	60.92	958
53	-26.281	0.031	-23.048	0.009	0.305	294.2055	44.7464	62.07	955
54	-26.262	0.031	-23.034	0.009	0.304	294.2105	44.7367	63.23	964
55	-26.263	0.031	-23.036	0.009	0.306	294.2155	44.7269	64.38	969
56	-26.249	0.031	-23.027	0.009	0.305	294.2205	44.7172	65.54	970
57	-26.265	0.031	-23.034	0.009	0.307	294.2256	44.7074	66.69	972
58	-26.282	0.031	-23.030	0.009	0.306	294.2306	44.6977	67.84	974
59	-26.274	0.031	-23.013	0.009	0.304	294.2356	44.6879	69.00	971
60	-26.344	0.031	-23.050	0.009	0.302	294.2406	44.6782	70.15	969
61	-26.307	0.031	-23.006	0.009	0.311	294.2456	44.6684	71.31	905
62	-26.015	0.031	-22.805	0.009	0.293	294.2506	44.6587	72.25	1547